California Institute of Technology

Graduate Aeronautical Laboratories

Department of Aeronautics

Numerical Simulations of Combustion Instabilities in Gas Turbine Combustors, with Applications

A Thesis in

Aeronautics

by

Grant Douglas Swenson

Submitted in Partial Fulfillment
of the Requirements
for the Degree of
Doctor of Philosophy

2000

(Submitted October 29, 1999)

Acknowledgments

I would like to thank the following people. Fred Culick for all his advice and help over the years. I would like to express my gratitude to Dr. Culick for allowing me the opportunity to study in Italy twice and to be involved in a side project on Amelia Earhart. The people of the University of Padova and the Center of Advanced Studies Research and Development in Sardinia for teaching me more about the numerical simulation of combustion systems. Ed Zukoski for waking me up on March 9, 1993, and informing me of my acceptance to Caltech. He was a great advisor during that first year and his efforts in the field of combustion are sorely missed.

Dorothy Eckerman, Marionne Epalle and Melinda Kirk for patiently answering my questions about all of those wonderful Caltech forms and for relaxing conversations when I needed a break. Claude Seywert and Giorgio Isella for answering all of my off-the-wall combustion dynamics questions and for introducing me to the great art of the afternoon coffee break. Michael Kaneshige and Winston Pun for putting up with me as an office mate.

Akshai Runchal for setting me up with the ANSWER code and for answering most of the questions I had when faced with a problem in the code. Victor Burnley and Windsor Lin for showing me the ropes when they were the senior members of the group. I hope I was able to pass on their wisdom and add a bit of my own to the others working so hard for this final day. Mark Brady, Steve Palm, Weng Ki Ching, Olivier Duchemin and Brad Dooley for their friendship here at Caltech. Finally, I would like to thank my family for all their support over the years; at least now they will stop asking me how my thesis is progressing.

Abstract

Recent advances in technology have opened up a potential market for small gas turbine power systems in the 50-100 MW range. In an effort to improve their systems, the gas-turbine industry is interested in understanding and controlling combustion instabilities as well as reducing pollutant production. To understand the dynamics inherent in a combustion system, information about the flow field behavior is required. Because of a scarcity of available experimental or numerical results for full-scale gas-turbine combustors, we decided to use numerical simulations to provide the required information about the flow field dynamics. The ability of the numerical simulations to reproduce unstable behavior in combustion environments will be presented. The investigation of the flow field dynamics has been conducted for three test cases; a planar heat source in a tube, premixed flow in a dump combustor, and premixed and diffusion flames in a full-scale gas turbine combustor. The numerically determined unsteady acoustic modes will be shown to compare well with theory and experiments. An investigation of the local heat release response to an unsteady flow field is conducted for incorporation into an approximate analysis method. The results of including a Helmholtz resonator in a dump combustor as a passive control mechanism will be presented. The production of NOx and CO will be compared between stable and unstable flow configurations. The pollutant results indicate that for the planar flame in a tube and the dump combustor, the NOx levels at the exit plane are reduced when the system is unstable.

Table of Contents

List of Figures

Chapter One

Introduction

1.1 Current Research

Power production facilities have evolved over the years. In the past, in order to reduce the operating cost per Megawatt of power, power production facilities utilized larger and larger power output devices. By the 1980's, this resulted in an optimal plant size in the 1000 MW capacity range (Bayliss, 1994). However, in the 1990's, advanced technologies in small gas turbine systems in the 50-100 MW range have reduced the cost per MW below that of the large power generation plants. This shift in optimization has opened up a potential market for small, pre-constructed, relatively portable gas-turbines. This potential market includes small communities and manufacturing plants that do not have the resources or the need to purchase a high production power plant. Because of this renewed interest in the small gas turbine market, increased funding has been made available for the research and development of such systems. The main concerns are reduced pollutant emissions and improved system efficiency.

Current experimental work with gas turbine combustors is concerned with pollutant emissions (with emphasis on NOx) in various steady state flow configurations (Rizk and Mongia, 1993; Newbury and Mellor, 1995; Leonard and Correa, 1990; Toh and Hosoi, 1994; Sturgess et al., 1993; Joshi et al., 1994; McVey et al., 1993; Nandula et al., 1996) and in the presence of oscillating flow conditions (Keller and Hongo, 1990; Casentini, 1995; Casentini et al., 1997); and control measures for reducing the levels of unsteady combustion (Houpt and Goodman, 1990; Schadow and Gutmark, 1992; Brouwer et al., 1990; Gutmark et al., 1991; Richards et al., 1995; Annaswamy et al., 1998; Torres et al., 1999; Chu et al., 1998). The need to determine NOx levels arises from environmental concerns that have led to increased restrictions on pollutant emissions

of gas turbine systems. In some parts of the world, the new source performance standards (NSPS) have gone below 10 ppm (corrected to 15% O_2) for stationary gas turbines used for electric power generation (Correa, 1992a). The strict regulations have increased efforts by researchers to understand the mechanisms behind pollutant formation. Chapter 6 describes the theory behind the three main NOx production mechanisms. The primary mechanism is the Zel'dovich thermal mechanism in which the level of NOx production is directly tied to the temperature of the combustion region. Therefore, when the flame is burning under stoichiometric conditions, as is the case for diffusion flames, the flame temperature is a maximum and so is the NOx production rate. Figure 1-1 shows a sketch of the relation between the equivalence ratio and the mass fraction of NOx and CO. Premixed flames, on the other hand, can burn under lean (rich) conditions in which the fuel-to-air ratio is lower (higher) than stoichiometric conditions. By burning a premixed flame away from stoichiometric, the flame temperature and the NOx production rate are reduced. However, a system that only burns rich does not use all of the potential chemical energy in the fuel and exhausts unburned hydrocarbons (UHC).

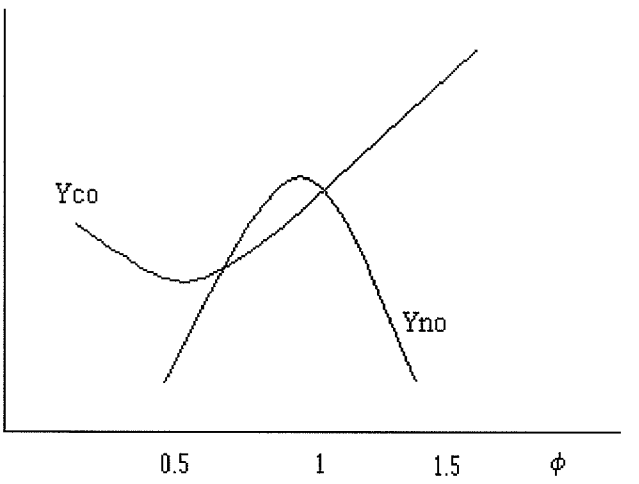

Figure 1-1 Sketch of CO and NOx Mass Fraction Relation to Equivalence Ratio

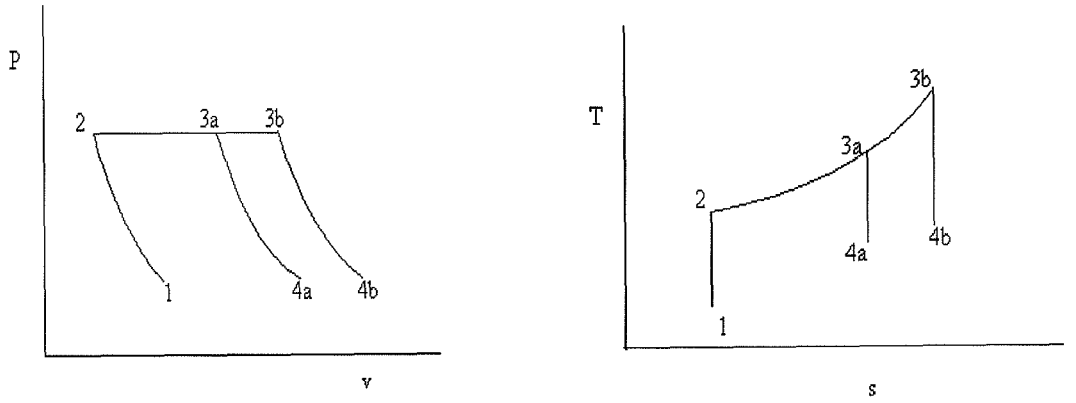

Figure 1-2 P-v and T-s Diagrams for Gas-Turbine Cycle

Two main efforts have been explored to reduce NOx emissions by decreasing the flame temperature: rich burn/ quick quench/ lean burn (RBQQLB), and lean premixed combustion (LPC). The first method uses a rich burn stage, which reduces the flame temperature and the available oxygen, then quenches the flame, and finally burns the remaining fuel under lean conditions. This method has shown promise (Sturgess et al., 1993), but the additional burn stages increase the complexity of the system. Lean premixed combustion only has one burn stage, which keeps the system simple. Recent efforts to examine NOx formation in LPC have been reviewed by Correa (1992b). One of the consequences of LPC is a reduced power density for an individual combustor. Figure 1-2 shows a P-v and a T-s diagram for an ideal gas turbine cycle. Cycle 1-2-3b-4b is for a combustor burning under stoichiometric conditions. The reduction in the fuel-to-air ratio in LPC decreases the maximum temperature in the combustor as represented by the cycle 1-2-3a-4a. In order to maintain the required power density for the system, the gas turbine is designed so the compressor feeds an array of combustion chambers that act in parallel to drive the turbine.

Additional concerns about LPC are being addressed experimentally. The first is the degree of mixing of the fuel and air (Fric, 1993). Since NOx is strongly affected by temperature, any pockets of fuel and air which are richer than the prescribed combustion conditions can lead to local regions of increased temperature and NOx production. Modeling of the mixing within a premixing chamber will be discussed in Chapter 5. Another concern is stabilization of the premixed flame. Some designs, including the gas turbine combustor studied in this thesis, use a central diffusion flame to keep the fresh premixed mixture burning. For the diffusion flame, the air comes from upstream and the fuel is injected at the location of the flame, which does not allow for premixing. However, since the diffusion flame burns under stoichiometric conditions, the central flame burns at a high temperature, which increases the NOx production in this region. Other methods of stabilizing the premixed flame include flow over a dump plane and the use of swirl vanes (Durbin et al., 1994; Feikema et al., 1990). The swirl vanes are also often used within the premixing chambers to improve the mixing properties.

Current research work in the field of LPC (Rizk and Mogia, 1993; Newbury and Mellor, 1995; Leonard and Correa, 1990; Toh and Hosoi, 1994; Sturgess et al., 1993; Joshi et al., 1994; McVey et al., 1993; Nandula et al., 1996) examines steady state or time averaged pollutant levels at a set operating condition. The research is designed to study the pollutant levels in various combustor designs, which might be used within gas turbine combustors. Some effort has been made (Newbury and Mellor, 1995) to develop characteristic time scale models for the NOx production levels that take into account the geometry, the flame structure and the relevant time scales in the combustor. These models would be beneficial in design considerations as a rough estimate of NOx production levels.

A further concern of LPC is that combustion is closer to the lean flammability limit. It has been shown experimentally that as this limit is approached, the flame stability is reduced (Sturgess et al., 1991, 1992; Roquemore et al., 1991). Undesired oscillations in the combustion

chamber can lead to structural damage; system inefficiencies; and varying pollutant levels. In order to reduce the oscillation levels near the lean flammability limit, work has been undertaken to understand how these oscillations develop and interact with the flow field. One of the goals of this thesis is to obtain a clearer look at the details of combustion driven oscillations for lean premixed combustion.

Other experimental work is concerned with the effect of oscillations on the flow structure and on the level of pollutants. The concept of an oscillating flow field is taken to the limit in the operation of pulse combustors. A pulse combustor is designed to set up a pulsing flow, which leads to an oscillating power generation characteristic. There are two types of pulse combustors. The first makes use of a mechanically driven valve to develop the oscillation by pulsing either the flow of fuel or air. The second makes use of the natural acoustic properties of the chamber, along with the heat release, to develop a condition of oscillating flow. The report by J. O. Keller and I. Hongo (1990) provides some results for pollutant emissions in a pulse combustor under pulsing and non-pulsing conditions. The pulsing conditions were developed by the natural resonant acoustics in the chamber and the interaction of the pressure fluctuations with an inlet flapper valve. Significantly lower NOx was expelled at the exit plane under pulsing conditions. The lower NOx output at the exit plane was due to a shorter residence time at high combustion temperatures. The shorter residence time at high combustion temperatures was due to the back flow of the burned products that mixed with the flame and caused a lower average temperature downstream of the flame. The lower average temperature downstream of the flame may have also been caused by an increased heat loss to the walls due to the fluctuations in the boundary layer. This lower average temperature reduced the average amount of NOx produced downstream of the main flame zone. In the non-pulsing case, the temperature remained high downstream of the flame, which kept the production rate high throughout the chamber. Additional work by Casentini et al. (1997) investigated the effect of a forced pulsed air flow rate on the NOx and CO

production in a diffusion flame. The results showed that depending on the pulsation frequency, the NOx levels could be reduced by up to 21% and the CO levels by up to 46%. These results show that a certain level of controlled oscillation might be beneficial to the overall reduction of pollutant levels in some combustor designs.

There have been experimental efforts designed to study the oscillating flow field within a given combustor design and to examine methods for the control of the oscillations. Most of the experimental control work (Houpt and Goodman, 1990; Schadow and Gutmark, 1992; Brouwer et al., 1990; Gutmark et al., 1991; Richards et al., 1995) studied the use of active control techniques, either by the use of actuators or with a secondary fuel source. The active control techniques are designed to sense the state of the system and make use of additional mass, heat or momentum sources to interfere destructively with the acoustic oscillations, leading to a more stable operation. Schadow et al. (1992) have done experimental work examining the relation between the vortex shedding frequency and the level of acoustic instability. The results show that when the vortex shedding frequency is in tune with a main acoustic mode, the instability within the chamber grows due to energy exchange between the vortices and the acoustic oscillations. Schadow and his colleagues are working on techniques for the passive control of acoustic oscillations based on the control of vortex shedding.

In addition to experimental work, numerical simulations are also valuable for the understanding of the behavior of a combustion system. A full numerical simulation should be more flexible than experimental work and provide more detailed information about the flow field, which experimental measurement techniques might not be able to determine. However, the quality of the numerical output is only as good as the models used. A comprehensive theory encompassing large-scale non-uniform motions, small-scale turbulence, detailed finite rate chemistry and interactions between turbulence and chemical kinetics is not available (Correa and Shvy, 1987). Chapter 2 will discuss some of the models proposed to alleviate these deficiencies.

There has been much progress in the area of steady state numerical calculations (Rizk and Mongia, 1993; DiMartino et al., 1994; Dupoirieux and Desaulty, 1995). These steady state results fairly accurately represent actual behavior and they provide a good framework for understanding the complexity of the flow in a given design along with species and heat release levels.

Numerical efforts to determine the production of NOx have mainly used methods involving perfectly stirred reactor (PSR) or plugged flow reactor (PFR) elements (Glarborg et al., 1986; Steele et al., 1996; Mellor, 1996). These methods involve dividing the combustion regime into regions that can be represented locally by a single PSR or PFR element. Complex chemical mechanisms are then used to calculate species levels within these elements based on generalized information on the local flow field. This technique is mainly useful for steady state calculations to obtain a general understanding of the reaction behavior in combustion chamber designs. An effort has been made to use these steady state results as the basis for algebraic functions relating the NOx levels to the pressure, temperature and time scales within the chamber (Steele et al., 1996; Mellor, 1996). Additional work has been initiated (Feitelberg, 1995) to examine the pollutant levels in a single PSR element under oscillating conditions. However, this numerical method involves the assumption of quasi-static behavior since it does not take into consideration the dynamical behavior of the full flow field in the presence of oscillations.

There is also numerical work devoted to the behavior of transient flows. Some work has been done which examines the flow field and the vortex dynamics within a given combustor (Kailasanath et al., 1991; Benelli et al., 1993; Liu and McGuirk, 1995; Menon and Jou, 1991). This information can be useful in understanding how the flow field dynamics might interact with the acoustic field in the development of instabilities. There has been some work on the simulation of oscillating combustion conditions, including the examination of pulse combustors (Benelli et al., 1993) and the interaction between vortex dynamics and the oscillating pressure field (Menon and Jou, 1991).

These simulations of transient reacting flows can provide valuable information on the structure of the heat release field and the interaction with the acoustics. The transient simulations can provide more details about the stability behavior of the acoustic modes. These details include linear growth or decay rates and phase differences between the frequency modes. The results can also be used to determine where the unsteady heat release may be driving or damping a given acoustic mode. This thesis will extend this work by examining how the numerical simulations can provide the necessary information about the unsteady flow field to develop models for the unsteady heat release. These models will be beneficial in application of the approximate analysis method that will be detailed in Appendix C.

1.2 Approximate Analysis of Combustion Instabilities

Due to the high-energy production densities in combustion chambers, and to the relatively low losses for unsteady motions in the flow, the problem of instabilities - generically called 'combustion instabilities' - has been observed in all types of propulsion systems and stationary power plants. Analyses have been carried out at various levels of complexity and with varying degrees of success. Much of the early work on the problem dealt with liquid and solid propellant rockets and ramjets. The development of the linear and nonlinear theory to explain the interactions within an unstable flow field was primarily based on experimental results. It was this theory along with numerous experimental firings that led to the passive control techniques (e.g., baffles, acoustic liners) for various liquid rockets including the F-1 engine used in the Apollo program.

The initial work on combustion instabilities examined linear interactions in a combustion system. This work was mainly concerned with the linear damping or production of the primary acoustic mode of the system. The work served as an impetus for passive control techniques, but it was not always accurate. It neglected other modes in the system and the response of various

factors to the combustion process. The analysis of combustion instabilities was extended to include nonlinear interactions by Sirignano (1964) and Sirignano and Crocco (1964) who first accounted for some of the possible influences between combustion and the flow field. However, this analytical work was limited to the consideration of periodic solutions and could only be used to study a single longitudinal acoustic mode.

In the early 1970's, Zinn and his students (Zinn and Powell, 1970; Zinn and Lores, 1972; Lores and Zinn, 1973) and independently Culick (1971, 1976) began to use a form of Galerkin's method, which is a special application of the method of weighted residuals, to investigate combustion instabilities. The classical Galerkin method has simple boundary conditions. However, combustion instability problems require complicated boundary conditions. For this reason, the classical Galerkin's method is modified so that the dependent variables are expanded in trial functions that do not satisfy the boundary conditions of the problem. The details of this approximate analysis will be presented in Appendix C. The advantages of this approach are: 1) spatial averaging allows the incorporation of realistic models for all processes; and 2) the analysis reduces the partial differential equations to a series of ordinary nonlinear differential equations. Time averaging can also be applied to this method to simplify the analysis further.

The approximate analysis is developed from a perturbation expansion of the conservation equations of mass, momentum and energy. This expansion leads to kinetic terms that are directly determined by the flow field variables and source terms including two-phase flows, noise sources and heat release which are not so easily represented by flow field variables. These additional source terms need to be modeled so they can be included in the approximate analysis to represent the important contributions to the system stability. It should be mentioned that the term 'models' will be used in two differing manners in the course of this thesis. The first definition relates to the 'reduced models' that are developed to describe the various systems in a given configuration for use in control analysis. The second meaning will be used to explain the development of

simplified equations representing flow field interactions for use in numerical simulations and for application in the approximate analysis.

The two-phase flow source terms will not be discussed in this thesis because the combustion simulations presented will involve pre-vaporized fuel injection. As mentioned in Section 1.1, since NOx is dependent on temperature, LPC is being explored as a means for pollution reduction. When pre-vaporized fuel is injected, the mixing effectiveness of the fuel and air is not dependent on droplet vaporization and there is no opportunity for stoichiometric burning in the vicinity of liquid fuel droplets. The noise source terms will be mentioned in regard to a more realistic representation of the stochastic behavior in a combustion system for the approximate analysis, but they will only be mentioned for completion of the proposed methodology. The main source term, which will be examined in the approximate analysis as part of this thesis, is the heat source term due to chemical reactions and convective heat release.

Most of the past efforts in the development of heat release models for use in the approximate analysis have been for solid and liquid rocket motors (Harrje ed., 1972). That kind of modeling is also described by the term 'combustion response' modeling because the main point of interest is how the burning surface of the solid propellant responds to the fluctuations in the flow field. These combustion response models are usually *ad hoc* formulas based partly on a relatively simple theory and partly on experimental results of burning rates in the presence of instabilities. Those formulas provide a means of including additional source terms in the approximate analysis, but the formulas are often deficient in that they do not properly model the interaction between the gas dynamics and the combustion field. A similar effort in modeling the combustion response in a gas turbine combustor will be important for design considerations and control efforts, based on how the heat release might impact the stability of a given combustor design.

1.3 Technical Problems

The gas turbine industry is interested in a basic understanding of the interaction between the combustion process and the flow field. This information would be valuable in the design process for new combustors and in the analysis of control measures to help stabilize undesired oscillations. Simplified heat release models would aid both of these efforts. However, unlike the stability work performed for solid propellant rockets, there is little experimental data available concerning the details of unstable gas turbine operation. Due to fierce competition in the current gas turbine industry, much of the experimental work is proprietary. Even if this data were available, it would be hard to find cases with enough information about the central reaction zone and the interaction of various flow properties to develop combustion response models. For this reason, numerical simulations have become increasingly attractive. Numerical simulations are conceivably more flexible for design considerations and can provide more detailed information about the flow field variables during steady or unsteady combustion.

The work presented in this thesis will make use of numerical simulations as a means of providing information about the flow field and the heat release, which can then be used to develop models for the approximate analysis. This thesis is not intended to discuss a novel numerical approach applied to a known combustion configuration. We will make use of a commercially available numerical code, ANSWER, developed by ACR, Inc., for the simulation of the combustion field. The simulation will solve for the complete kinetics and will use the k-ε turbulence model, described in Chapter 2, to account for the Reynolds stress terms. The chemical reactions will be modeled by a reduced mechanism for a methane and air flame. The method for the development of combustion response models will be described in Appendix C. The results for the Rijke tube configuration will be used to suggest a time delay model between the fluctuating heat release and velocity.

A possible drawback of relying on numerical simulations to develop heat release models is that the results may be too problem specific. Eventually a theoretical basis is necessary for global heat release models. As a first step towards this end, theoretical relationships for the heat release term in the energy equation will be investigated. These relationships will involve different theoretical models for the flame structure and chemical reactions, including the species conservation equations and the Arrhenius forms of the reaction rates. This work will be presented in Chapter 6.

Besides information on the interaction between the flow field and the heat release, the numerical simulations can provide valuable information about the acoustic field in a given combustor design. Knowledge of the acoustic mode shapes and the steady state regions of heat release can be beneficial for determining what modes might be unstable during operation. This information can be useful in design considerations and for examination of possible means of active or passive control. The acoustic field can be determined theoretically from the geometry and mean temperature field in a given combustor configuration as summarized in Appendix A. Appendix B summarizes another method for determining the theoretical acoustic modes for a one-dimensional approximation and a single step change in temperature. However, it is often difficult to obtain experimentally a detailed temperature field in a gas turbine combustor. To rectify this problem, numerical simulations can be used to provide a good representation of the temperature field in steady state operation. The acoustic frequencies and mode shapes can be determined more directly with a numerical simulation of the transient behavior in a given combustor. Numerical simulations of the transient behavior in a closed configuration containing a stationary non-reacting flow can provide information on the main acoustic frequencies and the linear damping rates without the presence of a driving mechanism. Also, numerical simulations of the full reacting flow configurations can provide information about the acoustics within the chamber and

some information about the growth rates of the primary acoustic modes. These results will be examined in Chapters 3, 4 and 5.

As mentioned earlier, in an effort to reduce NOx production in gas turbine combustors, there is interest in lean premixed combustion. In laboratory combustors, the fuel and air often has a long time to mix before reaching the flame. However, in practice, the premixing section of the combustor is short. It has been shown experimentally that ineffective mixing can lead to increases in the NOx production (Fric, 1993). To increase the mixing effectiveness, some systems have a swirl component and the pre-vaporized fuel is injected with high velocity driven by a large back pressure. Those methods may increase the level of mixedness, but the large back pressure in the fuel stream may also impact the stability of a given combustor design. Because of the high back pressure, any pressure fluctuations within the premixing chamber will impact the air flow rate to a greater extent than the fuel flow rate, leading to a fluctuation in the overall stoichiometry of the flow. This fluctuation in stoichiometry will lead to a fluctuation in the heat release and the NOx production. Depending on the convection time to the flame front, this fluctuation in heat release may lead to a driving or damping of the pressure oscillation. This behavior will be explored in more detail in Chapter 5 as part of an investigation of the behavior in the premixing chamber of a full-scale gas turbine combustor.

In addition to information about the oscillating heat release and the acoustic field, numerical simulations can also provide valuable information about the chemical kinetics in the presence of an oscillating combustion field. The formation of pollutants under unsteady conditions can be examined and better understood in all regions of a combustion chamber. Previous numerical methods used detailed chemistry and simple geometry methods with PSR and PFR elements to investigate the behavior of the unsteady pollutant production. However, these methods are only quasi-steady representations of the effects of oscillations and do not effectively consider the coupling with the dynamic flow field. The full simulations presented in this thesis do

not involve detailed chemistry, but do treat accurately the influences of the unsteady flow field. Those results will be shown in Chapter 4 and discussed in more detail in Chapter 6.

1.4 Summary

Chapter 2 will consist of a summary of numerical methods available for the simulation of combustion chambers. The summary will include details concerning the modeling of turbulence, chemical reactions and their interactions. The next three chapters will present the results for simulations of the steady state and transient behavior within three combustor configurations: a Rijke tube with an anchored premixed flame and a constant planar heat source; a dump combustor with a premixed flame; and a full-scale gas-turbine combustor with a central diffusion flame which sustains the surrounding premixed flame. Acoustic information along with analysis of the steady and unsteady heat release will be examined in all three cases. The influence of the mass flow rate and the equivalence ratio will be explored in Chapter 4 along with the use of a Helmholtz resonator as a means of passive control. The mixing behavior in the gas turbine combustor will be discussed in Chapter 5, producing a possible heat release model coupling the pressure oscillation with the mixing. Chapter 6 will discuss in more detail the local and global influences of unsteady combustion on the production of pollutant species, with emphasis on NOx and CO. Results from the numerical simulations will be examined to determine how pollutant levels change with fluctuations in the flow field. Chapter 6 will also initiate analysis of theoretical heat release models based on the species conservation equations. Appendix C will describe the basis for the approximate analysis and discuss the development of heat release models based on the numerical simulations.

The results of this work demonstrate the ability of numerical simulations: to determine the proper acoustics in a given combustor design; to develop heat release models; and to capture the behavior of chemical reactions in the presence of oscillations. This thesis will show that the

heat release models developed from the numerical simulations are very detailed, but possibly too problem-specific. Other theories for flame behavior, as discussed in this thesis, should provide a means towards the development of more global heat release models. The thesis will also initiate an investigation of the mixing effectiveness in a gas turbine premixing chamber and examine how an unsteady pressure field might interact with the fuel and air streams to produce an oscillating fuel-to-air ratio. This interaction, which is strongly dependent on the distance between the injector and the flame front, may play a large factor in the unstable nature of some combustor designs and may lead to higher than expected levels of pollutant production. This thesis will examine the effects of a Helmholtz resonator on the passive control of oscillations in a dump combustor and the effects of an unsteady flow field on the production of NOx and CO.

Chapter Two

Numerical Methods for Modeling Chemistry, Turbulence and Acoustic Waves

This chapter will review modeling methods used for the numerical simulation of chemically reacting, turbulent flows. The emphasis will be on the abilities of the commercially available code ANSWER used for the simulations in this thesis. Additional computational methods will be presented to complete a summary of the available models. The last section will discuss some of the concerns of numerically representing the acoustic field in a transient flow field. The ability of ANSWER to properly determine the acoustic frequencies and damping rates for unsteady motions in a combustion chamber will also be examined. It should be emphasized that the purpose of this thesis is not to develop numerical methods, but to use an existing code that uses the below methods for the investigation of certain applications surrounding combustion instabilities.

2.1 Flow Solvers

As computational ability has increased over the years from the early calculating machines, so has research into better methods for computational fluid dynamics. Those efforts have improved the accuracy and speed of numerical simulations as they are applied to realistic flow configurations.

The numerical methods described in this section are intended for application to the Navier-Stokes equations:

$$\frac{\partial \rho}{\partial t} + \nabla \cdot (\rho \vec{u}) = 0 \qquad (2\text{-}1a)$$

$$\frac{\partial(\rho\vec{u})}{\partial t}+\nabla\cdot(\rho\vec{u}\vec{u})=-\nabla p+\nabla\cdot\vec{\vec{\tau}}+\vec{F} \tag{2-1b}$$

$$\frac{\partial}{\partial t}\rho\left(e+\frac{u^2}{2}\right)+\nabla\cdot\rho\left(e+\frac{u^2}{2}\right)\vec{u}=Q+\vec{u}\cdot\vec{F}-\nabla\cdot p\vec{u}-\nabla\cdot\vec{q}+\nabla\cdot\vec{\vec{\tau}}\vec{u} \tag{2-1c}$$

For ideal gases the pressure is related to the density and temperature through the equation of state, $p = \rho RT$.

Most of the flows in gas turbine combustors are low-speed and nearly incompressible, i.e., negligibly small changes of density associated with changes of velocity and temperature. The only real changes in the density are due to chemical reactions and the changing species levels. There are two main schools of thought on solving for low-speed incompressible flows. The first involves solving the set of uncoupled incompressible equations directly. The second involves implementing a compressible flow solver with an artificial compressibility term to solve for the pressure using the mass continuity equation.

2.1.1 Incompressible Flow Solvers

An incompressible flow solver starts from the assumption that the density is fixed. Equation (2-1a) reduces to $\nabla\cdot\vec{u}=0$, which acts as a constraint on equation (2-1b). One possible method for the solution of the pressure involves a time-independent equation. The pressure is determined by solving the following equation obtained as the divergence of the momentum equation:

$$\frac{1}{\rho}\nabla^2 p=-\nabla\cdot(\vec{u}\cdot\nabla)\vec{u}+\nabla\cdot\vec{F}+\nabla\cdot\left(\nabla\cdot\vec{\vec{\tau}}\right) \tag{2-2}$$

The solution methods available for solving equation (2-2) are not as stable numerically as methods that include a time derivative term, and can lead to simulations that either converge slowly or not at all. For this reason, most modern codes do not use equation (2-2), but instead use a modified

continuity equation for the determination of the pressure (Chorin, 1967). A description of this form will be discussed in more detail in Section 2.5. Also for incompressible flows, if the system is isothermal, the momentum equations uncouple from the energy equation. A review of some of the numerical methods available for the solution of the incompressible system of equations can be found in the work by Hirsch (1988) and Oran and Boris (1987).

The ANSWER code makes use of an implicit finite difference method for solution of the conservation equations. Depending on the location of the grid node, the code uses either a fully implicit central method or a fully implicit upwind method. The code uses an alternating direction implicit (ADI) method to account for the gradients in multiple directions. There are other difference methods and solvers available with the standard ANSWER package, but the simulations in this thesis only use the methods mentioned. To step towards a solution, the uncoupled conservation equations are solved implicitly along one axis direction and the solution is used to solve additional implicit equations along the other axis directions. For the incompressible steady state solutions, the Chorin (1967) decomposition method for the continuity equation is used to determine the pressure. However, this incompressible solution method cannot properly describe acoustic waves. Section 2.5 discusses how the incompressible method used in the ANSWER code is adjusted to account for the compressibility effects, acoustic behavior and artificial viscosity.

One point about the energy equation used by ANSWER needs to be made at this time. The variable of choice for the energy equation is the enthalpy, which as a matter of convenience for the ANSWER code contains the enthalpy of formation values. The original form of the equation therefore was:

$$\rho\frac{\partial}{\partial t}h+\rho\vec{u}\cdot\nabla h=-\nabla\cdot\vec{q}+\vec{\vec{\tau}}\cdot\nabla\vec{u} \qquad (2\text{-}3)$$

whereas the theoretical form for the enthalpy, without the inclusion of the formation enthalpy values is:

$$\rho\frac{\partial}{\partial t}h+\rho\vec{u}\cdot\nabla h=\frac{\partial p}{\partial t}+\rho Q-\nabla\cdot\vec{q}+\vec{\vec{\tau}}\cdot\nabla\vec{u}+\vec{u}\cdot\nabla p \qquad (2\text{-}4a)$$

and $Q = -\frac{\partial}{\partial t}\sum_i Y_i h_{f_i}^{o}$, is the heat release due to chemical reaction. The original form of the equation used by ANSWER was therefore missing the $\partial p/\partial t$ and $\vec{u}\cdot\nabla p$ terms. Because we are interested in the coupling between the heat release and the pressure, these terms were added back into the ANSWER code. By including the formation enthalpy in the enthalpy term, the ANSWER code incorporated the Q term into the left-hand side of the equation. However, the total derivative, D/Dt, of the formation enthalpy leads to an additional term on the left-hand side of the equation that is not matched on the right-hand side. To accommodate this term, the function $\rho\vec{u}\cdot\nabla\sum_i Y_i h_{f_i}^{o}$ was added to the right-hand side of the equation in the code, giving:

$$\rho\frac{D}{Dt}\left(h+\sum_i Y_i h_{f_i}^{o}\right)=\frac{\partial p}{\partial t}-\nabla\cdot\vec{q}+\vec{\vec{\tau}}\cdot\nabla\vec{u}+\vec{u}\cdot\nabla p+\rho\vec{u}\cdot\nabla\sum_i Y_i h_{f_i}^{o} \qquad (2\text{-}4b)$$

2.1.2 Compressible Flow Solvers

Compressible flow simulations are formulated in a different manner, taking into consideration the entire coupled set of equations. The first order partial differential equations are put in the form of a hyperbolic system:

$$\frac{\partial U}{\partial t}+\frac{\partial}{\partial x}F(U)=S \qquad (2\text{-}5)$$

where $U = (\rho, \rho u, e)^T$, $F(U) = (\rho u, p+\rho u^2, (p+e)u)^T$ and S is the source term. The compressible solvers then solve for the U matrix via Riemann solvers which make use of the eigenvalues of the given set of equations to step through time. In these methods, the time step is used for marching towards a steady state solution. For transient simulations, a secondary time step needs to be included in the solution to take into consideration the real time dependent behavior.

The eigenvalues for the set of equations in (2-5) are u, u ± a. For flows near the transonic regime, these eigenvalues are of the same order and provide good stability. However, for low speed flows, the technique often experiences difficulties due to the large variations between the eigenvalues. A preconditioning technique has been developed to help fix this problem and to allow the numerical methods developed for compressible flows to be used for incompressible flows (Chorin, 1967; Merkle and Choi, 1988; Choi and Merkle, 1993). The technique makes use of an artificial compressibility parameter to couple the pressure variation with the density. A perturbation expansion in the parameter γM^2 can be applied to the conservation equations. Grouping the terms in the momentum equation according to like powers of M^2 leads to a zero-order pressure term, p_o, which is independent of space. This term can be assumed constant in the system. Therefore, the pressure variation is related to the first-order pressure term, or gage pressure, $p_g = p_1$. This first-order pressure term, along with the artificial-compressibility parameter, β, replaces the density in equation (2-1a):

$$\frac{1}{\beta}\frac{\partial p_g}{\partial t} + \nabla \cdot \rho \mathbf{u} = 0 \tag{2-6}$$

The inclusion of the artificial-compressibility parameter changes the eigenvalues for the system of equations (2-5) from u, u ± a to:

$$u,\ u/2 \pm \sqrt{(u/2)^2 + \beta(\mathbf{S}\cdot\mathbf{S})} \tag{2-7}$$

where **S** is the directed surface area at the interface of the grid cells. The variations between the eigenvalues in a low-speed flow are smaller than the differences between u, u ± a and therefore the stability of the numerical solution is improved.

2.2 Modeling Chemical Reactions

The addition of conservation equations for individual species to the numerical simulation creates another level of complexity. Each of the species, having concentration $Y_i = \rho_i/\rho$, is described by the equation:

$$\rho\frac{\partial Y_i}{\partial t}+\rho\mathbf{u}\cdot\nabla Y_i=\nabla\cdot\left(\rho\mathcal{D}\nabla Y_i\right)+w_i \tag{2-8}$$

assuming Fick's law with the diffusion coefficient, $\mathcal{D}$, as a scalar here. The diffusion coefficient is equal to the viscosity multiplied by the Schmidt number for the specified species. For ANSWER, the diffusion coefficient is the sum of the laminar and turbulent diffusion terms. The source term in equation (2-8) is the reaction rate w_i. The reaction rate is commonly represented by the Arrhenius model:

$$w_i = AT^kP^n\exp(-T_a/T)[\text{oxidizer}]^a[\text{reactant}]^b \tag{2-9}$$

where A is a constant, T_a is an activation temperature and the oxidizer and reactant are the concentrations of species involved in the described reaction.

Including all of the species and reactions for a given reaction system is computationally expensive. For example, the Miller-Bowman mechanism for methane reacting with air, including NOx production, has 46 species and 212 reactions (Miller and Bowman, 1989). Modeling the complete mechanism requires the solution of 46 additional conservation equations at every point in the flow. For a basic 2-D laminar system, the 46 conservation equations would need to be solved in addition to the conservation equations of $\vec{u}$, p, and T which would require 10 times as much computational space and time. This does not include the extra time needed to code in the properties of the 212 reaction rates. To lessen the computational expense of a complex chemistry simulation, reduced mechanisms have been developed to describe the global combustion behavior while sacrificing information about the minor species.

Reduced mechanisms, which usually involve less than ten species, are developed by adjusting the parameters in (2-9) to match temperature, species and velocity values obtained from experimental results and full-scale numerical chemistry calculations. The reaction rates are adjusted for a limited number of reactions in order to approximate the real chemical behavior. For the development of these reduced mechanisms, information on the relevant reactions for a given set of flow parameters is important. The Computational Singular Perturbation (CSP) method (Lam and Goussis, 1994; Hadjinicolaou and Goussis, 1999) has been proposed as a method to identify the important reactions for a given system. The CSP method orders the time scales of the various chemical reaction mechanisms and uses this information, along with information about the flow field, to identify the important reactions within a given system. Since it is not an aim of this thesis to construct reduced chemical mechanisms, but to use them for numerical simulations, this method is not pursued.

The results that will be presented in later chapters make use of two different reduced mechanisms. The first is a 4-step mechanism for C_nH_m based on propane oxidation (Hautman et al., 1981). The second is a 3-step mechanism specifically tuned for methane combustion at pressures near 14e5 Pa. Dr. Malte, of the University of Washington (1996), provided this mechanism. In order to make a qualitative examination of the influence of pressure instabilities on the production of NO, an additional NO reaction rate, based on equilibrium conditions (Bowman, 1975), is added to the 3-step methane mechanism for results shown in Chapter 6.

2.2.1 Single Scalar Chemistry Models

Other models have been developed to reduce the chemistry detail even further. The single scalar models described below have been reviewed with example simulations by Khalil (1982). For diffusion flames, the flame region can be assumed to be single step, irreversible, infinitesimally thin, so that fuel and oxidant do not co-exist anywhere, and the reaction rate infinitely fast. The

assumption is also made that the chemical reaction rate is frozen everywhere except at the flame sheet. The flame sheet occurs where the fuel-to-air ratio is stiochiometric. The assumption of a frozen chemical reaction rate was found to be unrealistic in diffusion flames and so changes were made to account for the co-existence of reactants in the model. The relevant parameter in this model is the mixture fraction, f. The flame region is broken up into two sections, as shown in Figure 2-1. For $0 < f < f_{st}$,

$$Y_{fu} = 0$$
$$Y_{ox} = Y_{ox_A}\left(1 - \frac{f}{f_{st}}\right) \tag{2-10}$$

where Y_{oxA} is the initial mass fraction of the air and f_{st} is the stoichiometric mixture fraction. For $f_{st} < f < 1$,

$$Y_{ox} = 0$$
$$Y_{fu} = Y_{fu_F}\left(\frac{f - f_{st}}{1 - f_{st}}\right) \tag{2-11}$$

where Y_{fuF} is the initial mass fraction of fuel. The mass fraction of the products is given by:

$$Y_{pr} = 1 - Y_{ox} - Y_{fu} \tag{2-12}$$

This method is interested in closely modeling the temperature and density gradients in the main flame zone and the expense of details about intermediate species such as CO, NO and H_2O.

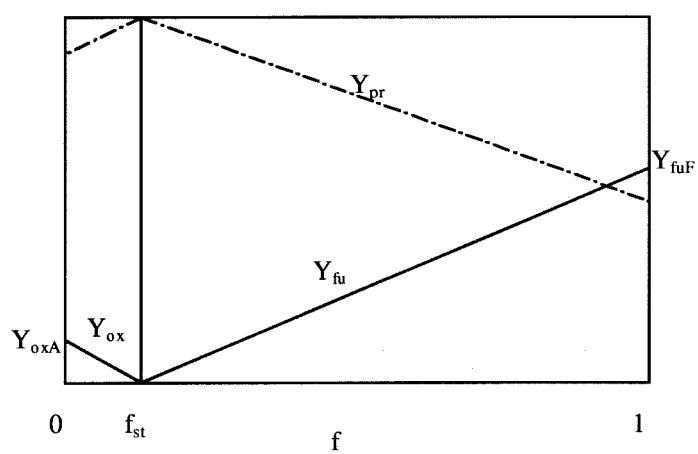

Figure 2-1 Relation between f and Scalar Variables in Flame Region

A single scalar model can also be used for premixed flames. An example of this is the statistical turbulent flame model of Bray and Moss (1977). The single scalar, c, represents the mass fraction of the products. The mass fraction is 0 upstream of the flame and 1 downstream of the flame. The distribution within the flame is defined by the probability density function f(c), which is an empirical input into the model. The form of the function f(c) depends on the dimensionless ratios l_{lam}/l and S_{lam}/u'_{rms}, where l_{lam} and S_{lam} are the undisturbed laminar flame thickness and flame speed at a given temperature, and l and u'_{rms} are a characteristic length scale and velocity of the turbulence. A sketch of a typical wrinkled premixed laminar flame profile is shown in Figure 2-2. As with the single scalar diffusion flame model, the model is mainly concerned with proper determination of the temperature and heat release profiles of the flame and does not determine detailed information about individual chemical species.

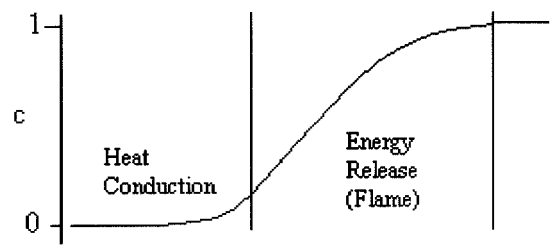

Figure 2-2 Sketch of Single Scalar Behavior in Premixed Flame

2.2.2 Characteristic Time Models and Perfectly Stirred Reactor Models

For simplified design considerations, analytical relations for some of the minor pollutant species (NO, CO) are being developed based on experimental results by a group at Vanderbilt University (Newburry and Mellor, 1995b, 1995c; McDonald and Mellor, 1995). Characteristic Time Models (CTMs) are developed that take into consideration various geometrical and residence time information for a given system. The models have shown some success in collapsing the data for different combustor designs depending on the exact time and length scales chosen. Knowledge

of the important length scales and residence times as they relate to pollutant levels can be beneficial in the early stages of combustor design to make educated estimates of the pollutant levels and to determine how sensitive these levels are to variations in the design.

Another way to reduce the complexity of complete numerical simulations involves simplifying the geometrical detail while retaining all of the detailed reactions. This is the basis of PSRs (Perfectly Stirred Reactors) and PFRs (Plug Flow Reactors) (Glarborg, Miller and Kee, 1986). The results from the numerical simulations and experimental results provide guidelines as to how the combustion chamber can be broken up into elements that approximate different flame zones. This division of the chamber into regimes of PSR and PFR elements is useful for investigating the overall chemical production in the context of an extremely simplified form of the complex flow field. This work has been useful in the determination of pollutant emissions where conventional experimental methods might not be available, for example in the main flame zone of a gas-turbine combustion chamber (Steele et al., 1997; Tonouchi et al., 1998).

Most applications of the PSR and PFR elements involve steady state calculations of the species field. While these results are important, they are not representative of species level behavior in the presence of nonlinear oscillations and noise. It was for this reason that Feitelberg (1995) began work to impose an oscillating condition onto a PSR element to determine how the pressure, temperature and species mass fractions were coupled together. The results showed an increase in the average amount of NOx produced under oscillating conditions. Since a PSR was used, the simulation modeled instantaneous mixing in what might be considered the main flame zone. Due to the exponential dependence of the NOx production rate on the temperature field, it should be no surprise that an oscillating temperature field with a constant amplitude $|T'|$ led to an increase in the average NOx levels.

This work with PSRs and PFRs will be examined in more detail in Chapter 6 along with a more basic calculation of NOx production in the presence of an unstable flow field. However, it

should be noted that there are deficiencies with using PSRs and PFRs for transient simulations at this time (Swenson, Pun and Culick, 1996). The models do not accommodate dynamic behavior in a rigorous way. The oscillations are applied in a quasi-steady manner. Also, a real nonlinear oscillating flow will impact the geometry of the flame and residence times which a set PSR-PFR system will not be able to compensate for.

2.2.3 Modeling Chemical Reactions in ANSWER

The reduced order chemical mechanisms used in this thesis were chosen to provide some detail concerning the chemical reactions, as opposed to the single scalar method, without including the full detail, as in the case of PSR and PFR modeling. The most important aspect of the studies described here is the flow field behavior. The effects on the reaction rates are important, but not required in such detail as to increase the complexity of the system by including a more detailed mechanism. The mechanism provided by Malte was evaluated using steady state values for the flow field within the high pressure gas turbine combustor modeled in this thesis; hence, it should best represent the methane reaction rates at the high pressure for this design. The ANSWER code used a maximum of eight species (CH_4, CH_2, CO, CO_2, H_2O, H_2, O_2 and N_2) for the chemical reactions. The Arrhenius chemistry model was used for the determination of the reaction rates and the 4-step mechanism is given by

$$CH_4 \rightarrow CH_2 + H_2 \qquad r_1 = 20893\times10^{18}\exp(-24800/T)\,[Y_{CH4}]^{0.5}[Y_{O2}]^{1.07}[Y_{CH2}]^{0.4} \qquad (2\text{-}13a)$$

$$CH_2+\tfrac{1}{2}\,O_2\rightarrow CO+H_2 \qquad r_2 = 50.117\times10^{18}\exp(-25000/T)\,[Y_{CH2}]^{0.9}[Y_{O2}]^{1.18}[Y_{CH2}]^{-0.37} \qquad (2\text{-}13b)$$

$$CO + \tfrac{1}{2}O_2 \rightarrow CO_2 \qquad r_3 = 39.811\times10^{18}\exp(-20000/T)\,[Y_{CO}]^{1.0}[Y_{O2}]^{0.25}[Y_{H2O}]^{0.5} \qquad (2\text{-}13c)$$

$$H_2 + \tfrac{1}{2}O_2 \rightarrow H_2O \qquad r_4 = 3.3113\times10^{18}\exp(-24800/T)\,[Y_{H2}]^{0.85}[Y_{O2}]^{1.42}[Y_{CH2}]^{-0.56} \qquad (2\text{-}13d)$$

2.3 Turbulence Modeling

Another area which is of major concern is the modeling technique used to approximate the turbulence for a given flow system. Direct Numerical Simulations (DNS) solve the time dependent conservation equations for a given system and resolve the full range of relevant turbulent scales. However, to include all of the relevant turbulent scales, the computational region must be big enough to include the largest scales, and the mesh spacing must be fine enough to include the smallest scales of importance. These simulations are computationally expensive, and for this reason most of the DNS have been for low Reynolds number flow configurations. The low Reynolds number simulations have been useful as a check for other turbulent models (Givi et al., 1990; Madina, Frankel and Givi, 1991; Miller et al., 1993). This section will describe some of the basic details relating to turbulence models used as alternatives to DNS: Reynolds stress models; the k-ε model; and LES (Large-Eddy Simulations). It should be noted that this thesis is not trying to cover the entire subject of turbulence modeling, but the thesis is trying to convey the main ideas with some examples.

The way many computational methods are configured, the flow field variables are either time-averaged or mass-averaged. For time-averaging, the sum of the mean and the fluctuating values are substituted for the flow variables (e.g., $u = \bar{u} + u'$) and the entire conservation equation is averaged over time. Time-averaging leads to density-velocity correlation terms, $\overline{\rho' \mathbf{u}'}$, in the continuity equation (2-1a) and the momentum equation (2-1b), as well as turbulent stress terms, $\overline{\mathbf{u}' \cdot \mathbf{u}'}$, and triple correlation terms, $\overline{\rho' \mathbf{u}' \cdot \mathbf{u}'}$, in the momentum equation (2-1b), that cannot be directly calculated from the primitive variables. The triple correlation terms are always assumed to be negligible. The density-velocity correlation terms can be modeled or removed from the equation with the use of mass (or Favre) averaging. In both the time-averaged and mass-averaged set of

equations, the turbulent stress terms must be modeled. If we take into consideration mass-averaging, $\tilde{u} = \overline{\rho u}/\bar{\rho}$ with $u = \tilde{u} + u''$, then the stress term is:

$$\nabla \cdot \left(\overline{\rho \mathbf{u}''\mathbf{u}''}\right) = \nabla \cdot \left(\bar{\rho}\,\tilde{\mathbf{u}''\mathbf{u}''}\right) \tag{2-14a}$$

which can be broken up into a deviatoric and a spherical part:

$$\bar{\rho}\,\tilde{\mathbf{u}''\mathbf{u}''} = \bar{\rho}\left[\underbrace{\tilde{\mathbf{u}''\mathbf{u}''} - \frac{\tilde{\mathbf{u}''\cdot\mathbf{u}''}}{3}}_{\text{Deviatoric}} + \underbrace{\frac{\tilde{\mathbf{u}''\cdot\mathbf{u}''}}{3}}_{\text{Spherical}}\right] \tag{2-14b}$$

Following the Boussinesq (1877) analogy for turbulent stresses, this can be simplified as:

$$\begin{aligned} -\bar{\rho}\left[\tilde{\mathbf{u}''\mathbf{u}''} - \frac{\tilde{\mathbf{u}''\cdot\mathbf{u}''}}{3}\right] &= 2\mu_t\left[\frac{\nabla\tilde{\mathbf{u}} + (\nabla\tilde{\mathbf{u}})^T}{2} - \frac{1}{3}(\nabla\cdot\tilde{\mathbf{u}})\bar{\bar{I}}\right] \\ -\bar{\rho}\left[\frac{\tilde{\mathbf{u}''\cdot\mathbf{u}''}}{3}\right] &= -\frac{2}{3}\bar{\rho}k\bar{\bar{I}} \end{aligned} \tag{2-15}$$

where μ_t is the turbulent viscosity and k is the turbulent kinetic energy. These relations can then be substituted back into the averaged momentum equation through:

$$\nabla \cdot \left(\overline{\rho \mathbf{u}''\mathbf{u}''}\right) = \nabla \cdot \left\{-2\mu_t\left[\frac{\nabla\tilde{\mathbf{u}} + (\nabla\tilde{\mathbf{u}})^T}{2} - \frac{1}{3}(\nabla\cdot\tilde{\mathbf{u}})\bar{\bar{I}}\right] + \frac{2}{3}\bar{\rho}k\bar{\bar{I}}\right\} \tag{2-16}$$

which makes use of the primitive averaged values of the velocity along with the scalar terms, μ_t and k, which need to be modeled. The terms can be modeled by using algebraic or differential equations that are adjusted to match experimental results.

2.3.1 Reynolds Stress Models

Algebraic and differential Reynolds stress models take into consideration the breakdown of the stress terms in (2-15) and are designed to model the turbulent viscosity μ_t. Prandtl's mixing length hypothesis (Prandtl, 1925) is:

$$\mu_t = \bar{\rho}\ell_m^2\left|\frac{\partial u}{\partial y}\right| \tag{2-17}$$

in which ℓ_m is the prescribed mixing length and is given by an algebraic expression determined from experimental results. Von Karman's similarity hypothesis (Von Karman, 1930) developed an expression for the mixing length:

$$\ell_m \propto \left|\frac{\partial u}{\partial y}\Big/\frac{\partial^2 u}{\partial y^2}\right| \tag{2-18}$$

which does not agree well with experimental results except near walls. This disagreement occurs because ℓ_m cannot be solely determined from local values, but is a result of the surrounding behavior. Also, the mixing length goes to infinity at points where $\partial^2u/\partial y^2$ goes to zero. A third algebraic relation for the turbulent viscosity is:

$$\mu_t = \bar{\rho}u_e y_e f\left(y/\delta\right) \tag{2-19}$$

where u_e and y_e are characteristic global velocity and length scales (Launder and Spalding, 1966). The values of u_e and y_e have been chosen differently by different researchers. For example, in a pipe flow, the friction velocity and the pipe radius have been chosen to represent these values (Jonsson and Sparrow, 1966). However, this model is not as widely applicable as Prandtl's mixing length hypothesis since the method requires more *ad hoc* adjustment depending on the specific flow configuration.

The differential turbulence models make use of differential equations for the solution of parameters in the model. These differential equations include some information on the local history

of the turbulence in the determination of the model parameters; in contrast, the local history is not included in the algebraic models. The one equation differential models include a model by Prandtl in which:

$$\mu_t = \text{Const} \cdot \overline{\rho}\, \ell_m \overline{|\mathbf{u}'|} \tag{2-20}$$

The mixing length is prescribed algebraically and the turbulent kinetic energy, k, is determined with the use of a differential equation (Bradshaw, Ferriss and Atwell, 1967). The structure of the differential equation will be discussed as part of the k-ε model which uses two differential equations for the determination of the turbulent viscosity. Another single differential model was developed by Nee and Kovasznay (1969) and uses a differential equation for the parameter μ_t/ρ.

2.3.2 k-ε Turbulence Model

The most common turbulence model in use today for numerical simulations is the k-ε model which uses two differential equations for the determination of the turbulent viscosity (Harlow and Nakayama, 1967; Jones and Launder, 1973). The turbulent viscosity μ_t can be calculated from a model based on the Prandtl mixing length theory:

$$\mu_t = \text{Const} \cdot \overline{\rho}\, \ell_m \overline{|\mathbf{u}'|} \tag{2-21}$$

where ℓ_m is the mixing length and $\overline{|\mathbf{u}'|}$ is approximated by $(2k/3)^{1/2}$. The rate of dissipation of turbulent fluctuations, ε, is defined as:

$$\varepsilon \cong k \frac{\overline{|\mathbf{u}'|}}{\ell_m} \cong C_\mu \frac{k^{3/2}}{\ell_m} \tag{2-22}$$

which leads to the Prandtl-Kolmogorov relation:

$$\mu_t \cong C_\mu \overline{\rho} \frac{k^2}{\varepsilon} \tag{2-23}$$

where $C_\mu = 0.09$ from experiment.

The k-ε turbulence model consists of differential equations for the conservation of k and ε. This adds another degree of complexity to a numerical simulation, but provides a reasonable estimate of the turbulence effects for many problems. This turbulence model may experience difficulties in strongly swirling and recirculating flows where strong non-similarity is dominant (Launder and Spalding, 1972). The difficulty arises due the inability of the k-ε model to account for a) strong anisotropy of Reynolds stresses, b) high stream line curvature and c) strong pressure gradients. These have to do with the way the terms are thrown out and pressure correlation is modeled. The problems with the k-ε model should not be a factor in the Rijke tube simulations; however, they might be important for the recirculating flow in the dump combustor and the strongly swirling flow of the gas-turbine combustor. The conservation equations for k and ε are:

$$\frac{\partial(\bar{\rho}k)}{\partial t}+\nabla\cdot(\bar{\rho}\tilde{\mathbf{u}}k)-\nabla\cdot\left(\frac{\mu_t}{Pr_k}\nabla k\right)=-\mu_t S_1-\frac{2}{3}\bar{\rho}kS_2-\bar{\rho}\varepsilon \tag{2-24}$$

$$\frac{\partial(\bar{\rho}\varepsilon)}{\partial t}+\nabla\cdot(\bar{\rho}\tilde{\mathbf{u}}\varepsilon)-\nabla\cdot\left(\frac{\mu_t}{Pr_\varepsilon}\nabla\varepsilon\right)=C_{\varepsilon 1}\frac{\varepsilon}{k}\left(\mu_t S_1-\frac{2}{3}S_2\bar{\rho}k\right)-C_{\varepsilon 2}\bar{\rho}\frac{\varepsilon^2}{k} \tag{2-25}$$

where $S_1=\left[\nabla\tilde{\mathbf{u}}+(\nabla\tilde{\mathbf{u}})^T\right]^2-\frac{2}{3}(\nabla\cdot\tilde{\mathbf{u}})^2$

$S_2=\nabla\cdot\tilde{\mathbf{u}}$

and $C_{\varepsilon 1}=1.44$, $C_{\varepsilon 2}=1.92$, $Pr_\varepsilon=1.3$, $Pr_k=1.0$.

Because of the no-slip boundary condition, the turbulence levels are sensitive near the wall. A reasonable way to handle the effects near the wall is with algebraic wall functions. An example of such a specification is that of the log-law variation of velocity for turbulent flow near the wall. A detailed treatment can be found in Launder and Spalding (1972). The log-law prevails in the region near the wall, such that:

$$U = U_w + (u^*/\kappa)\ \ln(E\ y^+) \tag{2-26}$$

where U is the velocity component parallel to the wall, U_w is its value at the wall, u* is a friction velocity, κ is the von Karman constant, E is a constant in the log-law and y^+ is a non-dimensional distance from the wall. The wall shear stress is given by:

$$\tau_w = \kappa \rho u^* (U - U_w) / \ln(E y^+) \quad (2\text{-}27)$$

For the k-ε model of turbulence, Launder and Spalding (1972) showed that in the vicinity of the wall where the shear stress is constant:

$$u^* = C_\mu^{1/4} k^{1/2} \quad (2\text{-}28)$$

$$\varepsilon = u^{*3} / (y \kappa) \quad (2\text{-}29)$$

and $$\mu_t = \kappa \rho u^* y \quad (2\text{-}30)$$

2.3.3 Large Eddy Simulation

The last method for modeling the turbulence to be discussed here is LES. As was mentioned previously, direct numerical simulations (DNS) determine the Reynolds stresses down to the smallest possible turbulent scale allowed by the grid. Because of this, DNS requires fine grids to include all of the important scales of turbulence. The small grids and lengthy computational time restricts DNS to low Reynolds number flows. Large-eddy simulations are also direct numerical simulations, but they assume that the large turbulent scales contain most of the turbulent energy and that the small scales follow given energy decay laws without significant energy fed from the small scales to the large scales. The small scales are modeled using subgrid turbulence models. Using these subgrid models, the grid size can be increased allowing for simulations at higher Reynolds numbers. Work has been performed using LES in combustion environments (Menon and Jou, 1991; Goldin and Menon, 1996; Smith and Menon, 1998) with promising results.

2.3.4 Turbulence Modeling in ANSWER

The code ANSWER has capabilities for making use of the Reynolds stress model and the k-ε model to determine the turbulence levels. For the simulations in this thesis, ANSWER uses the k-ε model and solves the mass-averaged conservation equations given by (2-1a)-(2-1c) along with the conservation equations for k and ε given by equations (2-24) and (2-25). The LES method has been incorporated into the current version of ANSWER, but was not used for any of the simulations in this thesis. Even though the differential equations representing k and ε have a term for the time derivative of these values, it is not understood how well the k-ε model behaves under transient flow conditions or whether k and ε even need to be solved for as a function of time. The turbulent models are developed based on the time-averaged properties of turbulence, and in most flow simulations the researcher will most often be concerned only with the time-averaged effects of turbulence, even when the flow is unsteady (Launder and Spalding, 1972). Therefore, in the simulations to follow, except where noted, the k-ε model will be used to determine the steady state properties of the flow and these steady state turbulent levels will be kept constant throughout the transient simulation.

The Reynolds stress models have difficulties during the simulation of transient flows when the turbulent time scale ($t_\tau = k/\varepsilon$) is of the same order as the acoustic time scale ($t_a = \Delta x/a$), and the models also require a computational time four times that of the k-ε model. A calculation of the turbulent time scales for the dump combustor and gas-turbine combustor configurations in this thesis yields turbulent time scales between 0.001 s and 0.01 s. In these cases, the relevant acoustic time scales are between 0.002 s and 0.006 s for the dump combustor and 0.002 s and 0.01 s for the gas-turbine combustor. Since the relevant turbulent and acoustic time scales are similar, the Reynolds stress model in ANSWER will not be used in the following simulations.

2.4 Connecting Turbulence and Chemistry Modeling

As can be seen by the above, simulating chemical reaction rates and turbulence separately can be a difficult task. This makes simulations combining the two even more challenging. One of the main concerns is determining how the two processes interact. The Damkohler number is defined as the ratio of characteristic flow time to characteristic reaction time. When the Damkohler number is much less than one, the chemical reactions are much slower than the turbulent mixing and the influence of turbulence is greatly reduced. The turbulence, for this case, factors into the mixing and diffusion properties of the flow but not in the determination of the reaction rate. When the Damkohler number is much greater than one, the chemical reactions are much faster than the turbulence, which leads to a thin flame regime controlled by turbulent mixing. However, when the Damkohler number is near one, then both the turbulent mixing and finite reaction rates must be considered. There have been a number of reviews detailing models that can be used to determine the influence of the turbulence and reaction chemistry on combustion (Libby and Williams, 1994; Manna and Vandromme, 1996; Buchlin and Planquart, 1995). The rest of this section will summarize a few of the methods used, including the eddy-breakup model, probability density functions and flamelet models. The ANSWER code makes use of the eddy-breakup model for all of the turbulent-reactive simulations in this thesis.

The structure of the flame is important in determining if the turbulence models are applicable for a given flow field simulation. The flame structure can be broken into different zones based on the turbulent intensity of the flame, $k^{1/2}/S_L$ where k is the turbulent kinetic energy and S_L is the laminar flame speed, and the ratio of the integral scale of turbulence, l_o, to the laminar flame thickness, δ_L (Borghi, 1985; Abdel-Gayed et al., 1989). Figure 2-3, taken from Abdel-Gayed et al. (1989), shows the various regimes for premixed turbulent combustion. For the eddy-breakup model to be valid, the flame should be in the flamelet regime in which there is a wrinkled flame. For the Rijke tube in this thesis, the flow field is assumed to be laminar with no influence of

turbulence on the flame structure. For the dump combustor simulation in this thesis, $k^{1/2}/S_L \sim (2$ m/s / 0.5 m/s) = 4 and $l_o/\delta_L \sim (0.01$ m / 0.0008 m) ~ 12.5, leading to a flame structure that is wrinkled. It should be acceptable to apply the eddy-breakup model to this flow field simulation, based on the structure of the flame. The gas-turbine simulation in this thesis does not contain premixed combustion and therefore the combustion zones in Figure 2-3 do not apply.

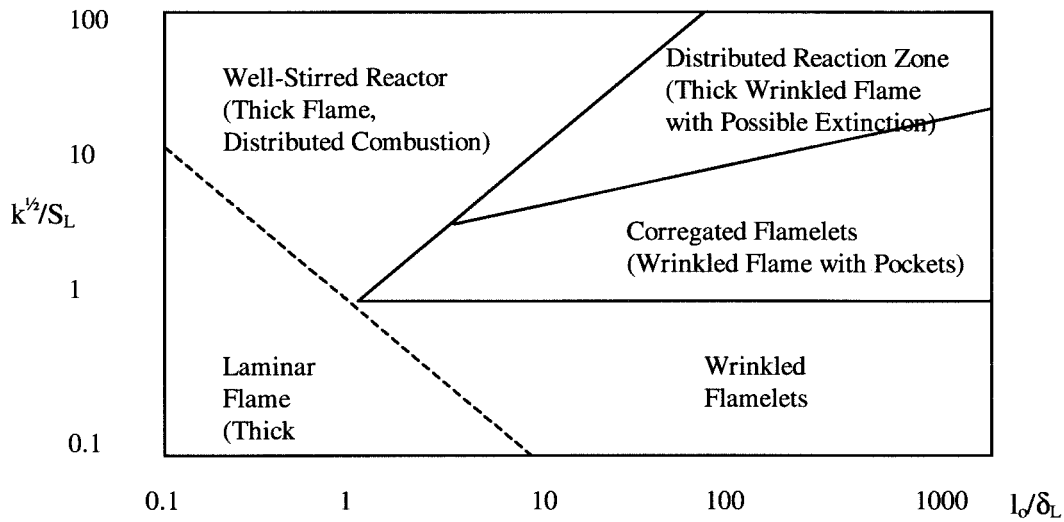

Figure 2-3 Premixed Turbulent Combustion Regions (from Abdel-Gayed et al., 1989)

2.4.1 Eddy-Breakup Model

One way to handle the possible reaction delay is to incorporate the eddy-breakup model (EBU) into the numerical simulation. The model makes use of k and ε along with the kinetic time scale and physically represents a time scale related to the breakup of turbulent eddies. The turbulent time scale is based on the time it takes for an eddy to decay, allowing the reactants to mix and react. The basic form of this model proposed by Spalding (1971) is:

$$w_i = C_{EBU} \rho Y_i^{rms} \frac{\varepsilon}{k} \tag{2-31}$$

where w_i is the source term in the species conservation equation (2-8), C_{EBU} is an empirical constant, Y_i^{rms} is a measure of the rms value of the local fluctuations in the mass fraction of species

i. $Y_i^{rms} = \min(Y_i, \alpha_i Y_{O2})$ where $\alpha_i Y_{O2}$ is the maximum amount of the i^{th} species that can react with the local oxygen concentration. The turbulent time scale is given by k/ε. Therefore, the reaction rate given by (2-31) is inversely proportional to the turbulent time scale. The overall chemical reaction rate is the minimum of the rate determined from the Arrhenius kinetics and the value from (2-31). Physically, this means that if the mixing time is larger than the chemical time, the mixing and breakup of the turbulent eddies controls the reaction rate. On the other hand, if the mixing time is small compared to the chemical time, then the reaction rate will be based on the chemical kinetics. Numerical efforts using the eddy-breakup model have demonstrated that the model is appropriate for premixed flame simulations where the rate of reaction is finite and very high, which is the case in furnaces and combustors (Khalil, 1982; Catlin and Lindstedt, 1991; Lee et al., 1993). The premixed flame in the dump combustor and the gas-turbine combustor fits this criterion and therefore the eddy-breakup model in the ANSWER code is used for these simulations.

2.4.2 Probability Density Functions

Other models currently being developed include probability density function (PDF) models and flamelet models. As has been mentioned, direct numerical simulations (DNS) can be valuable as research tools for very simple flows and large-eddy simulations (LES) can be useful for more complex flows, but they both break down when dealing with the nonlinear complexity of chemical reaction rates. In realistic cases, the Navier-Stokes equations are averaged and closure models are used to account for the resulting loss of information. Because the chemical reaction rate is highly nonlinear, in species concentrations Y_i and temperature T, the averaged reaction rate cannot simply be determined by using the average of the terms:

$$\overline{\dot{\omega}} \neq \dot{\omega}\left(\overline{Y}_A, \overline{Y}_B, \overline{\rho}, \overline{T}\right) \tag{2-32}$$

To account for the nonlinearity, the joint pdf method has been used to develop the average of a given function (e.g., turbulence or reaction rate) from the probability density function of the required arguments. If Q[q(**x**, t), q′(**x**, t)] is a function of two variables, the joint pdf is defined as follows:

$$Pr\{q < p; q' < p'\} = \lim_{N\to\infty} \frac{\#\text{ of experiments in which } q < p, q' < p'}{N} \tag{2-33}$$

The joint distribution function F(p, p′) is defined by:

$$F(p, p') = Pr\{q < p;\ q' < p'\} \tag{2-34}$$

and the joint probability density function is given by:

$$P(p,p') = \frac{\partial^2}{\partial p \partial p'} F(p,p') \tag{2-35}$$

From this, the average or first order moment of Q is given by:

$$\overline{Q}(\mathbf{x},t) = \int_{-\infty}^{\infty}\int_{-\infty}^{\infty} Q(p,p')P(p,p',\mathbf{x},t)\,dp\,dp' \tag{2-36}$$

The pdf can be developed from experimental results or detailed DNS or a transport equation can be solved for suitably chosen probability density functions. The method can also provide high order moments for closure needs in other simulation methods.

A more empirical method consists of assuming a given mathematical shape based on the first and second order moments of the coupled scalars used to define the distrubution function. This method is called the assumed shape pdf. The most common distribution functions used in the literature are beta functions, clipped Gaussians and delta functions.

The use of probability density functions has shown good agreement with experiments for simple flame structures (Khalil, 1982; Jones and Kakhi, 1998; Subramaniam and Pope, 1999; Saxena and Pope, 1999); however, the modeling technique needs further refinement before it will be useful in general flow simulations. The concern with probability density functions is in making

sure that the assumed shapes of the functions are representative of the actual flame structure. This would require more experimental results concerning the correct flame structure that might not be attainable in complex combustor configurations. For this reason, the probability density function model approach was not investigated in more depth for use in the combustor configurations modeled in this thesis.

2.4.3 Flamelet Modeling

Another method involves the use of flamelets (Peters, 1986; Veynante, Lacas and Candel, 1989; Candel et al., 1990; Meneveau and Poinsot, 1991; Duclos, Veynante and Poinsot, 1993). The essential property of this method is that a turbulent flame front is divided into a series of stretched, laminar flame elements, which are better understood analytically. Figure 2-4 shows a sketch of the flamelet technique for a diffusion flame (from Meneveau and Poinsot, 1991). The distributed reactive sheets are assumed to have a structure that can be identified and analyzed. This turbulent flame sheet is then assumed to be made up of a collection of stretched laminar flame elements. The use of flamelets decouples the complex chemistry problems from the turbulent flow field. In practical applications, a flamelet library is constructed to provide details on properties such as consumption rate per unit flame area and ignition and extinction conditions which might be important in a turbulent regime. The flamelet model can be used in both premixed and non-premixed flames, with slight differences between the two due to additional modes of propagation for premixed flames.

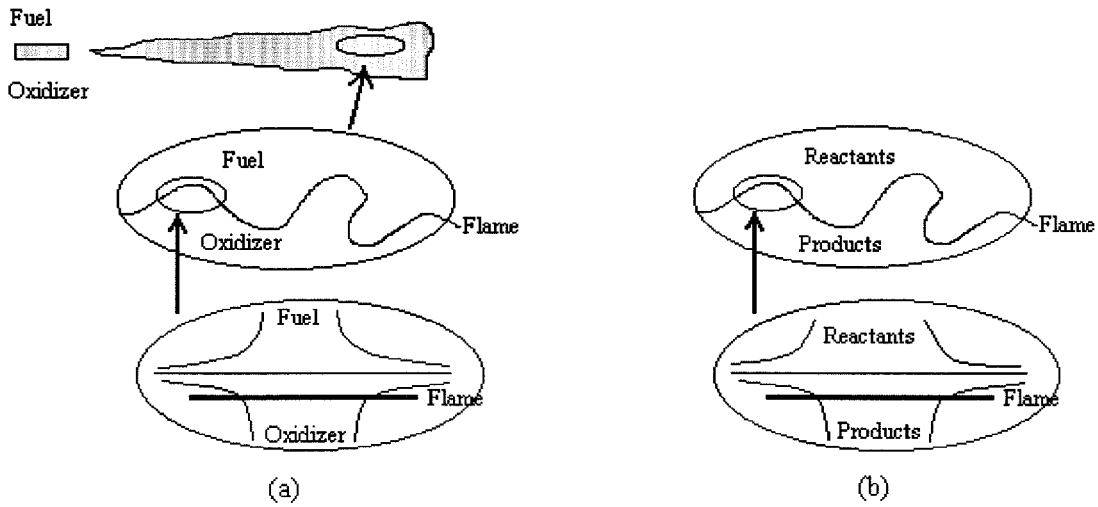

Figure 2-4 Sketch of Flamelet Model from Turbulent Flame Sheet to

(a) Laminar Diffusion Flame Elements; (b) Laminar Premixed Flame Elements

A central parameter for turbulent combustion modeling with flamelets is the flame stretch. The flame stretch is a measure of the variations of the flame surface A and is defined by:

$$K = \frac{1}{A}\frac{dA}{dt} \tag{2-37}$$

Flame stretch controls the growth of the flame surface via flame surface production and flame quenching. The flamelet model reduces to the evaluation of the flame surface density Σ. The coherent flame model provides a conservation equation for Σ moving with the turbulent flame:

$$\frac{d\Sigma}{dt} = \overline{K}\Sigma - Q_c \tag{2-38}$$

where $\overline{K}$ is the mean stretch rate and Q_c corresponds to flame surface annihilation between two flame fronts. The mean turbulent reaction rate is given by:

$$\overline{\dot{w}} = w_L \Sigma \tag{2-39}$$

where w_L is the mean consumption rate per unit surface along the flame front. For a lean reaction, $w_L = \rho_O U_L Y_O$, where ρ_O is the density of the fresh gases, Y_O is the fuel mass fraction in the fresh gases, and U_L is the mean consumption speed along the flame front.

A number of different models have been proposed in which a transport equation is developed to keep track of the flame surface density term, Σ. The existing models differ in the structure of the proper source and consumption terms that are part of the conservation equation for Σ written as:

$$\frac{\partial \Sigma}{\partial t} + \nabla \cdot (\overline{\mathbf{u}}\Sigma) = \nabla \cdot \left(\frac{\nu_t}{\sigma_\Sigma} \nabla \Sigma \right) + S_1 + S_2 + S_3 - D \tag{2-40}$$

where σ_Σ is a turbulent Schmidt number and source terms are given by S_i, including flame stretching and the consumption term by D. Different forms for these terms are summarized in Duclos, Veynante and Poinsot (1993). Equation (2-40) is coupled to the conservation equation for the mean fuel mass fraction by including (2-39) as a consumption term:

$$\frac{DY_i}{Dt} = \sigma \nabla \cdot \left(\mathcal{D} \nabla Y_i \right) - w_L \Sigma \tag{2-41}$$

The flamelet model is valid for configurations in which the flame thickness is small when compared with the dimensions of the flame surface; however, when the reaction rates are slower and the flame broader, the flamelet model will not work as well. The manner in which the flamelet model decouples the turbulence and the chemistry works when the flame thickness is small, but this benefit in modeling becomes a deficiency when the turbulent mixing has a strong influence on the reaction rates, which is what the eddy-breakup model takes into consideration. In the flamelet model, the reaction rates are based entirely on a database of the laminar flame behavior. This information might not be accurate for much of the turbulent flame configurations. The flamelet model might be beneficial to the study of the premixed flame in the dump combustor simulated in this thesis, but not for the other configurations, due to the structure of the flame.

2.4.4 Connecting Turbulence and Chemistry in ANSWER

For the simulations in this thesis, the eddy-breakup model is used to compute the turbulent time scale for the reaction. The eddy-breakup constant, C_{EBU}, is specified as 3.0 in all of the simulations. The reaction rates are evaluated using the Arrhenius model given by equation (2-9) and the eddy-breakup model given by equation (2-31). These two rates are compared and the smallest reaction rate is used as the w_i source term in equation (2-8). For the Rijke tube simulations shown in Chapter 3, the eddy-breakup model is not included in the solution and the chemistry reaction rates are specified only in terms of the chemical kinetics given by the Arrhenius model.

2.5 Simulation of Acoustic Waves in Incompressible Flows

One of the major issues that needed to be resolved in the present work before further analysis was conducted was the ability of the code to predict accurately the theoretical acoustic modes within a given system. In the combustion configurations investigated as a part of this thesis, the flow is low speed and incompressible. For this reason, the simulations performed in the results to follow have used incompressible flow solvers. However, if the flow is assumed to be incompressible, the speed of sound is infinite; therefore, the proper acoustic wave motion cannot be established. Any change in the pressure field instantly propagates to the rest of the chamber. In order to handle this problem, the ANSWER code modifies the continuity equation to take into account fluctuations in the pressure. The density term is then solved for using the ideal gas law, $p=\rho RT$.

At any stage in the calculation, the old values of the flow field are used to compute the new flow field values. The correct fluid velocity, density and pressure which satisfy the governing equations are given by:

$$\begin{aligned}\vec{V}_i &= \vec{V}_i^{\,*} + \vec{V}_i'' \\ \rho &= \rho^* + \rho'' \\ p &= p^* + p''\end{aligned} \tag{2-42}$$

where the starred quantities are the approximation of the new flow field variables at the next step in the calculation and the quantities with a double prime are corrections to these approximations. Substituting these in the mass continuity equation, and neglecting second order terms, leads to:

$$\frac{\partial \rho''}{\partial t} + \nabla\cdot\left(\rho''\vec{V}^*\right) + \nabla\cdot\left(\rho^*\vec{V}''\right) = m_{inj} - \nabla\cdot\left(\rho^*\vec{V}^*\right) \tag{2-43}$$

Following Chorin (1967), it can be shown that the approximate average velocity field, $\vec{V}^*$, differs from the final, $\vec{V}$, by the gradient of a scalar field, ϕ. Therefore, $\vec{V} = \vec{V}^* + \nabla\phi$. Now assuming that this scalar field is related to the density correction, by $\rho'' = c_\rho\phi$, equation (2-43) transforms to:

$$\frac{\partial}{\partial t}\left(c_\rho\phi\right) + \nabla\cdot\left(c_\rho\vec{V}^*\phi\right) = \nabla\cdot\left(\rho^* c_V\nabla\phi\right) + m_{inj} - \nabla\cdot\left(\rho^*\vec{V}^*\right) \tag{2-44}$$

which can be solved for ϕ. From the equation of state, $p'' = \rho''\partial p/\partial\rho$, which for a perfect gas becomes

$$p'' = \rho''CRT = CRTc_\rho\phi \tag{2-45}$$

where C = 1 for an isothermal process and γ for an isentropic process, R is the gas constant, and T is the temperature. The pressure correction can be determined from ϕ and related to the acoustic speed of sound. This should provide a proper determination of the acoustics within a low speed flow system.

Initially, the factor CRT in (2-45) was set equal to a constant in the ANSWER code. This was not a problem for constant temperature simulations, in which the term could be directly

specified using the proper temperature. However, for simulations in which the temperature varied over the flow field, the determined acoustic frequencies were a function of the constant value of CRT and not of the given temperature field. In order to correct this problem, the value of CRT was set equal to a local value, using the local values of R and T, to better represent the proper acoustic speeds. The use of the local flow properties will allow for the capture of the correct local acoustic speed in simulations where the temperature field might be changing dynamically.

2.5.1 Boundary Conditions

There are three basic boundary condition forms used by ANSWER: Dirichlet, specification of a variable value; Neumann, specification of a normal gradient value; and mixed (or Robbins), specification of the relationship between the boundary value and the normal gradient. The default boundary condition values used by ANSWER are Dirichlet at the inlet, except for a Neumann treatment of the pressure, and Neumann at the outlet.

The fundamental pressure standing mode is a quarter-wave for a basic flow through a tube with default boundary conditions. The upstream (or inlet) numerical boundary behaves like an acoustically closed boundary. The gradient of the pressure is zero for the default upstream boundary and a positive incoming wave is reflected as a positive wave in the other direction (i.e., no change in phase). The reason for this is that the default condition for the numerical simulation fixes the velocity at the inlet. An acoustically open upstream boundary condition can be obtained by removing the inlet specification and replacing it with a Dirichlet pressure condition and a Neumann velocity condition. The fundamental pressure standing mode for the acoustically open upstream boundary and the default downstream boundary condition is a half-wave identical to the theoretical prediction. The pressure is fixed at the upstream and downstream boundary such that a positive incoming wave is reflected as a negative outgoing wave (i.e., 180° change in phase).

The downstream (or outlet) boundary behaves like an acoustically open boundary under the default boundary conditions. The specification of a zero velocity gradient at the outlet dominates the behavior at the outlet, leading to a pressure that is nearly fixed at the outlet, in relation to the fluctuating value at the inlet. As with the upstream boundary, the downstream boundary can be changed to represent a closed acoustic boundary condition.

The default boundary conditions for ANSWER are therefore closed acoustically at the inlet and open acoustically at the outlet for the transient simulations. For the dump combustor case described in Chapter 4, the flow domain starts at the end of the plenum and ends at the opening to the atmosphere. The theoretical modes for this flow domain, determined by Zsak (1993), indicate that the inlet behaves like an acoustically closed end and the outlet behaves like an acoustically open end. Because the default boundary conditions determined by the numerical code match the theoretical boundary conditions, the results for the dump combustor require no adjustment. The ENEL gas-turbine combustor, which will be described in Chapter 5, is similar to the dump combustor in that the upstream boundary is a solid wall and the downstream boundary opens into the turbine blades. The default numerical boundary conditions are therefore also acceptable for this case as well.

The default boundary conditions are not ideal for the study of Rijke tubes, which will be described in Chapter 3. The Rijke tube is defined as a tube with some form of heating at a transverse section that is approximately acoustically open at both ends. Also, the experimental test cases that are being conducted here at Caltech involve tubes that are acoustically open at both ends. By altering the upstream boundary condition as described above, the acoustic information for an open-open Rijke tube can be obtained. However, the mode shapes are not smooth upstream of the flame, most likely due to the discontinuous jump in velocity across the flame. The difficulty with obtaining a smooth mode shape is not as pronounced for the default boundary conditions. It is therefore more desirable to simulate the simple flame in a tube that is acoustically closed at the

upstream end and acoustically open at the downstream end. The interaction of the heat release with the pressure and velocity fluctuations should still be the same regardless of the boundary conditions. As will be mentioned in Chapter 3, there have been a wide variety of configurations similar to the Rijke tube (Raun et al., 1993). Some of these configurations have had one end acoustically closed and others have had both ends acoustically closed. Therefore, the numerical results will be compared, where appropriate, to the experimental results for devices that are similar to Rijke tubes, if not exactly fitting the definition of one.

Even though the default conditions can model the test cases in this thesis, the numerical code is not as flexible as it could be. Work is being considered to make use of methods being developed for non-reflecting boundary conditions, characteristic boundary conditions and impedance boundary conditions. One of the main problems in this modification is that most of the methods have been developed for compressible flow solvers, and therefore, the method are not easily portable to ANSWER, which uses an incompressible flow solver.

Non-reflecting and characteristic boundary conditions can be used to ensure that the outgoing acoustic waves do not unduly influence the incoming acoustic waves. These boundary conditions are used to reduce the presence of spurious waves, which can be generated by numerical approximations at the boundary (Poinsot and Lele, 1992; Lepelletier and Raichlen, 1987; Watson and Myers, 1991; Rowley and Colonius, 1998). These methods have shown promise, but they do not constitute a definite answer to the problem. Also, a possible concern with non-reflecting boundary conditions is that in a real combustion system, the partial pressure reflecting is crucial to the coupling between the pressure and heat release and to the development of standing waves inherent in the system. A non-reflecting boundary would absorb all of the outgoing wave information, which might not allow for the development of a large-amplitude limit cycle.

Impedance boundary conditions would make use of experimentally determined behavior at a specified boundary. For steady waves, an acoustic boundary condition is specified in the form:

$$u' = (a+ib)p' = (a^2+b^2)^{1/2} \exp(i \tan^{-1}(b/a))\, p' \qquad (2\text{-}46)$$

It should be possible to define a relationship between the acoustic pressure and acoustic velocity at a boundary in order to describe the behavior of an acoustic wave at a boundary. Knowledge of temporal and spatial resolution of a and b could be used to describe an open boundary closely related to experimental results. Work on this is continuing, but will not be used in this thesis.

2.5.2 Calculation of Standing Wave in Closed Tube

Figure 2-5 shows the results of a cold flow laminar simulation made in a 2-D axisymmetric closed cylinder with length 2m and radius 0.1 m. The temperature is kept constant at 600 K and there is no inlet or outlet flow. The viscosity is set to 3.0e-5 kg/m-s. All of the boundaries behave like a solid wall, in that the normal velocity at the boundary is zero. The simulation is designed to examine the pure linear acoustic field when there is no other motion in the chamber. Theoretical acoustics predicts that under these conditions, the fundamental longitudinal frequency $f_l = a/(2*L)$ and that subsequent harmonics will be given by: $f_n = n * f_l$. The theoretical fundamental frequency for this case is 122.75 Hz. The results shown in Figure 2-5 are for a simulation with uniform grid spacing along the longitudinal axis of $\Delta x = 0.05$ m. The numerically determined fundamental frequency for this case is 135.9 Hz. The discrepancy with the theoretical frequency is due to the grid spacing near the boundary. To numerically simulate a zero pressure gradient at the wall, the first and second grid elements next to the wall are kept constant with the value at the wall. This effect causes the effective acoustic wavelength to be equal to $L_{eff} = L - 4\Delta x = 1.80$ m, leading to a fundamental frequency of 136.4 Hz, which is only a 0.4% difference from the numerically determined value. The simulation was repeated with the grid spacing near the walls equal to 0.001 m. The resultant fundamental frequency is 122.6 Hz which is 0.3% less than the theoretical fundamental frequency with an effective wavelength of 1.996 m. This demonstrates

that the simulation is correctly determining the acoustic frequency within a small margin of error and emphasizes the importance of the grid spacing near the boundaries.

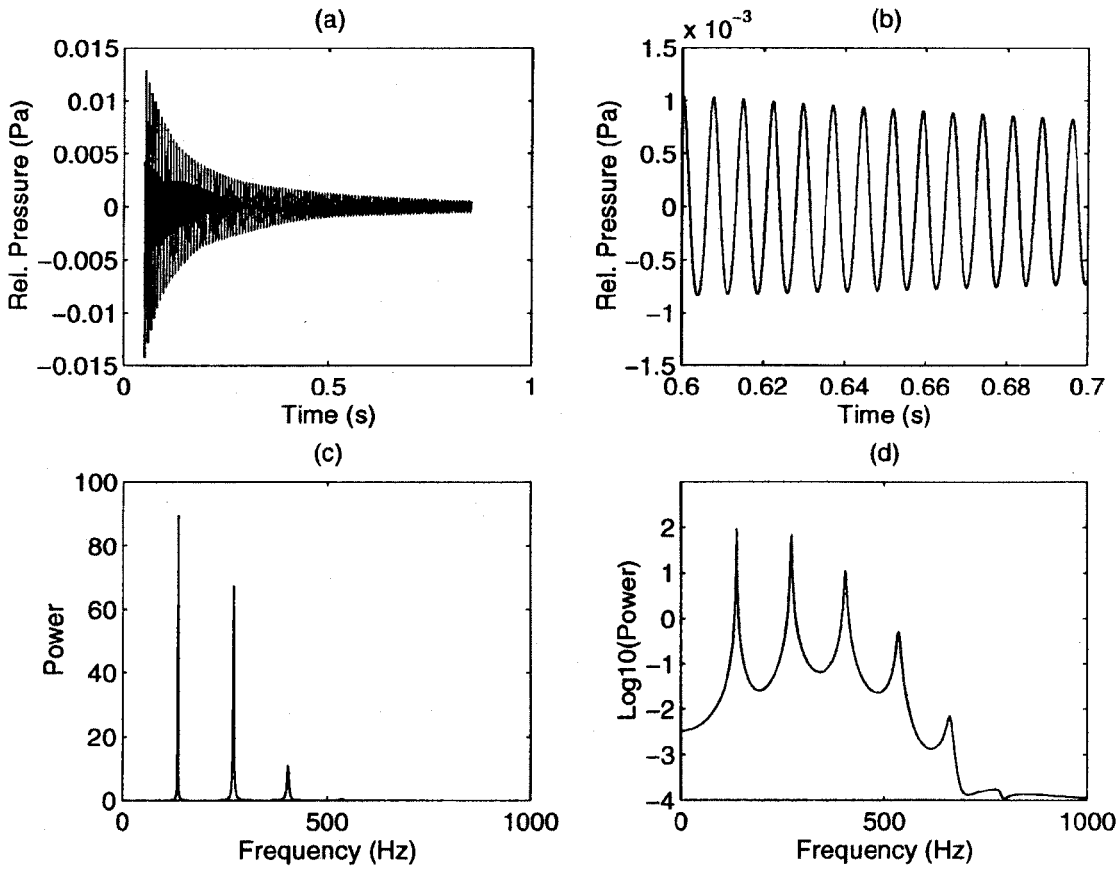

Figure 2-5 Numerical Simulation of Acoustic Waves in a Closed Tube

(a) and (b) Non-Steady Pressure at Quarter Chord Location;

(c) and (d) Fast Fourier Transforms of Pressure Signal

2.5.3 Attenuation and Time Step

As can be seen by the pressure records of Figure 2-5, there is exponential damping in the chamber. Since the system is not reacting and has no other energy source terms, there is no exponential growth term to take into consideration. The damping in the chamber is due to several sources: bulk attenuation; reflection losses at the outlet and inlet plane; and attenuation due to

dissipation in the boundary layer. Also, because the code uses a second-order finite difference method, artificial dissipation and dispersion must be accounted for. The amount of artificial damping will be discussed later in this section. The bulk attenuation values are normally more than an order of magnitude lower than the other loss terms for the low frequency levels we are interested in. The major sources of attenuation are due to the viscous and thermal losses in the boundary layer. Morse and Ingard (Flugge, ed., 1961) showed that for no-slip conditions and stationary isothermal walls, the velocity boundary layer thickness and thermal boundary layer thickness are given by:

$$\delta_v^2 = \frac{2\mu}{\rho\omega}$$
$$\delta_t^2 = \frac{2\kappa}{\rho\omega C_p} = \frac{2\mu}{\rho\omega\, Pr} \qquad (2\text{-}47a,b)$$

For a circular duct of radius R, the sound level intensity for a sound wave propagating in the x-direction is given by $\Phi_X = \Phi_O \, Exp(-2\alpha x)$ where:

$$2\alpha = \frac{\omega}{aR}\left[\delta_v + (\gamma - 1)\delta_t\right] \qquad (2\text{-}48)$$

This shows that the linear damping rate is related to the viscosity and the frequency. Since the sound wave is propagating at speed a, this damping rate can also be written in terms of time with $\Phi_X = \Phi_O \, Exp\,(-2\alpha at)$. The damping for the acoustic pressure field is half the damping rate for the sound intensity since the sound intensity is proportional to the square of the acoustic pressure. The exponential decay rate was determined as a function of time for the pressure record in Figure 2-5. Initially, when higher harmonic frequency components are noticeable, the decay rate is around 0.015 m^{-1}.

As the higher harmonics decay with time, the exponential decay of the fundamental frequency also decreases in value, approaching a value around 0.0045 m^{-1}. The theoretical value of the damping, using equation (2-48) yields a damping rate of 0.00442 m^{-1}. This shows that as

time increases and the losses to the higher harmonics become negligible, the main sources of decay for the fundamental frequency are the losses due to the thermal and viscous boundary layers. The numerical simulation is therefore correctly handling the acoustic losses due to the viscous and thermal boundary layers when the flow rate approaches zero. In this case, as the acoustic limit is approached, the artificial damping, due to the finite difference approximations, is negligible.

However, the viscous damping needs to be better understood when the flow field variables and gradients are not negligible. Finite difference methods use finite values to approximate the flow field gradients. These approximations include error terms of higher order gradients, which can enter into the equations as an extra (or artificial) viscosity or dispersion term. Runchal (1977) examined the added viscosity and dispersion terms for a series of finite difference methods. For the two methods used by ANSWER, namely the fully implicit central and fully implicit upwind methods, the dispersion component adds a negative value to the propagation speed, leading to a slight under prediction of the propagation speed. The artificial viscosity, while dependent also on the grid spacing, can be on the order of the actual viscosity. This increase in the viscosity could lead either to a lower limit cycle amplitude for an unstable simulation or to a damping of the oscillation altogether. This issue will be discussed later in connection with the results. In some cases, the viscosity has been reduced by an order of magnitude to decrease the effect of the artificial viscosity. The change in the propagation speed will have a slight effect on the fundamental frequency for a given chamber, but it is only a minor effect.

In addition to the viscous damping in the main flow region and near the wall, the other main source of sound attenuation is due to reflection losses at the boundaries (Flugge, ed., 1961). The normal acoustic impedance, z_n, is given by:

$$\frac{z_n}{ik\rho a} = \frac{p}{\partial p/\partial n} = \frac{\varsigma}{ik} = \frac{1}{ik}(\chi - i\xi) \qquad (2\text{-}49)$$

where p is the non-steady component of the pressure, $k = \omega/a$, ζ is the dimensionless specific impedance of the surface and χ and ξ are its resistive and reactive components. If the acoustic wave impacts at an incident angle ϕ, then the ratio of the reflected wave amplitude to the incident wave amplitude is given by:

$$R = \frac{p_r}{p_i} = -\frac{(1-\chi\cos\phi)+i\xi\cos\phi}{(1+\chi\cos\phi)-i\xi\cos\phi} \tag{2-50}$$

From this the absorption coefficient, α, of the surface is determined as:

$$\alpha = 1-|R|^2 = 1-\frac{(1-\chi\cos\phi)^2+\xi^2\cos^2\phi}{(1+\chi\cos\phi)^2+\xi^2\cos^2\phi} \tag{2-51}$$

One more comment needs to be made regarding the time scale for the proper acoustic determination. An acoustic wave propagating across a grid of size Δx at the speed of sound a, takes time $t = \Delta x/a$. Therefore, the maximum time step to ensure that all the pressure wave information is passed along to the next grid element is $\Delta t_{max} = \Delta x_{min} / \bar{a}$. This is one of the limiting factors in the speed of the numerical transient simulations. The time scale needs to be small enough not only to handle the proper acoustic wave motion, but also to ensure numerical stability.

However, while simulating chambers with no flow, we also noticed that there was a limit as to how small the time step could be. The time step was varied for the simulation of laminar flow in a closed cylinder with length 2 m and a radius of 0.1 m at a constant temperature of 600 K. Figure 2-6 shows the results for two different time steps. The top figure is for a time step of 5e-7 s. As can be seen in this figure, a high frequency signal is reaching unstable levels on the order of a few percent of the reference pressure of 1.01e5 Pa. Since the simulation is for a closed cylinder with no source terms and no heat release, there should be no instability, only a damping of the pressure term. Therefore, the instabilities in this simulation are due to the time step and are completely numerical. This is the opposite behavior from that seen in Figure 2-6(b) in which the

time step is 5e-6 s and the pressure record is decaying exponentially. Figure 2-6(b) also shows some of the damping behavior of the higher harmonics.

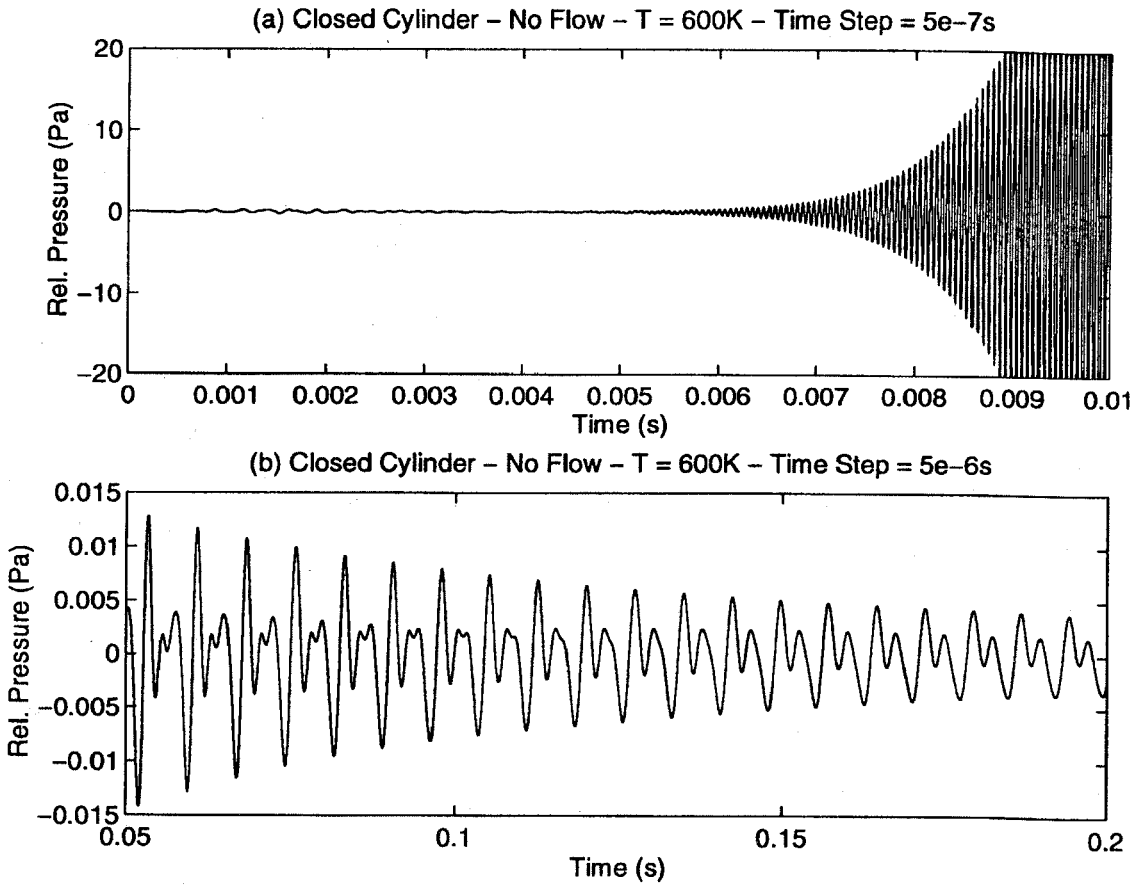

Figure 2-6 Pressure Traces for Closed Cylinder with No Flow (a) Δt = 5e-7 s (b) Δt = 5e-6 s

These two factors put a bound on the range of time steps that can be used for the transient simulations. The time step must be small enough to allow for transmission of the proper pressure information between the grid elements. The time step must also be large enough to avoid the introduction of high frequency, numerical instabilities, which are not real. For all of the cases in this thesis, a time step between 1e-6 s and 5e-6 s will be used for the simulations and will fall into the prescribed range of time steps.

A final comment needs to be made concerning the grid spacing used in the following simulations. Except for the influence of grid spacing at the boundaries on the acoustics shown in Section 2.5.2, the effect of grid spacing on the solution was not examined in great depth. A few test cases were computed for the Rijke tube, but not for the more complex flow regimes of the dump combustor and gas-turbine combustor. The reason for not using a finer grid spacing in the following simulations is a computational time constraint. A more detailed grid would have required a numerical time step an order of magnitude lower than that used in the simulations, which would have required a longer computational time to determine even one acoustic period. It was desired to generate reasonable acoustic results in a reasonable amount of time and for this reason the grid spacing and time scale were set as described. However, the influence of grid spacing on the overall flow properties should be a goal of future work on this matter.

Chapter Three

Simulations of Rijke Tubes

The main concern in this thesis is the application of a numerical code to the simulation of transient combustion flows. This chapter and the next will present some results, for two simplified combustion flow systems, which can be compared with past experiments. A Rijke tube system is defined as a planar concentrated heat source in an open-ended pipe. As mentioned in the previous chapter, the simulations in this chapter will mainly focus on Sondhauss-type tubes in which there is a planar heat source in a tube acoustically closed at one end and acoustically open at the other. The heat source will be modeled by two methods: a premixed flame and an insensitive fixed heat source. The dump combustor, discussed in the following chapter, involves a premixed flow over a dump plane with the potential for large-scale vortex dynamic interaction with the acoustic field. These simple flows provide a basis for understanding transient combusting flows in more complex flow regimes.

The frequencies and amplitudes of oscillations in the numerical, experimental and theoretical cases are comparatively similar for both the Rijke tube and the dump combustor configurations. The numerical simulations can improve upon the experimental information by providing more details about the flow behavior near the heat source. The ability of the numerical results to match accurately the theoretical acoustic frequencies will be discussed. The details of incorporating these results for the development of heat release models, to be used in the approximate analysis, will be discussed in Appendix C. Finally, the production of NOx in a steady and unsteady flow field will be discussed in this chapter.

3.1 Rijke Tube and Sondhauss Tube

The phenomenon of oscillatory heat release producing acoustic oscillations has appeared in many combustion applications from solid propellant rockets to gas-turbine combustors. There are three key elements connecting all of these systems that need to be better understood: the coupling between the flow field and the heat release; the dynamics of the combustion process; and the dynamics of the medium and chamber. An understanding of all of these elements is necessary to describe and predict combustion instabilities.

One of the simplest experimental tools for such understanding is the Rijke tube (Rayleigh, 1877; Merk, 1957; Carrier, 1955; Collyer and Ayres, 1972; Houpt and Goodman, 1990; Raun et al., 1993). A Rijke tube is a long tube with a circular or square cross-section and a heat source at a specified location along the length of the tube. For the original Rijke tube, both boundaries are acoustically open; however, there have been a number of experimental devices, similar to the Rijke tube, in which the boundary conditions are either closed-closed or closed-open (Raun et al., 1993). The heat source can be applied by various means, including an electrically heated wire mesh or an anchored flame. The acoustic modes excited by the heat source are the harmonics of the fundamental longitudinal mode.

The strength of the excited harmonics is dependent on the location and the strength of the heat source. Collyer and Ayres (1972) showed experimentally that the position of the heat release affects which harmonic frequency is excited. For example in a Rijke tube, which is acoustically open at both ends, placing the heat release at L/4 from the inlet will drive the first harmonic, while placing the heat release at L/8 and 5L/8 from the inlet will drive the second harmonic. The reason for this has to do with the interaction between the heat release and the fluctuating components of the velocity and pressure. Rayleigh's criterion states that when the pressure and heat release fluctuations are in phase, then the system will be driven at that frequency. Rayleigh's criterion is described by the equation:

$$R=\int_{V}\int_{t}^{t+\tau}\frac{p'Q'}{\bar{p}\,\bar{p}}\,dt\,dV \tag{3-1}$$

If we examine the first acoustic mode in an open-open Rijke tube and assume that the heat release differs from the pressure mode by a time delay, we have:

$$\begin{aligned}\frac{p'}{\bar{p}}&=A\cos(\omega t)\cos(kx)\\ \frac{Q'}{\bar{p}}&=B\cos(\omega t+\phi)\cos(kx)\end{aligned} \tag{3-2}$$

with A and B positive. Assuming that the flame is at $x = x_f$ and integrating (3-1) using (3-2), we have:

$$R=AB\left(\frac{\pi}{\omega}\cos^2(kx_f)\right)\cos\phi \tag{3-3}$$

If ϕ is between –90° and +90°, the heat release fluctuation and pressure fluctuation are in phase and Rayleigh's parameter, R, is positive, indicating a driven system. When R is negative, the system is considered damped.

Theory predicts that the heat release fluctuations lag the velocity fluctuations by around 60° (Raun et al., 1993). When the heat release is between $0 < x < L/2$, the pressure fluctuation lags the velocity fluctuation by 90°, therefore, the pressure and heat release fluctuations are in phase and the system is driven. However, when the heat release is between $L/2 < x < L$, the pressure fluctuation leads the velocity fluctuation by 90°; therefore, the pressure and heat release fluctuations are not in phase and the system is damped. A similar analysis can be performed for the higher harmonics to show optimal driving for the n^{th} mode at $(1+4k)L/2n$, where k = 0,1,2…,n-1.

Work at the California Institute of Technology has made use of the Rijke tube as a basic experimental device. The main focus of this work has been the development of a database for use in the theoretical analysis of combustion instabilities. The two main experimental configurations

are a horizontal square tube with an electrically heated wire mesh and a premixed flame in a vertical cylindrical pipe. A blower is used to force air through the horizontal tube, while the flow rate through the vertical pipe is driven by convection. The experimental work has mapped out the stability of the Rijke tube and examined the behavior of the pressure field when the heat release is placed at various locations in the tube. Recent work has also made use of the Rijke tube to study control techniques, including negative feedback with a speaker and a secondary fuel source in the premixed flame configuration. The Rijke tube works well as a test case for active control techniques because the modes are well-characterized (Houpt and Goodman, 1990). Simple feedback loops can be developed to stabilize the system. A third experimental system under study at Caltech is a flare burner that is acoustically closed at the upstream end (the entrained air enters along the radial axis). This burner is similar in structure to a Sondhauss tube.

Numerical results will be presented that are acoustically open at both ends. The frequencies obtained will be shown to be similar to the experimental and theoretical frequencies. The main focus of the numerical results will be for a tube similar to the flare burner in which the upstream end is acoustically closed and the downstream end is acoustically open. A few cases will be presented in which the system is acoustically closed at both ends, similar to the research by Putnam and Dennis (1954) and Friedlander et al. (1964). The change between an open-open, closed-open and closed-closed cases will only impact the form of the acoustic modes. The interaction between the acoustics and the heat release will still be correct and the analysis of this response in the behavior will still be applicable to a Rijke tube.

Because of the simple design and the well-defined acoustic modes, the Rijke or Sondhauss tube provides a good starting point for examining how well the numerical techniques simulate transient behavior of pressure instabilities. The numerical results of the excited frequencies, mode shapes and limiting amplitudes will be compared with theoretical and experimental results. The simple flow regime allows rapid calculation of various heat release

configurations. These results can provide a detailed picture of the interaction between the heat release and pressure field. Models of the heat release response to pressure and velocity fluctuations can be developed from the numerical results for inclusion in the theoretical methodology that will be described later in this chapter. In this way, the transient heat release results are useful as a guide for the more complex transient results in full-scale gas-turbine combustors.

3.1.1 Configurations

The first experimental configuration is a square aluminum tube with a length of 1.0 m and a width of 0.1 m (Pun and Hixson, 1999). Figure 3-1(a) shows the sketch of the apparatus. This tube is used for the experimental case of an electrically heated wire mesh. In the experiment a damping chamber of length 1.0 m and width of 0.3 m is used to uncouple the acoustics in the tube with the behavior of the blower, which produces the mean flow. In the experiments, the blower volume flow rate of air is varied in 1 L/s intervals (1.293 g/s of air at STP conditions). The wire mesh is heated with a power source at intervals of 100 W. Both ends of the experimental tube are acoustically open, meaning there is a pressure node and a velocity anti-node at the inlet and outlet. In actuality, this pressure node is positioned outside the tube by a fixed distance related to the width of the tube.

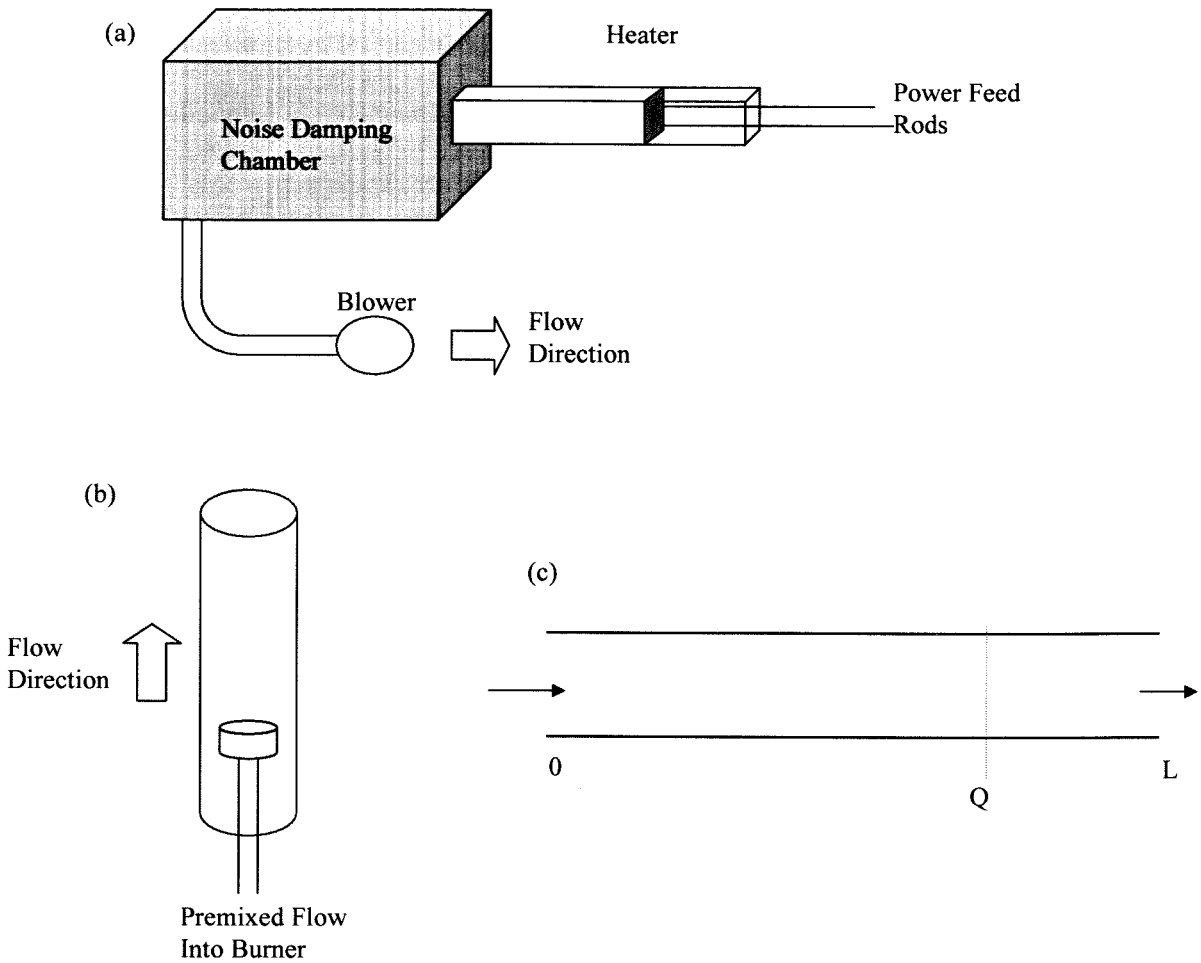

Figure 3-1(a) Sketch of Experimental Rijke Tube with Planar Heat Source;

(b) Sketch of Rijke Tube with Premixed Flame; (c) Sketch of Numerical Domain

The numerical simulations will assume a 2-D flow structure (i.e., the z-direction will be ignored) with a parabolic profile for the inlet velocity. Figure 3-1(c) shows a sketch of the numerical domain. This same domain will be used for all cases in this chapter, except where noted. The variation in the simulations will include changing the power level, position of heat release, and the boundary conditions. A power source will be included in the enthalpy equation to model the heat source in the tube. The reference pressure for the simulation is 1.013e5 Pa and the

inlet temperature is 300 K. The numerical grid is 82 by 62. It should be noted that all results will be scaled by the length of the chamber, L, in order to generalize the conclusions.

A cylindrical glass pipe with a length of 1.5 m and a radius of 0.05 m is used for the other experimental case with a premixed flame (Seywert and Isella, 1999). The premixed fuel and air is injected through a porous plate in the center of the pipe. A sketch of the configuration is shown in Figure 3-1(b). The porous plate has a radius of 0.03 m, which leads to a 36% blockage at the flame holder location. Methane fuel is used for all the premixed flame cases. The numerical simulations of this case will assume a parabolic inlet velocity profile and will neglect the influence of the z-axis, which is into the page in Figure 3-1(c). The assumption of a 2-D flow should be valid since most of the extra energy in the system is expected to excite the longitudinal modes. The inlet temperature in this case is set to 300 K for the numerical simulations and the reference pressure is set to 1.013e5 Pa. In the experimental case, the additional airflow through the pipe is drawn in by natural convection due to the premixed flame. In the numerical simulations, the mass flow rate will be fixed.

For the premixed flame simulation, the flame is ignited numerically by setting a high value of temperature in a group of cells downstream of the flame location. The flame location is specified by fixing the fuel mass fraction upstream of the flame. Fixing the fuel mass fraction upstream of the flame does not allow the flame to "flashback" in these simulations, but a flame "blow-off" can still occur since the simulations do not impede the flame movement downstream of the flame. "Flashback" occurs in an experimental test case when the propagating flame speed is greater than the incoming flow speed. "Blow-off" occurs when propagating flame speed is much lower than the incoming flow speed. In an experimental premixed burner, the fuel mass fraction would be constant upstream of the flame front and a wire mesh or porous burner would be used to prevent "flashback" of the flame. The wire mesh or porous burner would act to anchor the flame and allow it to adjust its shape so that the flame speed is equal to the flow speed normal to

the flame. The high temperature zone acts like an experimental spark in the numerical simulations. This numerical spark creates a flame front propagating into the combustible mixture with a flame speed proportional to the square of the flame temperature (Kuo, 1986). In an open tube, the flame propagates upstream if the convection velocity is lower than the flame speed, and the flame is forced downstream if the convection velocity is larger than the flame speed. In addition to "flashback" and "blow-off", the flame can also "blowout" when the energy provided by the burned products is not enough to ignite the incoming mixture. Local regions of blowout can destroy an anchored flame front or lead to further instabilities as the surrounding flame front adjusts to the tear in the flame. Blowout can occur on the lean and rich side of stoichiometric when the flame front can no longer sustain itself. For the numerical simulations with a planar premixed flame in this chapter, the velocity and equivalence ratio are set in a stable region not close to the lean blowout limit. However, we found that the flame did blowout numerically when the equivalence ratio was decreased and/or the velocity increased to a point near the lean blowout limit.

As mentioned in Chapter 2, the boundary conditions are a concern for proper understanding of the acoustic modes and the interaction between the flow field variables in the numerical simulation. In both of the experimental cases, the ends of the tubes are open to the atmosphere, leading to an acoustically open boundary in which the oscillating pressure is at a node. It was determined in the numerical simulations that the inlet boundary conditions in the code constituted an acoustically closed boundary in which the fluctuating pressure is at an anti-node. Similarly, it was determined that the downstream default boundary condition indicated an acoustically open boundary. The expected theoretical modes for this case are given by $f_n = (2n-1)\,\bar{a}/4L$. The fundamental mode should not be driven at any point in the tube for this case. However, the second harmonic should be driven between L/3 and 2L/3. The reason has to do with the phase relation between the heat release and the pressure as described in Section 3.1. In the

cases where the upstream boundary is also set to an acoustically open condition, the theoretical modes for this case are given by $f_n = n\ \bar{a}/2L$. It is expected that the first harmonic is driven at L/4 in this case. The exact theoretical values of the fundamental mode and the harmonics will be discussed along with the results.

3.1.2 Electrically Heated Mesh in Square Tube

This section will describe the numerical results obtained from the simulation of an electrically heated wire mesh in a square tube. For these simulations, the time step was 5 μs and the sampling frequency was 10 kHz. All results in this section are for the configuration sketched in Figure 3-1(c). Since the numerical domain is only 2-D, the third dimension is assigned a value of 1.0 m. In order to match the experimental flow velocity in the chamber, the simulations match the value of $\dot{m}/A$ and P/A, where P in this case is the power supplied to the tube. The mean velocity for the following cases is 0.5 m/s, which corresponds to a volume flow rate of 4.5 L/s in the experimental configuration. The major difference between the numerical simulation and the experiment is the flow blockage imposed by the wire mesh. This blockage is not included in the numerical simulations.

For the simulations of an electrically heated wire mesh, the conservation equations for the momentum, equation (2-1b), and the stagnation enthalpy, equation (2-4b), are solved along with the modified continuity equation using the Chorin (1967) evaluation of the pressure, equation (2-44). The flow is assumed to be laminar and therefore the k-ε model is not included in the simulation. The heat release term for the simulations in this section is a constant source term for the stagnation enthalphy equation. The stagnation enthalphy in ANSWER is the sum of the enthalpy, the kinetic energy and the turbulent kinetic energy. The temperature increase, and therefore the energy addition to the flow, at the source location for the following simulations is

therefore a function of the constant stagnation enthalpy and the velocity. In this way, fluctuations in the velocity lead to fluctuations in the energy input into the flow, which can then couple with the pressure fluctuations, leading to a large-amplitude oscillation. It is expected that the explicit form of this coupling will be determined by post-processing the numerical results. In all the simulations, a steady state solution was first computed as an initial condition for the transient simulations. For the cases in which an oscillation develops, the transition from a steady state simulation to a transient simulation was enough to initiate the oscillation. In some of the results to follow, there is a jump in pressure when the transient simulation is initiated. It is believed that this jump in pressure is caused by the evaluation of the continuity equation given by equations (2-44) and (2-45) at the heat source. The discontinuity in the temperature and the mean velocity at the heat source may be the cause of the pressure jump in the transient simulations. The initial pressure field can also be specified in the code, but it was not used in these simulations to demonstrate growth or decay of unsteady motions.

As a first test case, the simulation was run with no heat release in the chamber. The temperature is 300 K and the mean velocity is 0.25 m/s. Figure 3-2 shows the pressure record at L/4. The main frequency is 173 Hz, which corresponds to the theoretical first harmonic for this case of 173.6 Hz. The maximum value of the peak pressure fluctuation during the time of the simulation is 0.35 Pa, which is 0.00035% of the mean pressure. This case is stable and demonstrates that the simulation does not develop oscillations that are a product of the numerical method. If the simulation were extended in time, the fluctuating pressure would tend to zero.

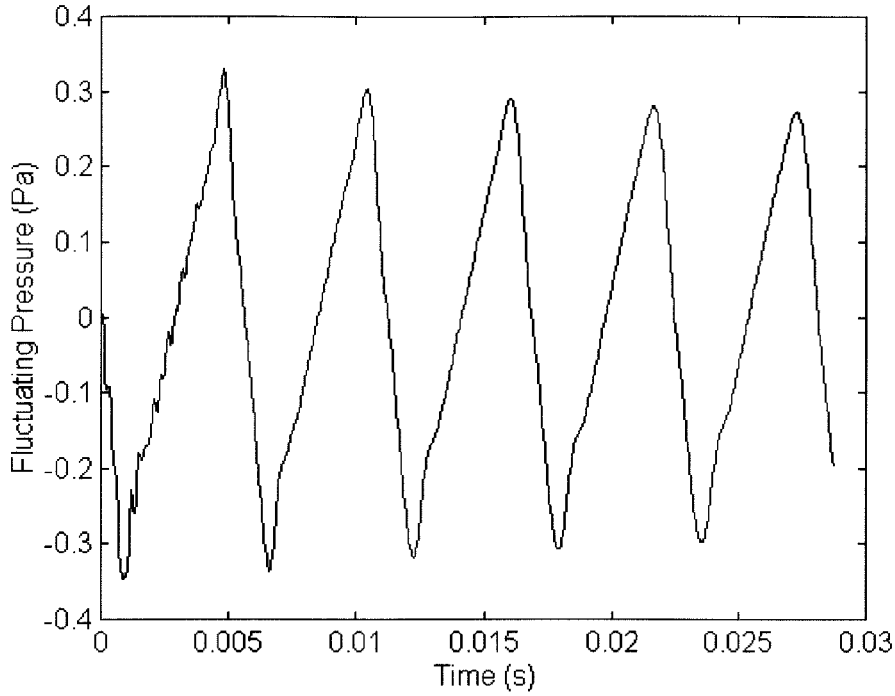

Figure 3-2 Pressure Record in Open-Open Tube with No Heat Release

The stagnation enthalpy source was increased at this point to 500 kW/m^2 in order to excite the oscillation. For the open-open boundary case, the heat source was placed at the L/4 point. Figure 3-3(a) shows the pressure record for this case. The fundamental frequency is 231 Hz and the pressure amplitude begins at around 80 Pa and quickly drops off. Figure 3-3(b) shows the exponential decay of the first mode in a semi-log plot of the successive negative pressure peaks.

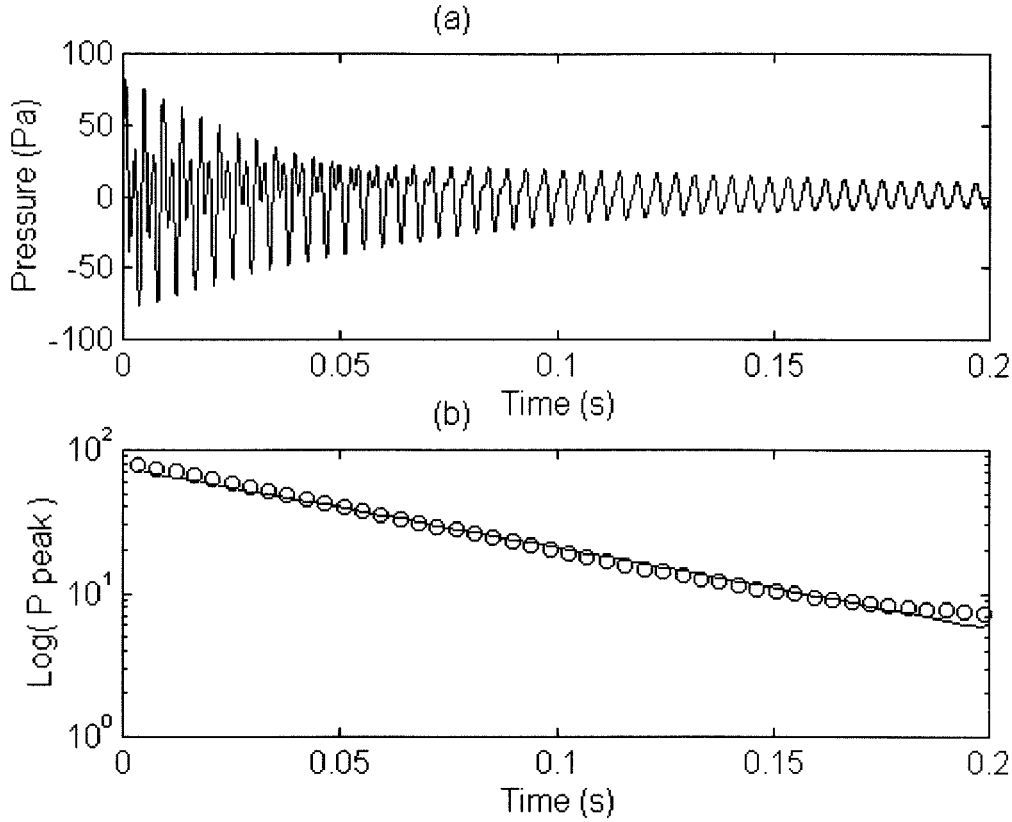

Figure 3-3 (a) Open-Open Rijke Tube with Heat Source at L/4

(b) Semi-Log Plot of Successive Negative Pressure Peaks with Linear Fit

The same source of 500 kW/m2 was used for a simulation in which the upstream boundary was closed acoustically and the downstream boundary was open acoustically. The heat source was placed at L/4 and L/2. Figure 3-4 shows the pressure records for the heat source at L/4 and Figure 3-5 shows the pressure with the heat source at L/2. When the heat source is added at L/4, the first mode (118 Hz) is excited and decays slowly. When the heat source is added at L/2, the second mode is also excited and both modes decay to zero. There may be a problem with fixing the pressure at the boundary (as was done for the open-open boundary condition simulations), in which the boundary condition attenuates the pressure signal, leading to a more rapid stabilization when the system may not be so stable. The source term was reduced by half in

the L/2 location and the results are shown in Figure 3-6. The frequencies are lower, (93 Hz versus 105 Hz) due to the reduced mean temperature downstream of the heat source, and the pressure amplitudes are much lower, indicating that there is not enough power to excite the modes or drive them unstable.

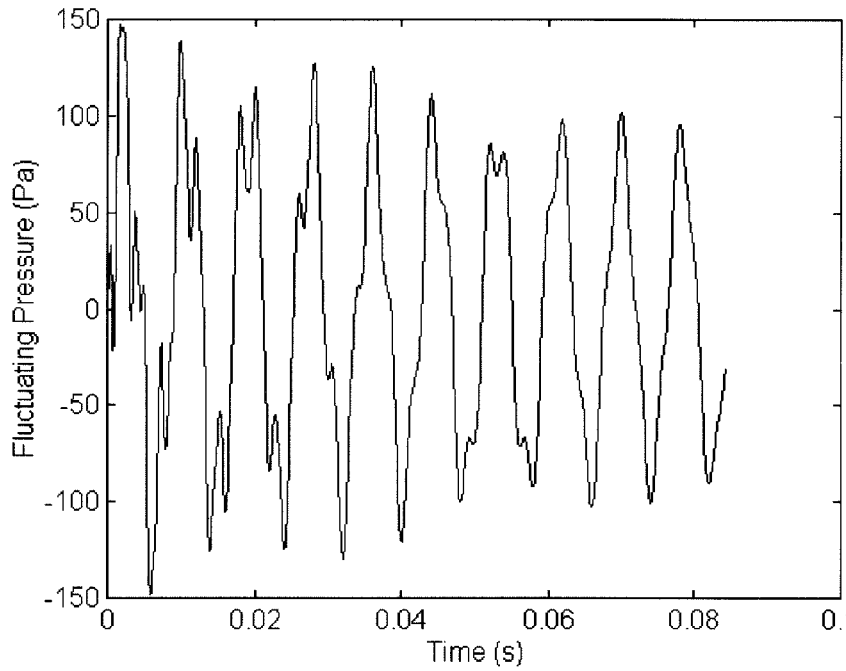

Figure 3-4 Closed-Open Tube with Heat Source at L/4

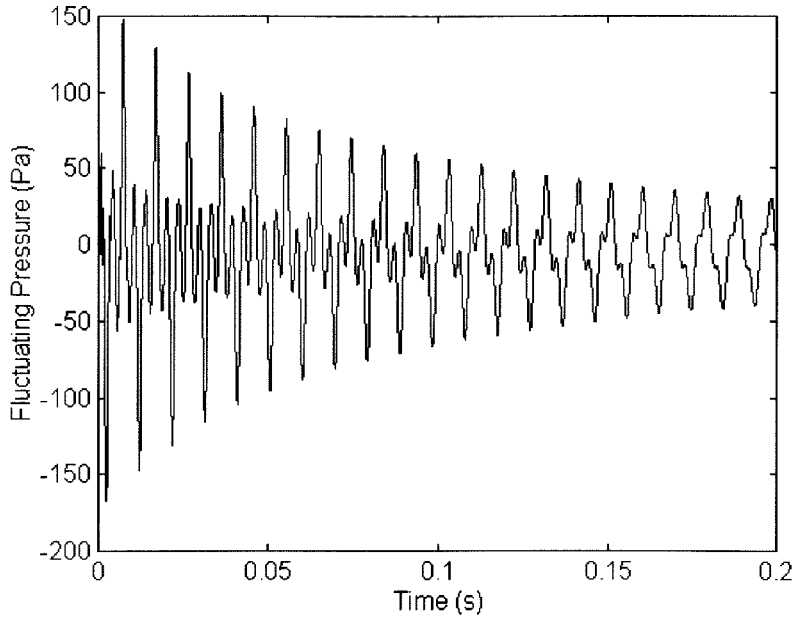

Figure 3-5 Closed-Open Tube with Heat Source at L/2

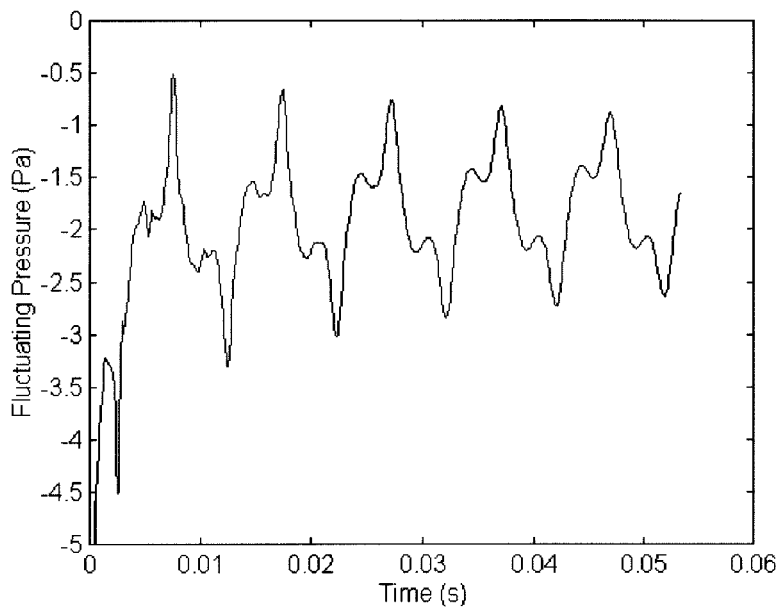

Figure 3-6 Closed-Open Tube with Heat Source Reduced by Half at L/2

Results were also obtained for a configuration in which the upstream and downstream boundaries where acoustically closed. The power source was 40,000 W/m^2, which corresponds to

the experimental case with the power source at 400 W. The power source was added to the system at two points, L/4 and 3L/4. Figure 3-7 shows the pressure records at L/3 for these cases. As expected, placing the heat release at L/4 led to a damped system and pressure oscillations on the order of the cold flow simulation. The 3L/4 case, as was expected, has the largest amplitude oscillation of the first harmonic. The unsteady numerical frequency is 190 Hz, which is comparable to the theoretical frequency of 183.6 Hz. Figure 3-8 shows the acoustic mode shapes from the numerical results. Since the system is acoustically closed at both ends, the pressure node is at L/2. The velocity mode is not a smooth sine function. There is a noticeable kink in the curve at the location of the heat release due to the jump in velocity across the temperature discontinuity. Also, the velocity perturbation is not zero at the outlet boundary. I am not exactly sure why this is the case. The kink in the velocity mode at the heat source may be the reason for this unexpected condition. However, it should be noted that the fluctuating mass flux, ρu, has a smooth sinusoidal shape across the entire chamber, indicating that the kink in the fluctuating velocity is likely not a numerical artifact.

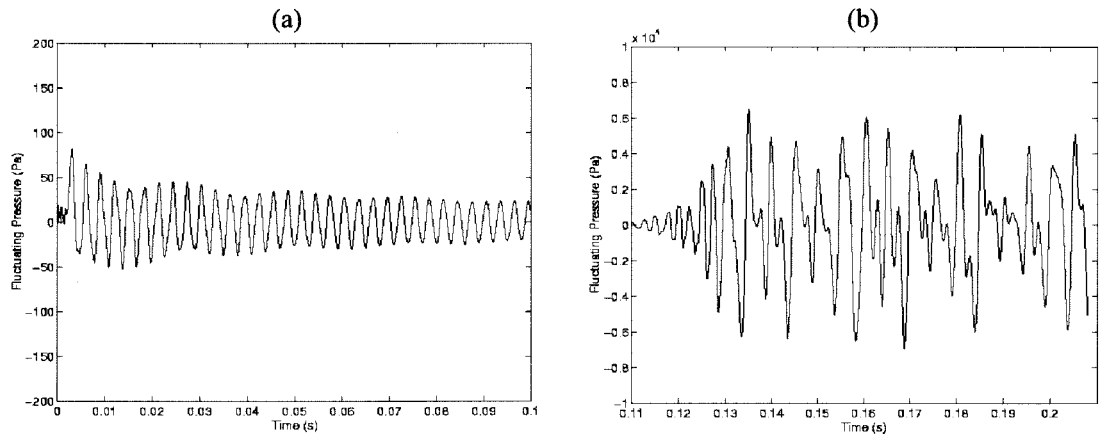

Figure 3-7 Results for Heat Source in Tube Acoustically Closed at Both Ends

(a) Heat Source at L/4; (b) Heat Source at 3L/4

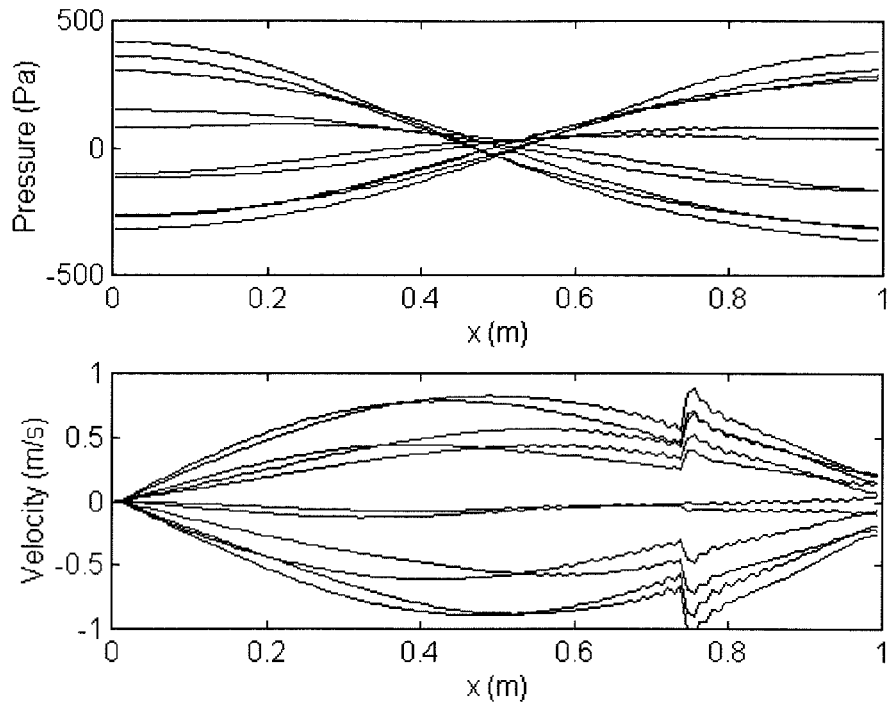

Figure 3-8 Pressure and Velocity Mode Shapes with Heat Source at 3L/4

Understanding how the heat release fluctuations interact with the flow field can be examined in the case where the heat release is at 3L/4. The heat release in this case is assumed to be the change in the stagnation enthalpy across the heat source. Figure 3-9 shows the time dependence of the fluctuating velocity, pressure and heat release. If we take τ as the period of the first harmonic, then the pressure term lags the velocity by $\tau/4$ and the heat release lags the velocity by $\tau/8$ at the flame location. Averaging over a period of the oscillation, the heat release is overall in phase with the pressure fluctuation, leading to a driven flow case.

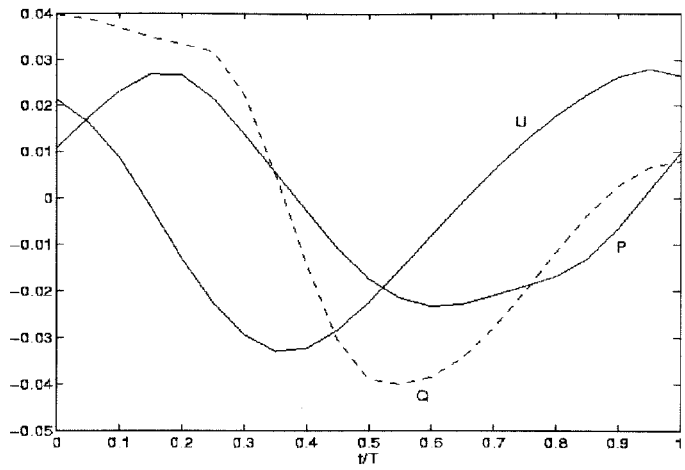

Figure 3-9 Fluctuating Flow Variables During Cycle of Oscillation with Heat Release at 3L/4

This relation between the heat release and the pressure was first described by Rayleigh in the 1800's and was given the form in equation (3-1). The pressure oscillation is driven when $R > 0$ and damped when $R < 0$. For the case with the heat release at 3L/4, R is greater than zero and the system is driven. When the heat release is placed at L/4, R is less than zero and the system is overall damped. In this case, the heat release lags the velocity by $\tau/8$, but the pressure leads the velocity fluctuation by $\tau/4$.

As these results demonstrate, the frequencies determined by the numerical simulations of the Rijke tube compare well with the theoretical predictions. Also, the location of the heat release and the subsequent driving or damping of the oscillations matches what has been observed experimentally. The problem at this point is the flexibility of changing the boundary conditions to better match the experimental configurations. Even with this problem, the numerical results demonstrate an easy method for the modeling of the heat release. In the above cases, it was shown that the heat release fluctuation lags the velocity fluctuation by $\tau/8$. This is a basic n-τ model, which can then be used, in the approximate analysis that will be described in more detail in Appendix C.

This result agrees with the theory for heat conduction in a Rijke tube (Raun et al., 1993). For the case of an electrically heated wire mesh, a positive velocity fluctuation will bring in more cold air, which will in turn enhance the heat conduction by increasing the temperature differential between the wire mesh and the air. A negative velocity fluctuation will have the opposite effect and will diminish the amount of heat conduction. However, the heat conduction does not respond instantaneously to the change in the velocity, leading to a time delay. Given the characteristic time for heat conduction $\tau_c = \kappa / \bar{u}^2$ in a low speed flow, and the period of oscillation $\tau = 2\pi/\omega$, we can figure out the lag for a given system. For the case shown in Figure 3-9, the mean flow velocity is 0.25 m/s, $\kappa = 22.5 \times 10^{-6}$ m^2/s and the frequency is 185 Hz, leading to a theoretical lag of 24°, which is about half of that shown in Figure 3-9.

3.1.3 Premixed Flame in a Pipe

The remaining simulations of the Rijke tube were performed with combustion of premixed fuel and air at a specified location. The fuel used in the simulations is methane, CH_4. For methane in air the fuel-to-air ratio is 0.0584 at stoichiometric conditions. The configuration domain for the simulations is the same as shown in Figure 3-1(c). The length of the chamber, L, is 1.0 m in the following cases and the inlet height in the y-direction is 0.1 m. The experimental case is driven by natural convection. However, the simulation assumes no gravity forces. In the simulation, it is assumed that the air and fuel mixture is being forced through the chamber by another mechanism (e.g., an upstream reservoir). Without gravity, the flame is assumed to be flat in the vertical plane. The time step for the simulations is 2 μs, which is less than the time step required to capture the pressure wave propagation across a grid element. The sampling frequency for the time history output is 25 kHz. A steady state solution was determined first in all the following simulations. This steady state solution was used as the initial condition for the transient simulations. The steady state solution for the premixed flame in a tube consists of a step jump in

the temperature at the flame location. The thickness of the flame is much less than the grid spacing, so the temperature jumps from 300 K to the adiabatic flame temperature from one grid point to the next at the flame front. There is also a step jump in the velocity and density corresponding to the jump in temperature. The pressure, for the steady state solution, is constant across the flame front.

All of the following simulations solve the momentum, enthalpy and species conservation equations along with the modified continuity equation for the pressure term. The density is solved using the ideal gas law. The flame in these simulations was assumed to be laminar and therefore the k-ε model was not solved to evaluate the turbulence. The mass fraction of the fuel was fixed for a given region of the flow domain to simulate a flame front held in place by a wire mesh at a given location in the flow domain. The flame front is allowed to move and the transient solutions will show that the flame front broadens and curves in the center of the tube in the presence of a large-scale oscillation.

The first attempts were made for a system in which the boundaries were acoustically open. The mean inlet velocity in these cases is 0.5 m/s and the flame is located at L/4. Figure 3-10 shows the pressure record for the case with an equivalence ratio of 0.57. The first three modes given by the numerical results have frequencies 267.9, 549.7 and 826.8 Hz, which compare well with the theoretical predictions of 277.5, 615.9, and 843.8 Hz. The method for determining the theoretical predictions is described in Appendix B. The largest discrepency is a 10.6% difference in the second mode. Figure 3-11 shows the pressure record for the case with an equivalence ratio of 1.0. In both of these cases, there does not seem to be enough power supplied to the system to sustain an instability. The inability to sustain a large amplitude oscillation may also be caused by fixing the pressure at the upstream and downstream ends of the numerical domain. The impact of fixing the pressure on the oscillation amplitude is just speculation based on the examination of various simulation configurations. The pressure is fixed to provide an open-open boundary

condition; however, fixing the pressure in the numerical calculation may be akin to imposing a non-reflecting boundary condition. The fixed pressure conditions acts as an additional damper on the system, leading to a stable solution.

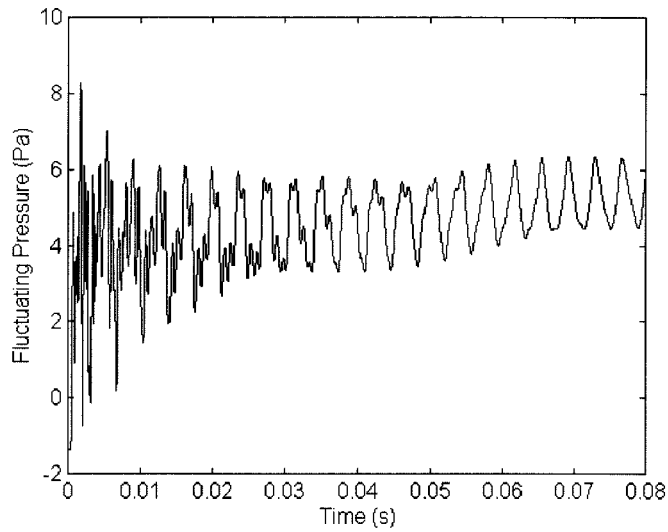

Figure 3-10 Open-Open Rijke Tube with Flame at L/4 (ϕ = 0.57)

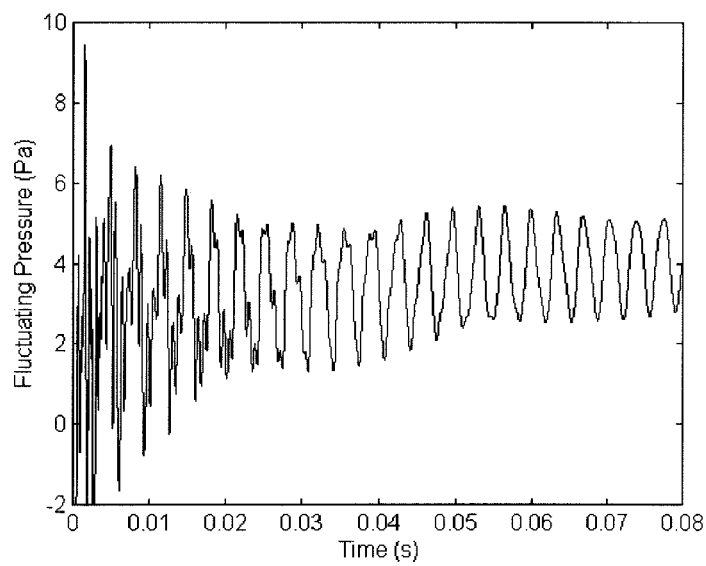

Figure 3-11 Open-Open Rijke Tube with Flame at L/4 (ϕ = 1.0)

The next set of simulations used the default boundary conditions for the ANSWER code so that the inlet was closed acoustically and the outlet was open acoustically. The mean velocity in all these cases was 0.25 m/s and the equivalence ratio was 0.57. Figure 3-12 shows the results of the simulation when the flame front was located at the L/4 location. The numerical modes had frequencies of 189, 383 and 725 Hz compared to the theoretical estimates of 188.8, 420.3 and 774.2 Hz. Again, the worst discrepancy is an 8.8% under-estimate of the second mode. The results show that the first mode is the main excited mode and that the oscillation is decreasing slowly. It may be that the amount of power supplied is not enough to balance the viscous and boundary losses. It is not readily apparent why the oscillation grows initially before decaying in this simulation. It may be that the system is unstable in the linear domain when the amplitude is small (< 500 Pa in this case), and that the non-linear effects that develop at higher amplitude lead to a damped system.

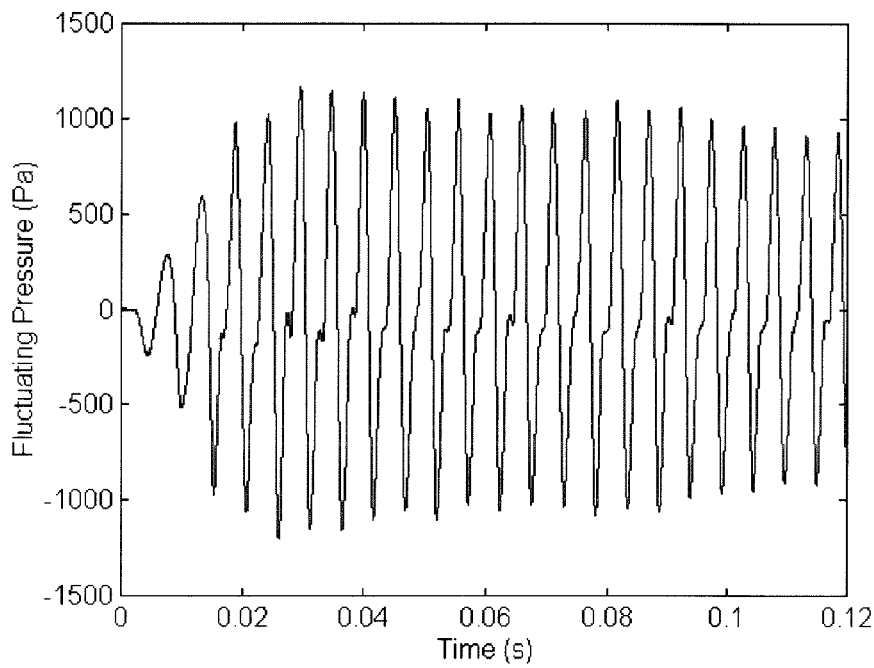

Figure 3-12 Closed-Open Tube with Flame at L/4 (ϕ = 0.57)

The results shown in Figure 3-13 are for a case in which the flame front has been shifted to the L/2 location. Theory based on Rayleigh's criterion indicates that for a closed-open system, placing a flame between L/3 and 2L/3 should drive the second harmonic if we assume that the fluctuating heat release lags the fluctuating velocity by no more than 180°. Since the fluctuating pressure of the second harmonic lags the velocity by 90° between L/3 and 2L/3, the heat release will be in phase with the pressure, leading to a positive value of Rayleigh's parameter and a driven system. Figure 3-14 shows the FFT for the pressure record in Figure 3-13. The second harmonic is indeed at a higher amplitude than the fundamental frequency and the higher harmonics. The unstable frequency does not change by more than 5 Hz between t = 0 s and t = 0.15 s in Figure 3-13.

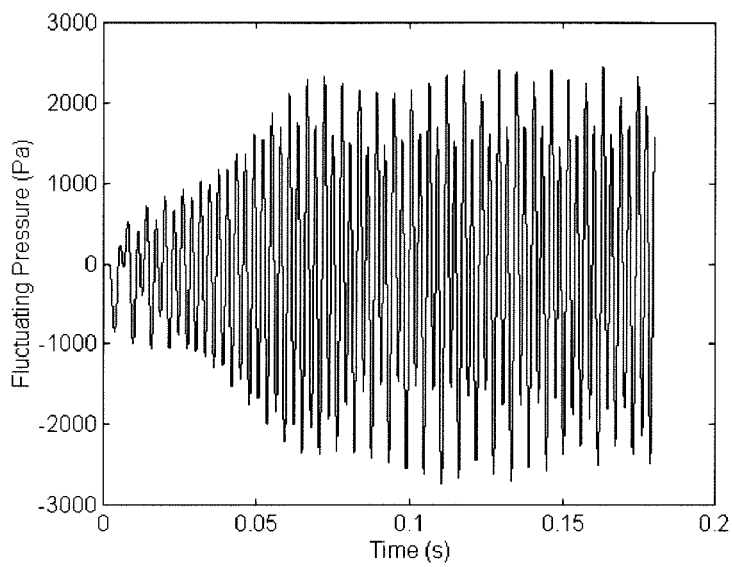

Figure 3-13 Closed-Open Tube with Flame at L/2 (ϕ = 0.57)

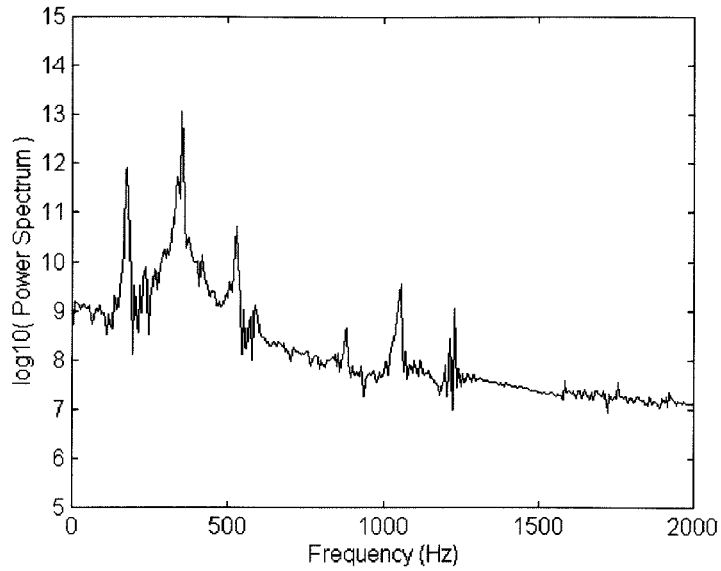

Figure 3-14 FFT of Pressure Record Shown in Figure 3-13

The interest in these simulations is in obtaining a model of the oscillating heat release within the chamber. Since the majority of the heat release is due to a chemical reaction, the heat release term can be determined with knowledge of the local species and temperature field via:

$$\dot{Q} = -\sum_{n} \bar{h}^{o}_{f_n} \omega_n W_n \qquad (3\text{-}4)$$

where $\bar{h}^{o}_{f}$ is the formation enthalpy, ω is the reaction rate and W is the mass fraction. The maximum heat release is localized near the fuel source. An examination of the local behavior is shown in Figure 3-15. The result is for the case shown in Figure 3-13 with the heat release at L/2. The heat release lags the pressure by about 30° for the second harmonic and the pressure fluctuation lags the velocity fluctuation by 90°. Rayleigh's parameter, equation (3-1), for this case is overall positive during a period of the second harmonic, indicating a driven system.

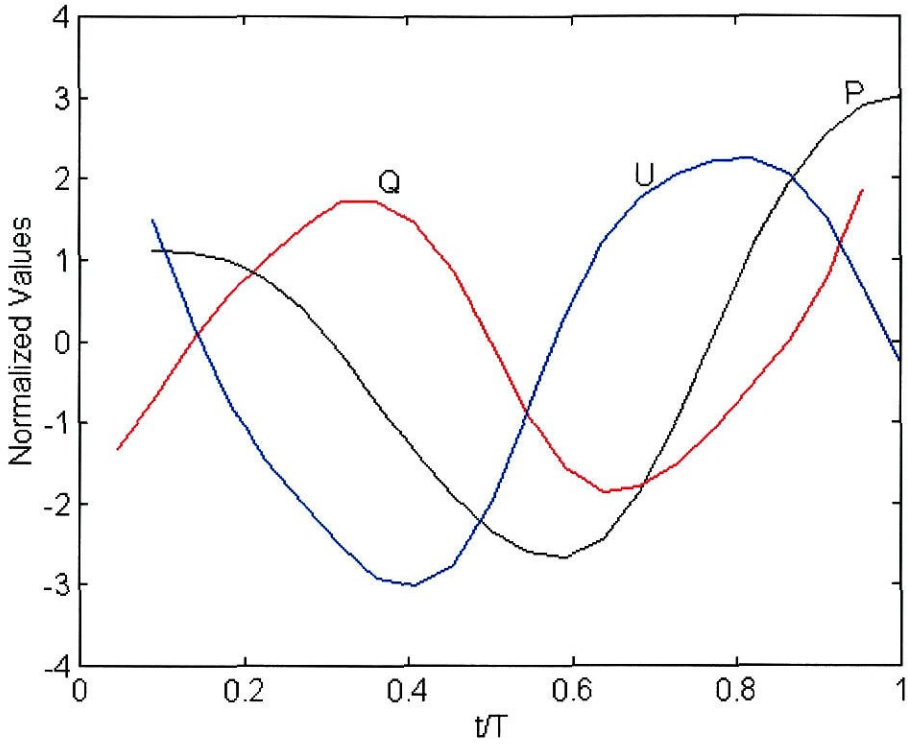

Figure 3-15 Localized Flow Field Fluctuations at Flame Front

Also of interest for the flame in a tube is the level of NOx produced in both a steady and an unsteady flow configuration. As was mentioned in Chapter 1, work by Keller and Hongo (1990) showed that in an experimental pulse combustor, the NOx levels at the exit plane were significantly lower when the combustor was run under pulsing conditions. It should be noted that the work by Keller and Hongo (1990) involved a fluctuating mass flow rate at the inlet to the chamber to drive the oscillations. The simulations performed as part of this thesis had a steady mass flow at the inlet and the oscillations were driven by the interaction of the heat release and the pressure. For this thesis, an additional reaction rate was included in the case shown in Figure 3-13 to provide at least a qualitative assessment of the NOx levels in this basic configuration. The flame was at L/2 and was burned lean ($\phi = 0.57$). When the oscillation was damped out (steady state case), the average NOx mass fraction at the exit plane was 2.19e-3. When the oscillation was

included (unsteady second mode) with a frequency of 348 Hz, the average NOx mass fraction at the exit plane was 1.85e-4, which is almost 12 times less than in the steady case. Figure 3-16 shows the mean mass fraction of NOx in the tube for the stable and unstable case. For the unsteady case, the residence time in the hot flame region is reduced over the residence time in the steady case, leading to a reduction in the production of NOx. It should be noted that the NOx production rate may not be as sensitive to fluctuations when the reaction is stoichiometric and there is not an excess of oxygen for the NOx reaction to take place.

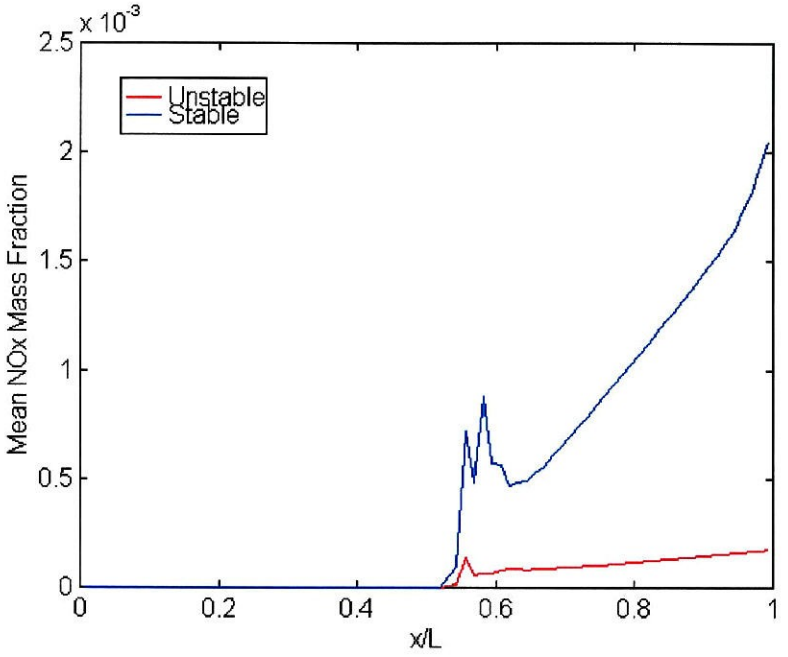

Figure 3-16 Mean NOx Mass Fraction During Stable and Unstable Conditions

Since the NOx production rate is extremely sensitive to the temperature, the mean temperature was examined in both of the cases shown in Figure 3-16. Figure 3-17 shows the mean temperature in the tube for the stable and unstable case. The mean temperature in the unstable case drops off severely between the flame and the exit plane, as compared to the mean temperature in the stable case, which does not change more than a few degrees. The reduction in the mean temperature downstream of the flame leads to a reduction in the production rate of NOx

and therefore a reduction in the level of NOx at the exit plane in the unstable case. The oscillations in the chamber lead to a thicker and curved flame front in the center of the pipe. The thicker and curved flame front leads to a reduction in the average temperature in comparison with the same position in the steady state simulation. However, the unstable flame front does reach the same maximum temperature as the stable case and there is complete burning of the methane. Downstream of the flame front, the temperature drops off significantly near the walls, indicating that the unstable behavior is increasing the heat conduction to the walls. This increased heat conduction, due to fluctuations in the velocity in the boundary layer at the wall, leads to a reduction in the mean temperature downstream of the flame front and subsequently a reduction in the NOx production. A similar reduction in the mean temperature was observed by Keller and Hongo (1990) and has also been observed for an unsteady flow in an experimental Rijke tube with an electrically heated wire mesh. Further discussion of the NOx production in an unsteady flow field will be discussed in Chapter 4 and Chapter 6.

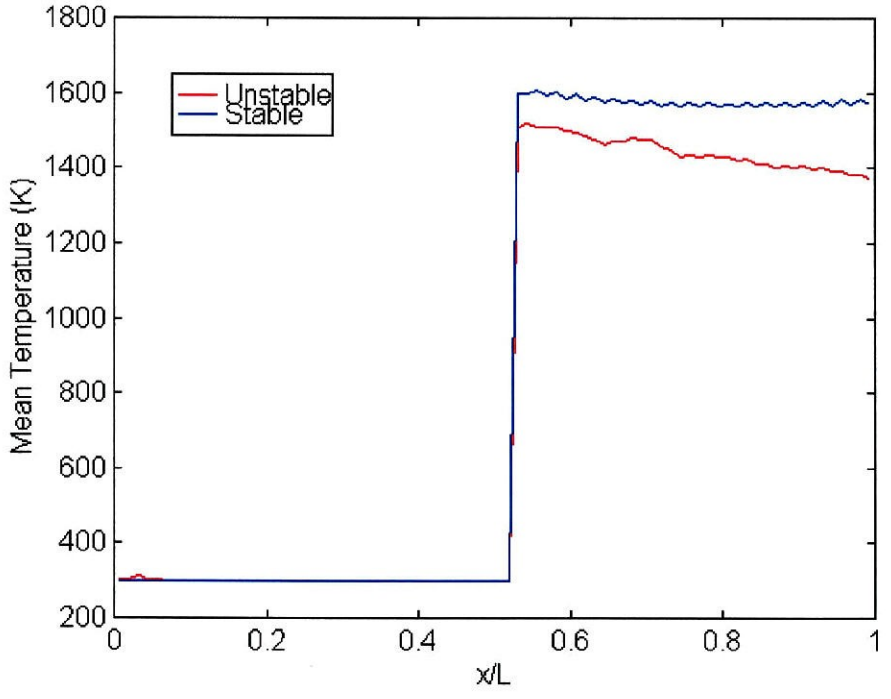

Figure 3-17 Mean Temperature During Stable and Unstable Conditions

Chapter Four

Simulations of Instabilities and Vortex Shedding in a Dump Combustor

Another basic chamber design is the dump combustor. The dump combustor can be used to represent the combustion region within a ramjet engine. In addition to chemical-acoustic interactions, the dump combustor also demonstrates interactions between the vorticity and the acoustic field. Those interactions exist most strongly when the vortex shedding frequency at the dump plane and the acoustic frequency are nearly coincident. The vortex energy can drive the acoustic instability; likewise, acoustic energy can drive a vortical instability.

Work on the unsteady nature of this flow has been carried out by a number of researchers (Schadow and Gutmark, 1992; Smith and Zukoski, 1985; Sterling and Zukoski, 1987; Yu et al., 1987; Schadow et al., 1987; Sterling, 1987; Zsak, 1993) to be mentioned within this section for comparison with the numerical results. The main comparison with experiments will be made for work conducted at the California Institute of Technology. That work was initiated to model the unstable behavior in a ramjet engine. The combustor was designed to run under atmospheric conditions and to represent 2-D flow. The fuel and air were mixed far upstream of the dump plane since the experiments were concerned with the behavior of premixed combustion. Menon and Jou (1991) give results for the coupling between combustion and vortex shedding in an axisymmetric ramjet combustor. They had a premixed flow, a dump ratio of 2:1 and a nozzle at the exit to deal with the problems of the downstream boundary condition. Menon and Jou showed very good results with a LES model of turbulence and a single scalar chemistry model. Depending on the area ratio at the nozzle Menon and Jou were able to show a large-scale or small-scale instability. The vortex shedding matched the form of the experimental work by Smith and Zukoski (1985). The differences between this work and that by Menon and Jou are the dump ratio, the exit

boundary conditions, the complexity of the chemistry models and the use of a k-ε turbulence model instead of LES.

One possible application of a transient numerical simulation is the study of control strategies for reducing the unstable motions within a combustion chamber. Both active and passive control techniques can be examined numerically at a lower cost than experimental methods. As a demonstration of a passive control technique, the numerical simulation of a dump combustor with two different Helmholtz resonator designs will be presented in this chapter.

In addition to information about the interaction between the acoustic field and the flow field, the numerical simulations can also provide information concerning the interaction between the flow field and the chemical reaction rates, with an emphasis on the production of pollutants such as NOx and CO. The results of pollutant production in a dump combustor will be presented at the end of this section and examined in more detail in Chapter 6.

4.1 Dump Combustor Configuration

A sketch of the dump combustor configuration is shown in Figure 4-1. For the inlet section, X_S is 0.43 m and H_S is 0.0254 m. The step ramps up to a 75% blockage at the dump plane. The height at the dump plane, D, is 0.00635 m and will be used as the reference length scale in the rest of the chapter. The dump section length is 0.86 m leading to a total length X_L of 1.29 m. The height, H_L, of the dump section was varied in the numerical simulations to compare with the experimental work performed at Caltech. An expansion ratio, H_L:D, of 4:1 and 12:1 was used in the simulations. However, in all of the simulations with an expansion ratio of 4:1, the instability caused the flame to "blowout" within a few periods of the oscillation, leading to a cold flow. For this reason, all of the results presented in this chapter will be for an expansion ratio of 12:1. Premixed fuel and air is preconditioned before the inlet section and the exit plane is open to

the atmosphere. In later cases, the mixture of the fuel and air will be spatially unmixed to examine the influence of an unmixed flow field on the instabilities. The flow is considered to be 2-D due to the small extent of the chamber depth. The numerical grid is 62 x 52 and is spaced to provide more detail about the flow field in the region near the dump plane inlet. The theoretical analysis of the acoustic modes in the chamber, to be covered in Section 4.3, shows that the interface between the plenum chamber and the inlet section behaves like a closed acoustic boundary. Because the default boundary condition for the numerical inlet is acoustically closed, it was determined that simulating the behavior in the plenum chamber was not necessary to obtain correct numerical results. Turbulence properties are determined by the k-ε model and these factors are included in the eddy-breakup model, which impacts the chemical reaction rates.

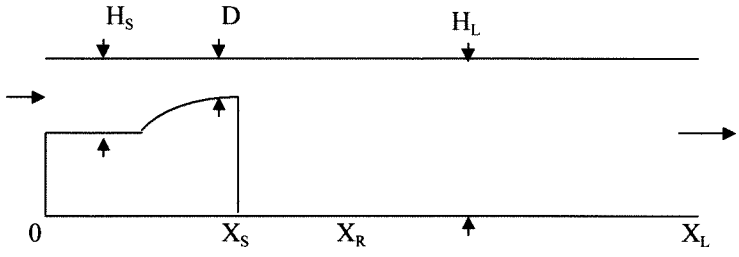

Figure 4-1 Sketch of Dump Combustor Configuration

4.2 Steady State Results

The main case examined in this section is configured to represent the experimental results of Zsak (1993) for an expansion ratio of 12:1 and a methane-air mixture at an equivalence ratio of 1.3. The mean flow velocity at the dump plane, U_{Step}, is 21 m/s. This case will be designated subsequently as Case A. The other results in the section on transient flows will be presented for comparison with this case.

Figure 4-2 shows the steady state temperature and axial velocity contours for Case A. In the figure for the axial velocity, the solid lines indicate a positive value and the dashed-dot lines indicate a negative value. The flame is stable and the reaction zone is thicker than is observed for the premixed flame in the Rijke tube. The increased flame thickness is due to the higher turbulence intensity in this system, which corresponds to a larger turbulent mixing time and a reduced reaction rate. The flow past the backward facing step also develops a clear recirculation zone. The recirculation zone is composed of hot burned products, which help ignite the incoming cold mixture. The recirculation length, X_R, is defined as the distance from the dump plane to the stagnation velocity point along the lower wall. For this steady state simulation, the recirculation length is 0.157 m. This value of the recirculation length is lower than that for a non-reacting simulation with the same properties as Case A. The recirculation length in the non-reacting simulation is 0.382 m. The numerically determined recirculation length for a cold flow simulation compares well with experimental data. Based on the length D and the velocity U_{Step}, the Reynolds number Re = 8890. For non-reacting flows and Re > 6600, the recirculation length, X_R, divided by the step height, S, has been determined to be constant. The step height, S, in our case is equal to 11D. The numerical simulation with ANSWER yields $X_R/S = 5.47$ which is in close agreement with the experimental results of de Brederode and Bradshaw (1972) who measured $X_R/S = 6$ and Moss, Baker and Bradbury (1979) who measured $X_R/S = 5.5$. The ratio for the reacting flow simulation is 2.24. The difference between the reacting simulations and the cold flow simulations is due to the increased amount of gas expansion caused by the flame. The expansion at the flame forces the recirculation zone further into the corner of the step, leading to a reduced recirculation length.

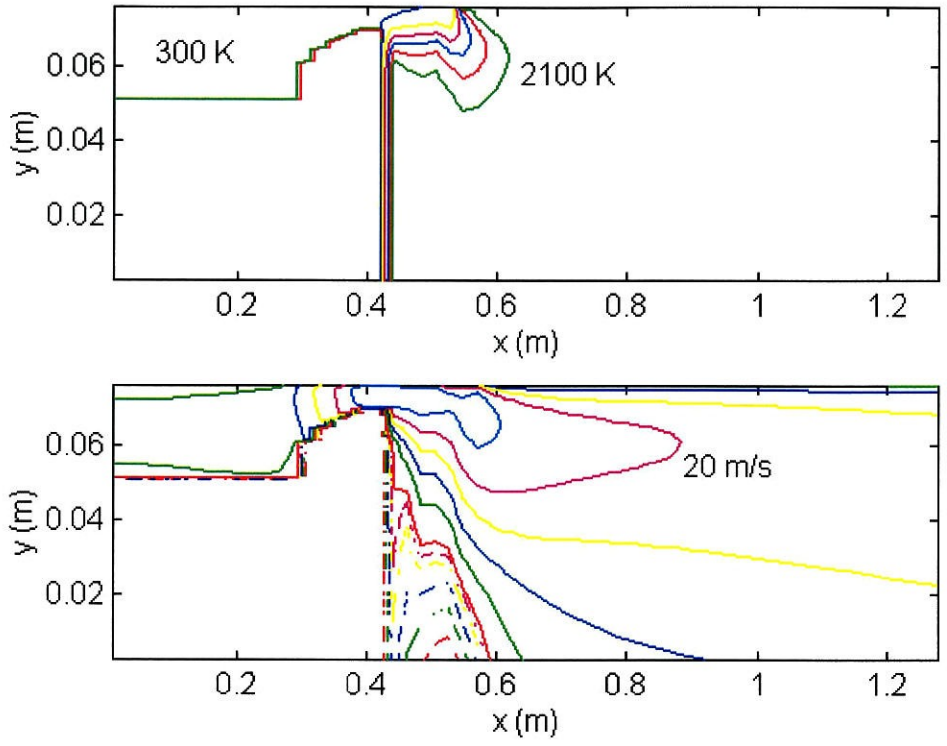

Figure 4-2 Steady State Results for Case A: (a) Temperature; (b) Axial Velocity

4.3 Transient Results

A linear one-dimensional acoustic analysis was performed by Zsak (1993) on the dump combustor configuration to determine the main acoustic modes. Allowing for small variations in the mean temperature field, the main acoustic modes for the 12:1 expansion ratio were 190 Hz, 222 Hz and 278 Hz. The experimental results closely matched the theoretical acoustic modes. The primary mode of oscillation was at 235 Hz, the second mode was 187 Hz and the third highest mode was 281 Hz. It should also be mentioned that the experiments for Case A showed acoustic beating between the 235 Hz and 187 Hz modes. With repeated tests for various velocities and equivalence ratios, a stability map can be generated for a given combustor design. A stability map was not generated for the 12:1 expansion ratio; however, Sterling (1987) did generate a stability map for a methane-air flame in a 4:1 expansion ratio dump combustor. The

stability range is shown in Figure 4-3 and is presented because it is expected that the 12:1 expansion ratio case should follow a similar form. Along with Case A, four other simulations noted in the figure will be presented in this section and will give some indication of the form of the stability map for this configuration.

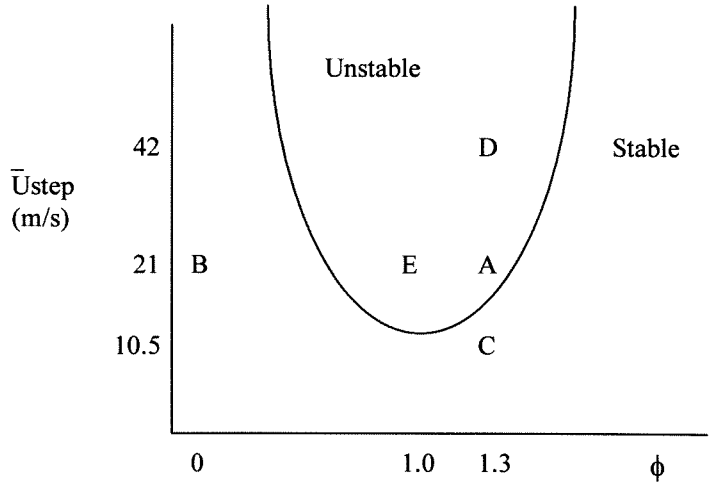

Figure 4-3 Stability Map for 12:1 Dump Combustor Simulation

Figure 4-4 shows the results of the transient numerical simulation of Case A. The steady state solution was used as the initial condition in the transient simulations. The velocity, temperature, turbulence and chemistry values were held fixed at the inlet for the transient simulations. The data is obtained for a point directly downstream of the dump plane and 4D below the top wall. The primary unstable acoustic mode for this simulation is 226 Hz and the second mode is 165 Hz. These values compare well with both the theoretical and experimental acoustic modes determined by Zsak (1993) (235 and 187 Hz). The peak amplitude of the pressure oscillation is around 2% of the mean pressure in the system, which is 1.013e5 Pa, about half of the amplitude determined in the experimental case.

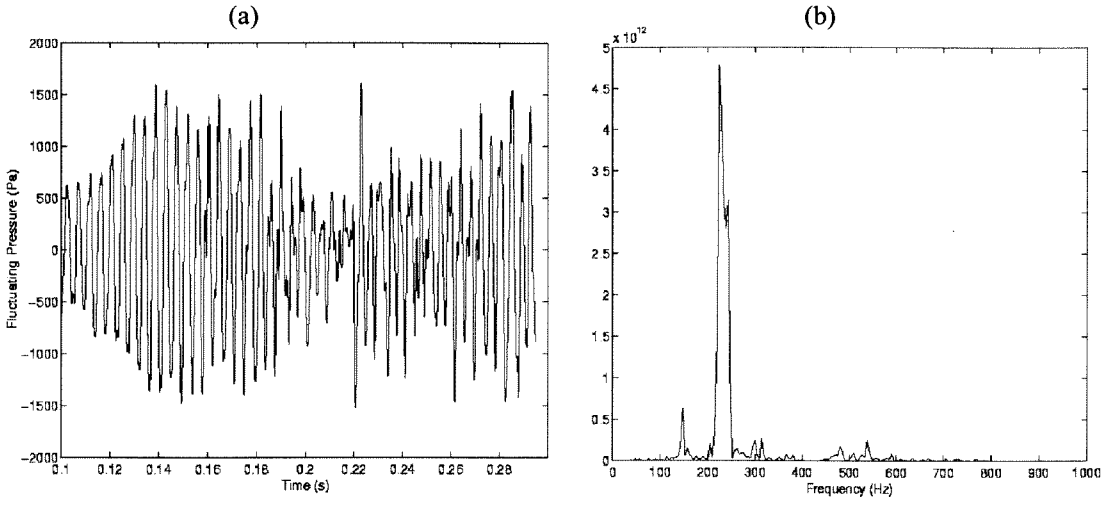

Figure 4-4 (a) Case A Transient Simulation; (b) FFT of Pressure Record

Figure 4-5 shows the behavior of the heat release during a period of the primary mode of oscillation. Rayleigh's parameter, R(x,y,z;t) can also be determined by averaging over the entire flow domain and one cycle of the oscillation. Figure 4-6 shows the value of R(x,y). The value of R averaged over time and space is positive for this case, indicating that the system is overall driving. Positive R is indicated by the solid lines and negative R by the dashed lines.

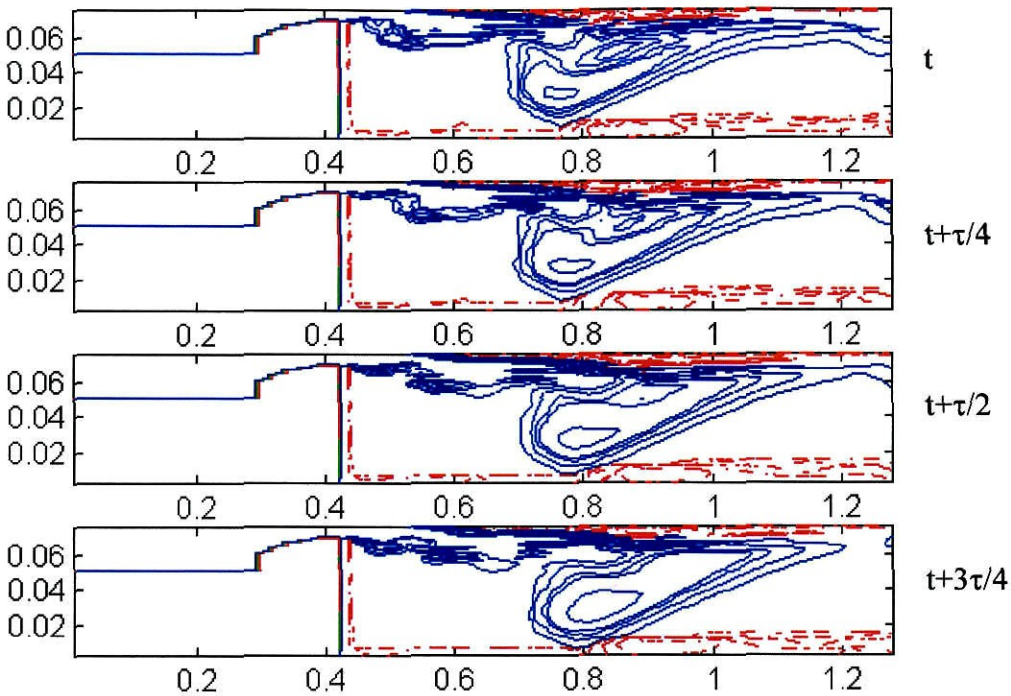

Figure 4-5 Heat Release During One Cycle of Oscillation

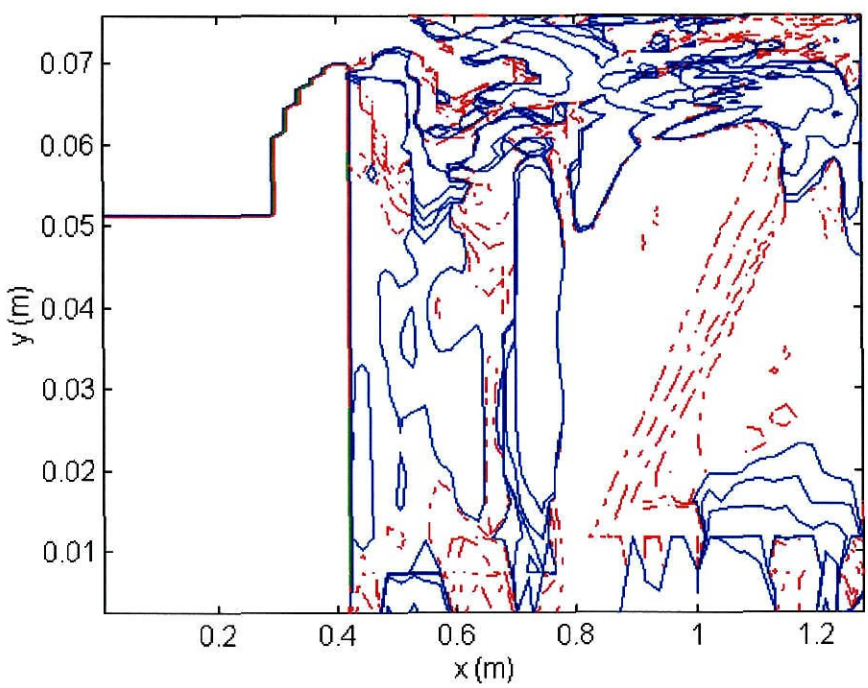

Figure 4-6 Rayleigh's Parameter Contour for Case A

Figure 4-7 shows the axial velocity contours during a period of the oscillation for Case A. The solid lines are positive velocity and the dashed-dot lines are negative. There is a clear vortex shed from the step. In the first image, the small vortex is at about x = 0.5 m, y = 0.05 m. As time progresses, the vortex seems to interact with a recirculation zone centered around x = 0.75 m. This interaction seems indicative of the vortex striking the bottom wall and dissipating. The effect of the vortex shedding is also shown clearly in the work by Menon and Jou (1991). The generated vortex strikes the wall and the reaction front broadens as the flame front propagates downstream.

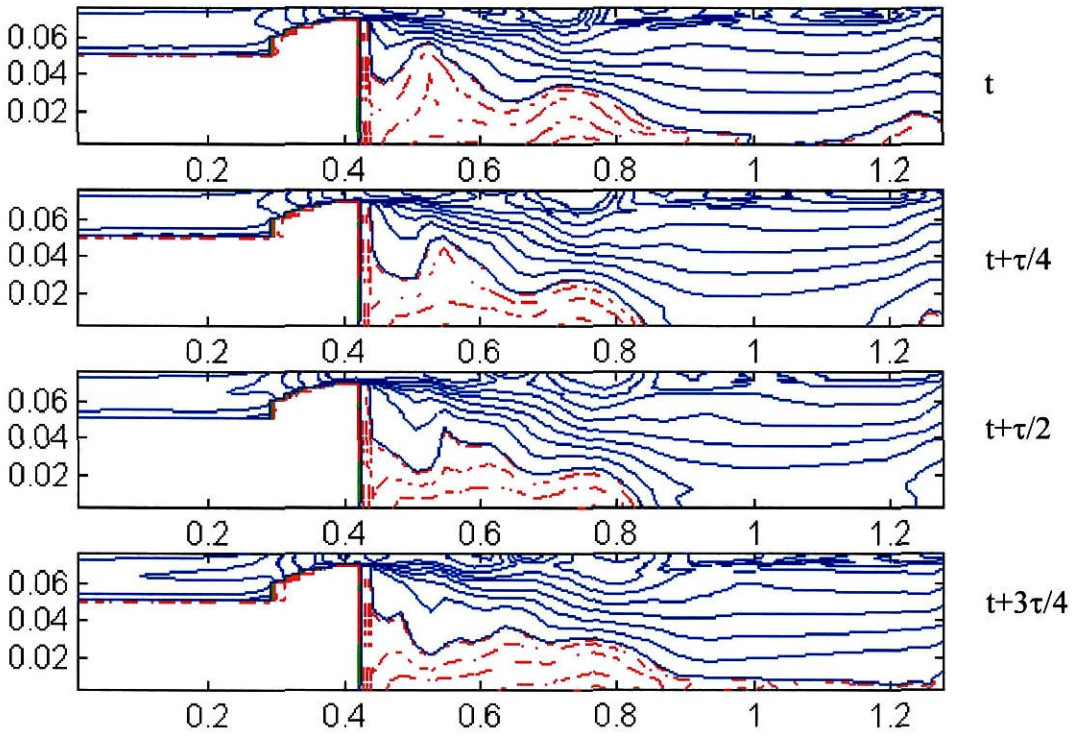

Figure 4-7 Axial Velocity During a Period of the Cycle for Case A

In order to show that the large scale oscillations were not a result of numerical effects, Case A was run with the reaction rates set to zero. In this case, designated in Figure 4-3 as Case

B, the interaction between the heat release and the other flow field variables has been removed and the only possible oscillation is due to vortex shedding. Figure 4-8 shows the pressure history for this case. The main mode of oscillation is 216 Hz and the peak amplitude never rises above 100 Pa, which is an order of magnitude lower than Case A. This demonstrates conclusively that in this simulation, the unsteady heat release, in conjunction with the vortex shedding, is driving the large-scale oscillations.

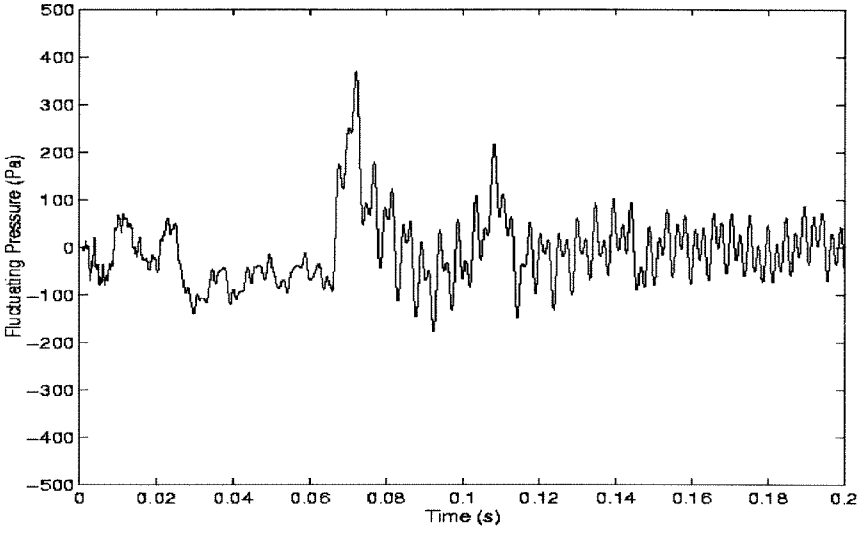

Figure 4-8 Case B, Mean Step Velocity = 21 m/s, No Reaction

Three other cases shown in Figure 4-3 were examined for the dump combustor. The first two, Cases C and D, were run at the same equivalence ratio as Case A with variations in the velocity at the step. In Case C, the average step velocity was reduced by half and in Case D, the velocity was increased by a factor of two over the step velocity in Case A. If the stability map of the 12:1 expansion ratio compares with that for the 4:1 expansion ratio shown earlier, then the reduction in velocity should make the system more stable and the increase in velocity should place the system in a more unstable region. The third case, designated as Case E, involved a reduction in the equivalence ratio from 1.3 to 1.0 with the same step velocity as Case A. A

simulation not shown here was run for an equivalence ratio of 1.8. In this case, there was no flame and therefore no heat release. Because of this, the results were similar to Case B with no reaction and the same mean flow velocity.

Figure 4-9 shows the results for Case C with a reduced step velocity. The pressure levels for this case are low compared with those in Case A. There is a noticeable absence of vortex structures, leading to a linear flame region downstream of the dump plane. Because of the steady flame structure, the heat release does not oscillate at the level seen in Case A; therefore, the unsteady heat release is not able to provide enough energy to the pressure field to drive a large-scale instability.

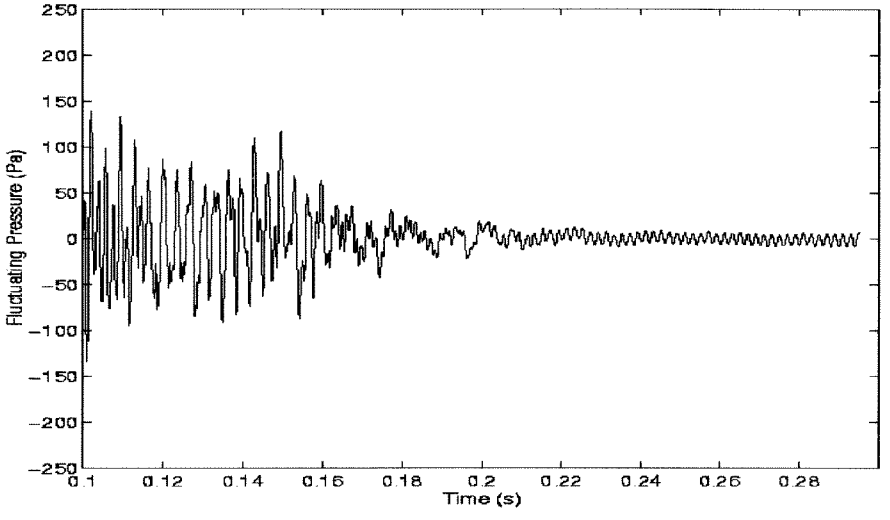

Figure 4-9 Dump Combustor Case C, Mean Step Velocity = 10.5 m/s

Figure 4-10 shows the results for Case D with an increased step velocity. The system demonstrates amplitudes of pressure oscillation that are slightly above those for Case A. Also, the frequency of the oscillation has changed. The increased step velocity corresponds to an increase in the expected vortex shedding frequency. Since the oscillation is in tune with the shedding of vortex structures, the primary unstable acoustic frequency for this case has increased to 250 Hz.

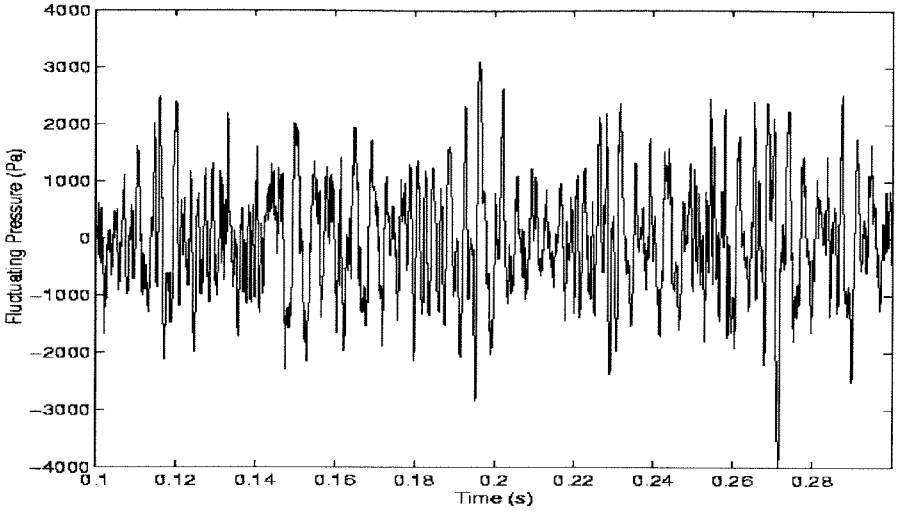

Figure 4-10 Dump Combustor Case D, Mean Step Velocity = 42 m/s

Figure 4-11 shows the results for Case E with a reduction in the equivalence ratio to 1.0. The pressure levels have increased from those of Case A and the frequency has shifted slightly to the higher value 245 Hz. This shift in frequency is mainly due to the increase in the mean acoustic velocity. Since the flame is burning all of the methane, the flame temperature is increased and therefore so is the mean temperature in the chamber.

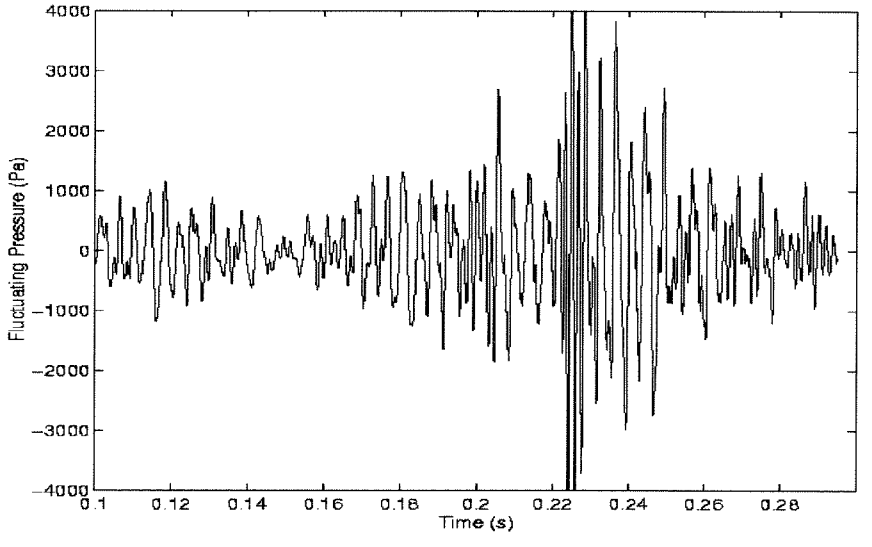

Figure 4-11 Dump Combustor Case E, Equivalence Ratio is 1.0

All of these cases have been mapped on Figure 4-3 and a possible zone between stability and instability has been sketched in a manner similar to that for the 4:1 expansion case. This stability map is clearly deficient because there are only five cases. However, it does demonstrate that the numerical simulations can be applied to a series of configurations for a given system providing results that demonstrate stable behavior and large-scale instabilities.

4.4 Passive Control Using Helmholtz Resonator

This section is designed to demonstrate the use of numerical simulations for the study of control techniques. A basic passive control method uses a Helmholtz resonator or a series of resonators at some location in the chamber. Helmholtz resonators have been used as sound filters and noise suppressers since the late nineteenth century (Harrje, 1972). The main source of energy loss is due to viscous damping as the mass of the fluid oscillates back and forth in the resonator. A series of resonators can couple together to form either a high pass or low pass filter depending on the resonator configuration. A Helmholtz resonator is a small cavity of volume V_{cav} connected to the main chamber by an orifice of length l_o and diameter d_o. Figure 4-12 shows a sketch of a typical resonator cavity.

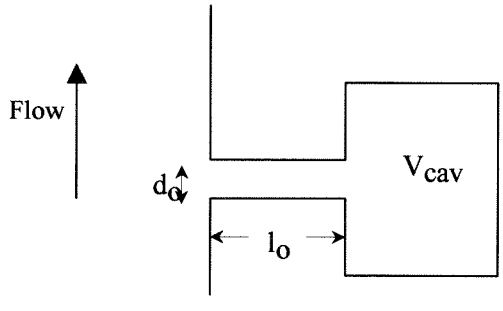

Figure 4-12 Typical Helmholtz Resonator Configuration

The dimensions of the resonator are typically small in comparison with the wavelength in the chamber. The motion of the gas in the resonator is analogous to a mass-spring-dashpot system. The resonant frequency for a Helmholtz resonator is given by:

$$\omega_r = \bar{a}\sqrt{\frac{A_o}{l_{eff} V_{cav}}} \tag{4-1}$$

where A_O is the area of the orifice connecting the chamber with the resonator cavity and l_{eff} is l_o + δ, where δ is an empirical length correction. Some difficulties with the Helmholtz resonator include tuning the cavity to a given unstable frequency. During the course of an instability, the temperature in the system and therefore the temperature in the resonator will change leading to a change in the resonant frequency. The change in the resonant frequency will lead to a de-tuning with the unstable frequency in the chamber and a reduced effectiveness in damping out a large-scale instability.

Figure 4-13 shows the two configurations examined for the dump combustor. The first resonator design (A) was configured to represent the generic resonator shape and still fit into the computational domain set up for Case A. The second resonator design (B) was configured to test the limit as the volume of the main cavity went to zero and we were left with only the orifice. A resonator made up of only the orifice represents a quarter-wave damping chamber. Any viscous damping in this configuration will be tuned to the fundamental quarter-wave in the chamber and the higher harmonics. The resonators were placed horizontally in the dump plane to simplify the simulation domain and may be placed vertically in later simulations for comparison purposes. Design (A) had a volume of 5.7e-3 m^3, an orifice length of 0.215 m and an orifice area of 0.012 m^2. The resonant frequency, based on a mean temperature of 300 K, is 171 Hz for this design. Design (B) had a length of 0.366 m and an orifice area of 0.012 m^2. The resonant frequency, based on a mean temperature of 300 K, is 246 Hz. Both of these configurations were used along with Case A and in both cases the temperature in the resonator was set to 300 K at the initiation of

the transient simulations. The temperature was started at this low value to allow for simpler calculation of the mean acoustic velocity on the resonator. However, during the course of the simulation, the interaction with the hot products only changed this value slightly, by no more than 50 K. Of course, the simulation was only run for a short amount of time and the effect of the hot products may change when the simulation is extended in time.

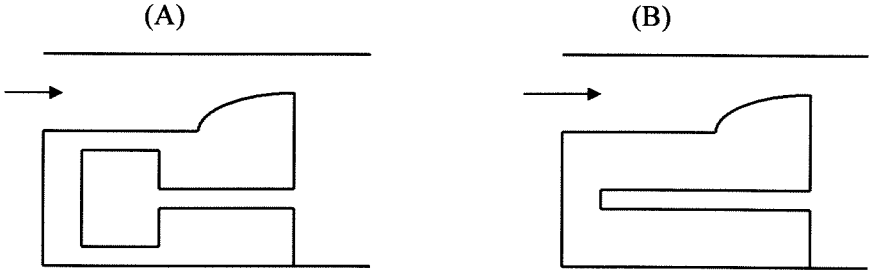

Figure 4-13 Helmholtz Resonator Configurations

Figure 4-14 shows the comparison between resonator (A) and the case without the resonator. The oscillations are damped in the case with the resonator. For resonator (A) the theoretical frequency of resonance is 171 Hz, which is between the first and second unsteady acoustic modes for Case A. Figure 4-14 shows the similar behavior with resonator (B). For this case, the quarter-wave resonance is 246 Hz, which is above the unsteady modes. However, in this configuration, the resonator still behaves well as a passive controller. Resonator configuration (A) seems to work better than (B) as a passive controller. One of the possible reasons for this is that there is a greater surface area in design (A), which allows for increased viscous damping. Tuning the resonant frequency of design (A) between the two unstable frequencies also may have improved the response to both frequencies. It could be that design (A) has a broader frequency response, allowing it to damp the high and low frequency instabilities. If the chamber had been tuned to only one of the unstable frequencies, it may not have had as large of an effect on the other unstable frequency. A de-tuned chamber may have also added to the larger oscillation amplitude

for design (B). The frequency started above the main unstable frequency and temperature effects may have increased the resonant frequency such that the viscous damping at the required frequency was reduced.

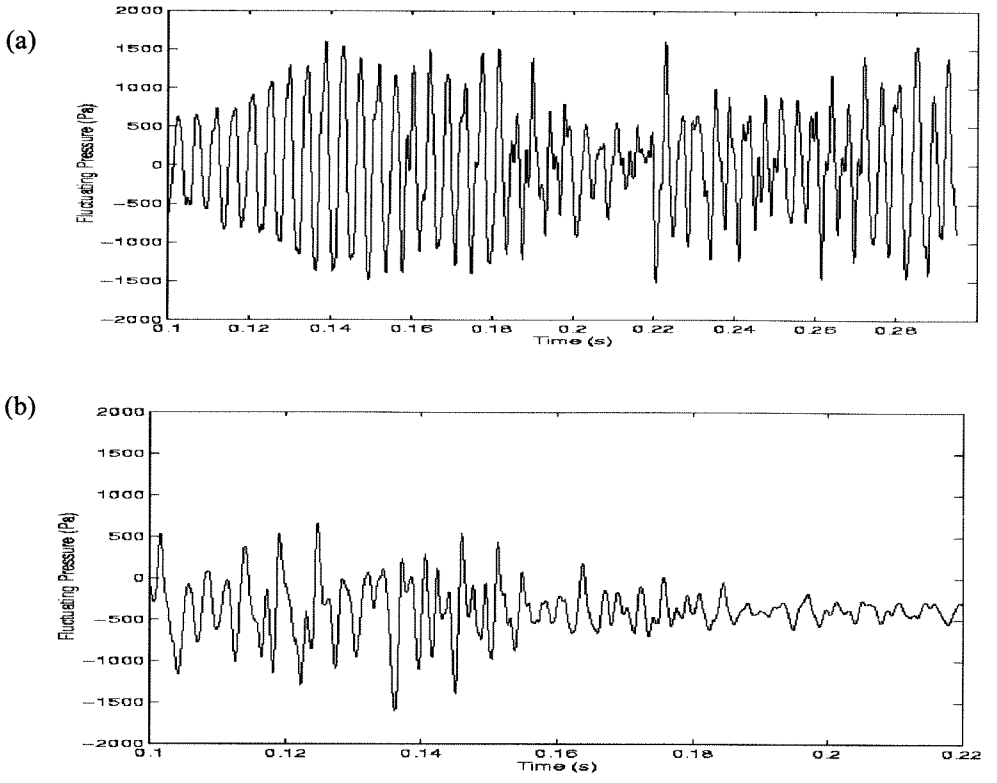

Figure 4-14 (a) Case A without Resonator; (b) Case A with Resonator (A)

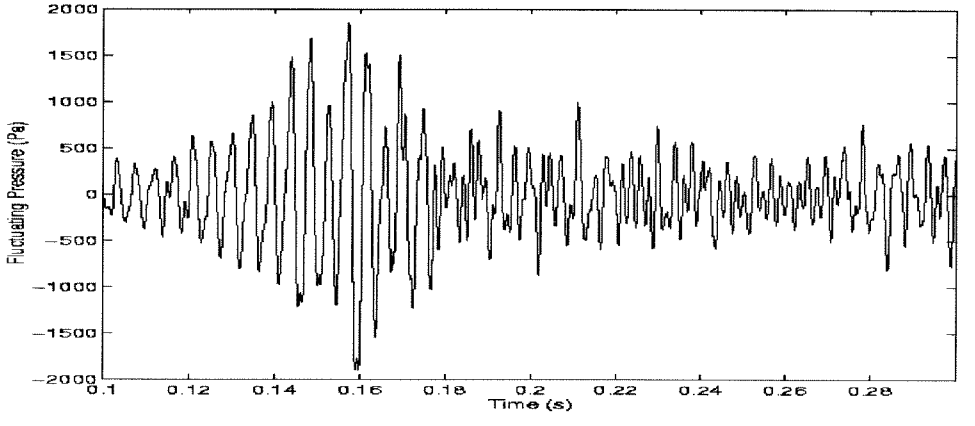

Figure 4-15 Case A with Resonator (B)

4.5 Pollutant Levels in Oscillating Flow

The analysis of the unsteady effects on pollutant levels is also investigated for this combustor configuration. The NOx levels and CO levels are examined on a local and global scale in relation to the oscillations. Figure 4-16 shows the steady state contour of the CO mass fraction for the same case shown in Figure 4-2. The maximum value of the CO mass fraction in this figure is 0.024 and the contour lines mark off the field in steps of 0.004. Figure 4-17 shows the steady state NO mass fraction contour. The maximum value is near 0.022. Because the flame is so well structured in the steady state simulation, the flame reaches the adiabatic flame temperature and produces a high level of NOx. The stable flame also causes the maximum CO production to occur upstream of the exit plane.

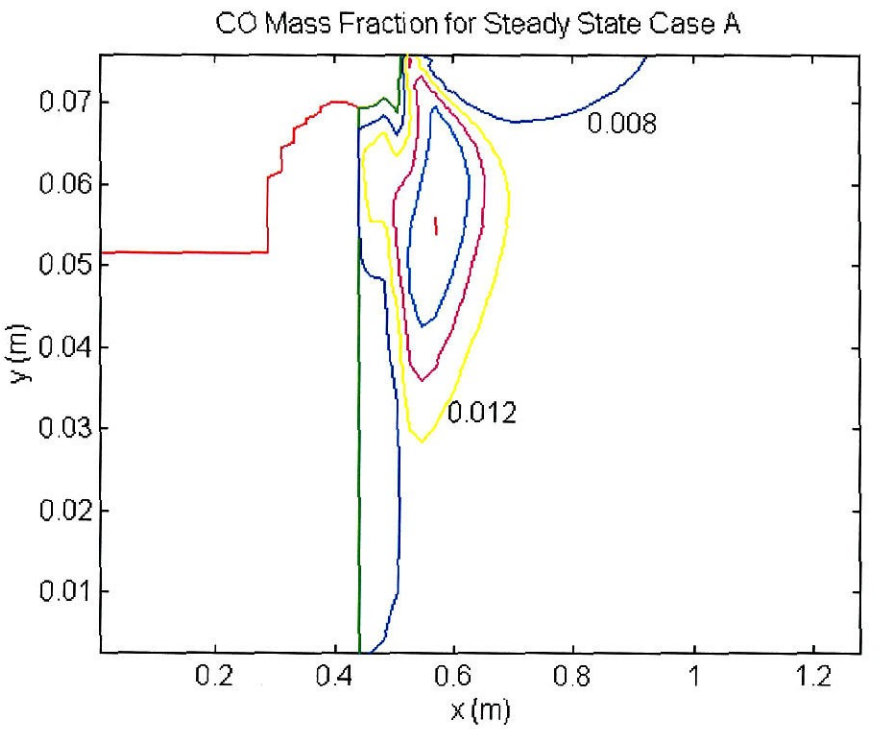

Figure 4-16 Steady State CO Mass Fraction Contour for Case A

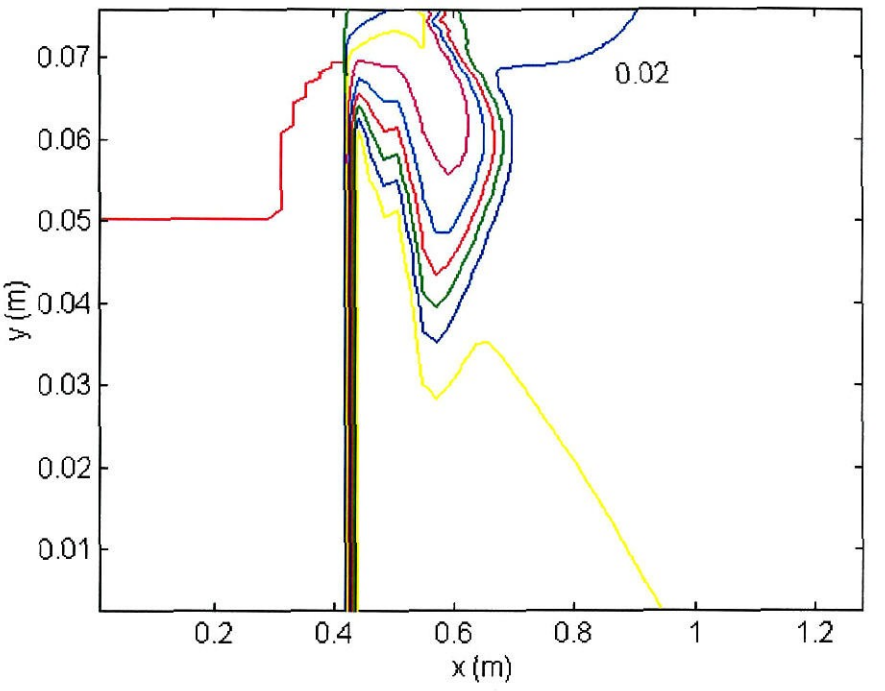

Figure 4-17 Steady State NOx Mass Fraction Contour for Case A

Figure 4-18 shows the NOx contour during the transient simulation. The vortex structure has altered the flame structure that in turn has lowered the flame temperature and changed the pollutant reaction rates near the top wall. The new flame structure has a significant effect on the NOx levels. The maximum NOx levels have been shifted downstream. At the exit plane, the average mass fraction for NOx is 0.007 and is lower upstream. The averaged NOx levels have dropped off by a factor of about three from the steady state to the transient simulations. This effect is also apparent for the CO levels. The volume averaged CO mass fraction at the exit plane for the steady state is 0.0039. Figure 4-19 shows the time-resolved value of the oscillating CO mass fractions at the exit plane. The time-averaged value was determined as 0.0064, which is a 60% increase in the mean level as compared with the steady state level. For this case, the oscillations have a negative impact on the production of the pollutant species CO at the exit plane since the main flame front is pushed downstream by the action of the vortex shedding. The shift

of the main flame zone causes a shift of the main zone of CO production. Therefore, at the exit plane for this simulation the CO levels are higher in the presence of vortex shedding.

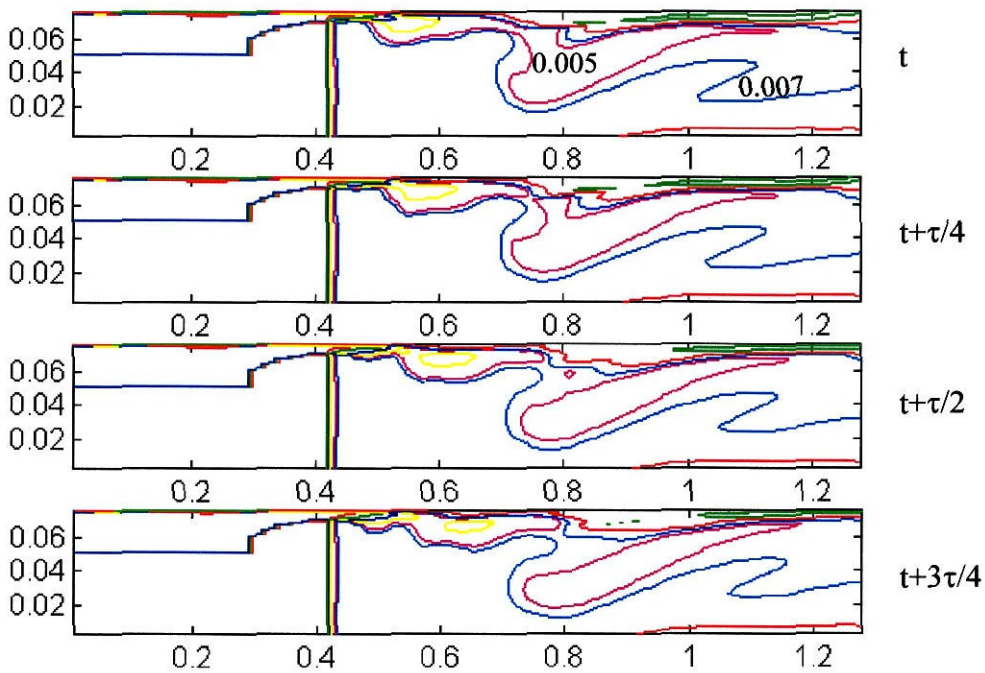

Figure 4-18 NOx Mass Fraction Contours During a Cycle of Oscillation for Case A

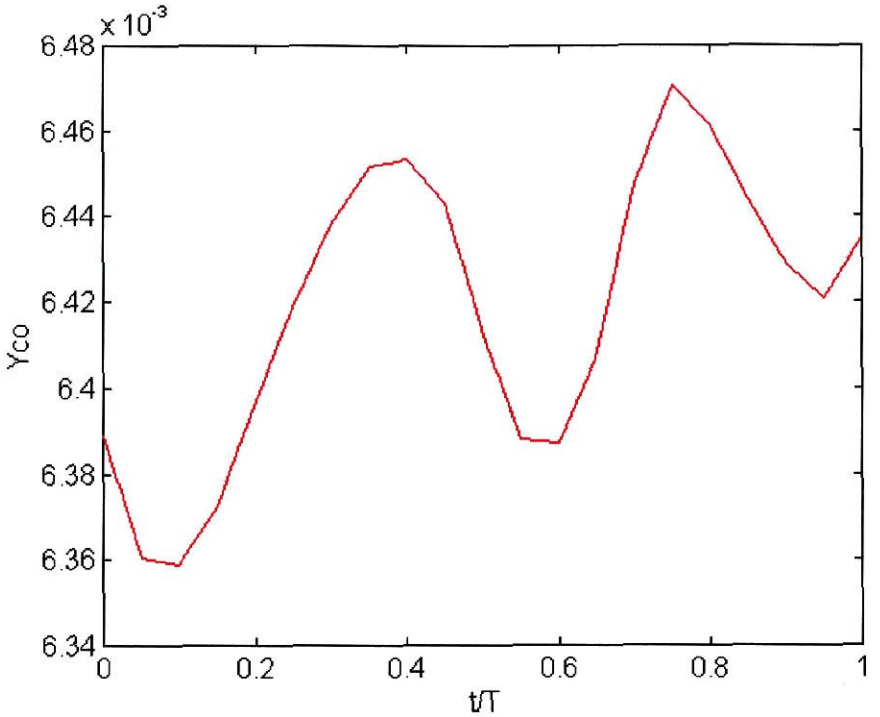

Figure 4-19 CO Mass Fraction at Exit Plane During Cycle of Oscillation for Case A

Overall, for both the Rijke tube and the dump combustor, the numerical method demonstrated an ability to accurately represent the flow field and the frequencies of the instabilities, with some possible concerns related to the boundary conditions and the effects of turbulence. The aspects of the numerical method learned during the simulation of these simple combustion flows are applied to the more complex simulation of a full scale gas turbine combustor in the next chapter.

Chapter Five

Mitsubishi/Westinghouse Gas-Turbine Combustor

This chapter presents the results of numerical simulations of unsteady flows in a Mitsubishi/Westinghouse gas-turbine combustor currently being tested experimentally in Italy by ENEL (Benelli, 1995). The gas-turbine system is designed for use as a stationary power plant. Certain specific details about the configuration and the flow field will not be presented since this information is proprietary. The combustor is run premixed and lean to reduce the temperature and the amount of pollutants produced. Running the combustor lean brings up additional stability issues, since past experience has demonstrated increased instabilities as the lean blowout limit is approached in gas-turbine combustors (Sturgess et al., 1991; Sturgess et al., 1992; Roquemore et al., 1991).

The combustion configuration is not as simple as the previous numerical examples since the combustor contains premixed and diffusion flames, the latter associated with stabilization by a pilot flame. The pilot flame is a diffusion flame because the fuel and air first interact at the flame front, leading to a stoichiometric combustion region. Figure 5-1 shows a sketch of the combustor design. The diffusion flame is a central pilot flame fed by swirled air and anchored by a flame cone. A strong recirculation zone develops in this region which ignites the premixed flow. There are eight premixer chambers around the central pilot. The ability of these chambers to mix completely the injected fuel and air, as well as the impact of pressure oscillations on the equivalence ratios, will be discussed in Section 5.1. Spatial and temporal variations in the equivalence ratio can produce temperature fluctuations that can lead to variations in the pollutant levels and a possible coupling with an oscillation pressure field.

Figure 5-1 - Sketch of Gas-Turbine Combustor used for Simulations (Not to Scale)

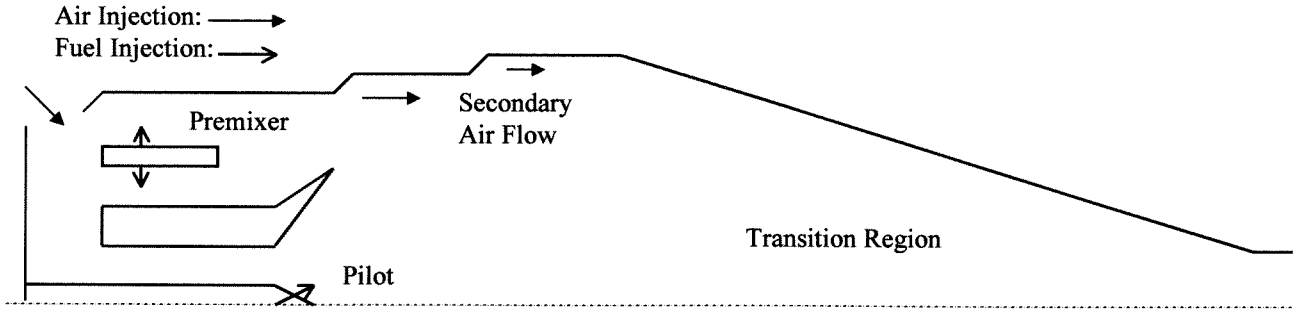

This research is being conducted to produce numerical data for the flow field in a gas-turbine combustor during unsteady oscillations. For simpler designs, like the dump combustor and Rijke tube, the oscillations can be studied by low cost experimental facilities at atmospheric conditions. However, because of the high pressures in gas-turbine combustors, the manufacturers perform most of the experimental research. Due to the highly competitive industry of gas turbines, the data is often proprietary and hard to obtain in order to study the oscillations. Even if the data was made available, it might not be detailed enough to develop a good understanding of the oscillating behavior in the combustor. The numerical work is designed to obtain data for gas-turbine combustors at a level of detail unavailable experimentally.

5.1 Mixing Effectiveness in the Premixer

As mentioned earlier, one of the main research efforts in the reduction of pollutant emissions involves lean premixed combustion. Due to the exponential dependence of NOx production on temperature, if the average temperature remains constant and there are local fluctuations in the temperature, the average amount of NOx produced locally will increase. We have seen cases in Chapter 3 and Chapter 4 in which the mean temperature was reduced leading to a reduction in the overall NOx production. Therefore, if the cold mixture is not perfectly

premixed, spatially varying mixture levels can produce local temperature and heat release fluctuations. These variations can have a negative impact on pollutant levels and system stability. Hence, it is desirable to have a perfectly premixed flow (Fric, 1993).

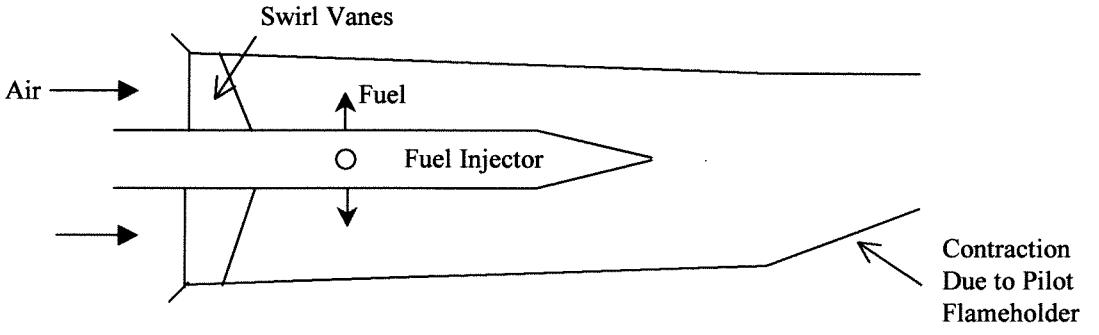

Figure 5-2 Sketch of Premixer Chamber

Because of the concern for a properly mixed flow, work was initiated to investigate the steady state mixing conditions in a single premixer chamber sketched in Figure 5-2. The mixing simulation was performed with ANSWER using the conservation equations for the momentum, enthalpy, pressure, turbulence (k-ε model), and species (O_2, N_2, CH_4). As was mentioned in Chapter 2, the diffusion term in the species conservation equation was a factor of the viscosity for the given species and the Schmidt number. The diffusion term also included the effects of turbulence by a turbulent viscosity value determined from the k-ε model. Instead of modeling the entire chamber, the configuration represented a 90 degree periodic slice of the chamber. The simulation used a 37 x 37 x 12 cell grid. The coarse grid was used due to computational time constraints. The full injection was simulated by a source term at the proper injection point at x-axis cell number 7. The simulation was carried out axially beyond the region of area convergence in order to see how the unmixedness would change with distance from the injector if there were no restrictions on the length of time needed for complete premixing. Figure 5-3 shows a series of slices showing the equivalence ratio levels at various locations downstream of the fuel injection plane.

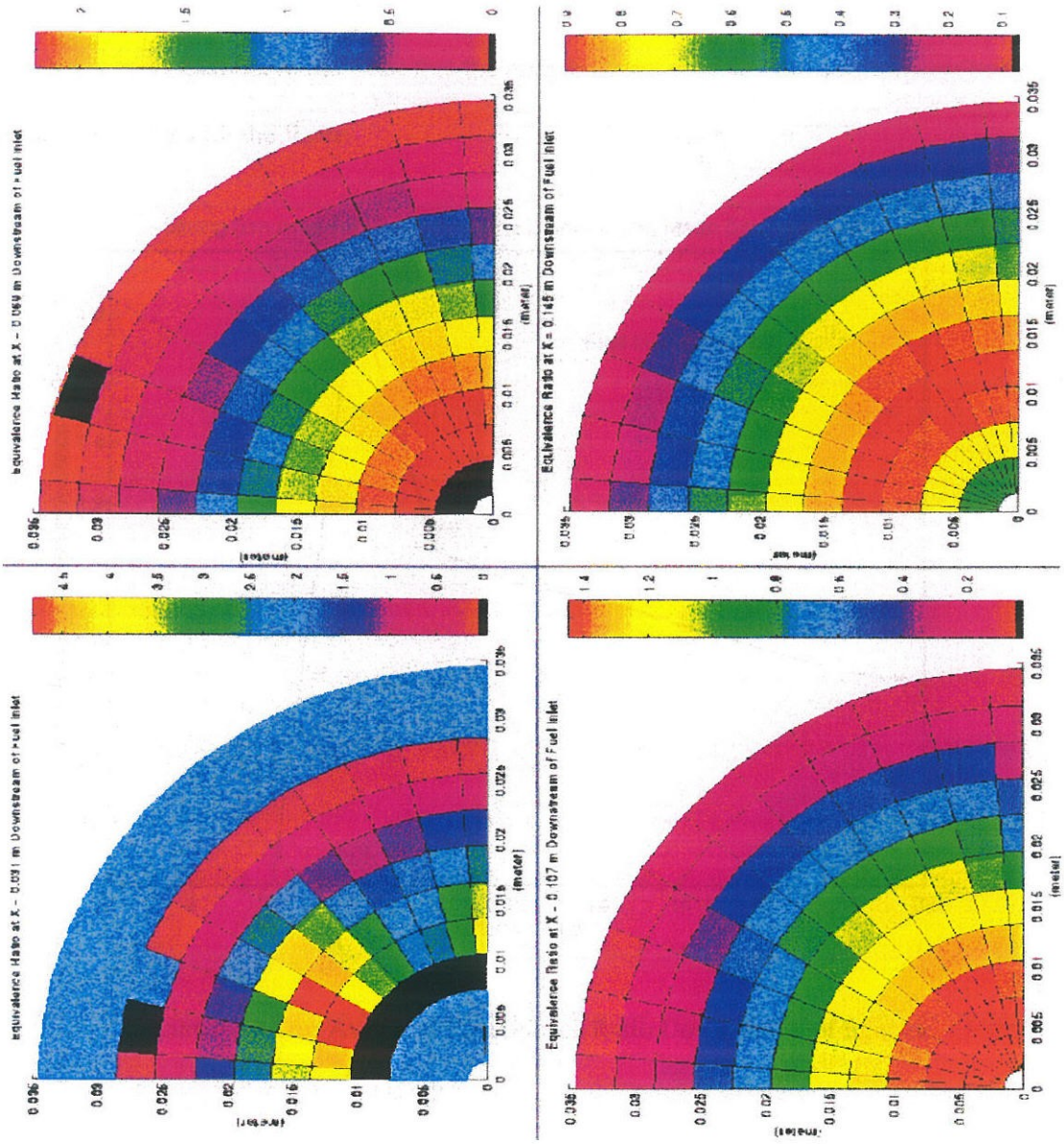

Figure 5-3 Fuel Mass Fraction Contours Downstream of Injector

As can be seen, the swirl does have some impact, but only in shifting the concentrations away from the injector centerline. Figure 5-4 shows the area averaged equivalence ratio as a function of distance from the injector. The level of mixedness, towards the global mean equivalence ratio, increases with distance downstream of the injector, but as Figure 5-3 shows, there is never a region where the mixture can be said to be perfectly premixed. Experimental data

into this problem would be needed to validate the findings of these numerical codes, but it seems like a fairly good qualitative indicator that the mixture is not reaching the desired premixed state before interacting with the flame.

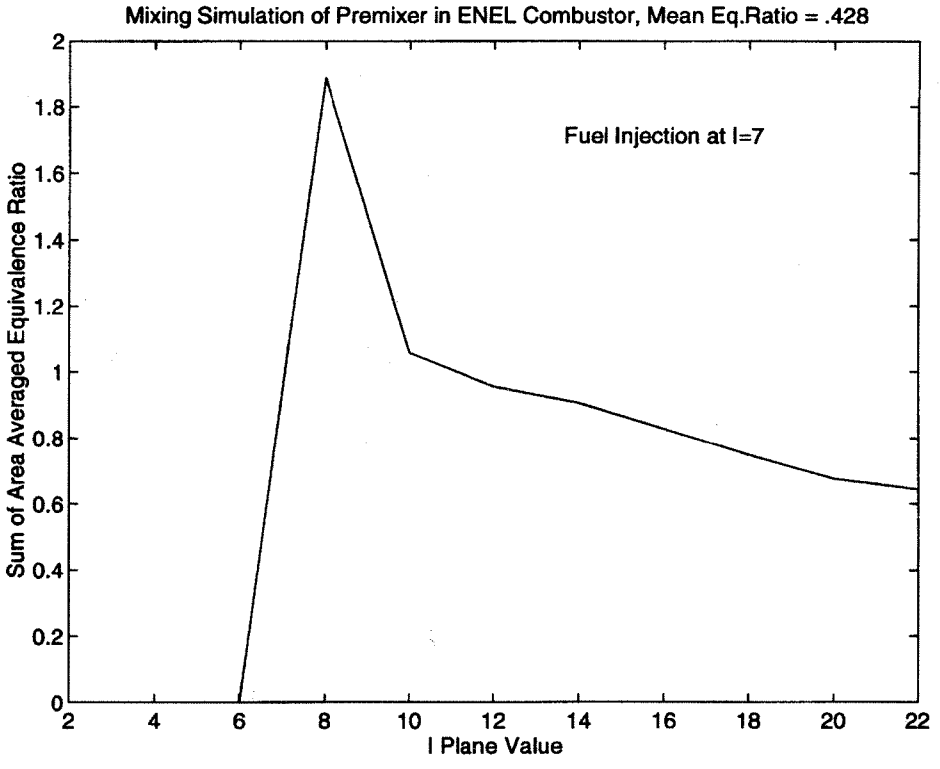

Figure 5-4 Area Averaged Equivalence Ratio Downstream of Injector

Another point of interest for some future study would be how a pressure oscillation in the premixer affects the mixing. For high-speed fuel injection, the back pressure in the fuel line is often larger than the air back pressure. This difference in back pressure can have a large influence on the fuel and air flow rates under unsteady conditions. Because of this large pressure drop across the fuel injector, it would seem that a pressure wave in the main chamber would adversely affect the air mass flow rate. For example, if the pressure in the chamber increases, the velocity of the air into the premixer will decrease more than the fuel, leading to a richer mixture. This rich

mixture will propagate downstream to the flame front with some characteristic flow time. If this rich mixture burns while the fluctuating pressure in the main chamber is increasing, the added heat release will drive the instability, leading to larger pressure oscillations. This feedback between the pressure and the incoming mixture ratio has been examined in experimental test cases (Lieuwen et al., 1998) and the instability has been shown to be a function of the characteristic time between the fuel injector and the flame front. In addition to affecting the mean equivalence ratio, the pressure oscillations may also influence the mixing quality. This information may be of use in possible control measures.

5.2 Calculations of Steady Flows

The next step in the analysis was to produce the steady state results for the entire chamber. The steady state simulation is performed to examine the flow properties in the chamber and to determine a baseline for the transient simulations. The initial steady state determinations are made with a 2-D axisymmetric slice of the chamber. In order to compensate for the behavior of the premixers that are not axisymmetric, the total area of the eight premixers is represented in the simulation by an annulus of a single axisymmetric inlet. The fuel injection holes for the pilot flame are also grouped together and represented by an annulus. To simulate the entire combustor from the air inlet to the turbine inlet, the transition region is also modeled. The transition region, as labeled in Figure 5-1, is the area between the end of the flame zone and the turbine inlet. In the actual combustor, the transition region shifts from a cylindrical cross-section to a rectangular cross-section. For the numerical simulations, the transition region is adjusted to be straight and axisymmetric.

The simulation takes into consideration the swirl vanes for the premixers and pilot flame by including a tangential velocity component. The swirl angle in the premixers is 45° and the swirl angle for the pilot air inlet is 66°. The air flow is input at a temperature of 650 K with a

back pressure of 1.4 MPa. The fuel is injected at a temperature of 300 K and is driven by an upstream pressure of 1.8 MPa.

The maximum load condition is simulated. In this configuration the pilot fuel-to-air ratio is 0.042 and the premixer fuel-to-air ratio is 0.025. The fuel is injected into the chamber at the same locations as in the real combustor and the mixing is allowed to proceed according to the conservation equations. The total air mass flow rate in the entire chamber at maximum load condition is 20.5 kg/s with 77.8% flowing through the premixer chambers, 7.6% through the pilot section, 6.3% for secondary air flow injected tangentially along the outer wall of the chamber and the rest used mainly as bleed air at various locations in the combustor.

The simulations with ANSWER use a 77 by 57 cell grid that fits the contours of the chamber. The most grid detail occurs in the region of the pilot diffusion flame and the interation region between the diffusion and premixed flame. The chemical reaction mechanism uses a three-step mechanism for methane (Malte, 1996) with determination of the intermediate product CO. The k-ε model is used to calculate the turbulence. The grid and the steady state temperature contour are shown in Figure 5-5. The maximum temperature in the recirculation zone is 2700 K and the average exit temperature is around 1340 K which is close to that determined experimentally.

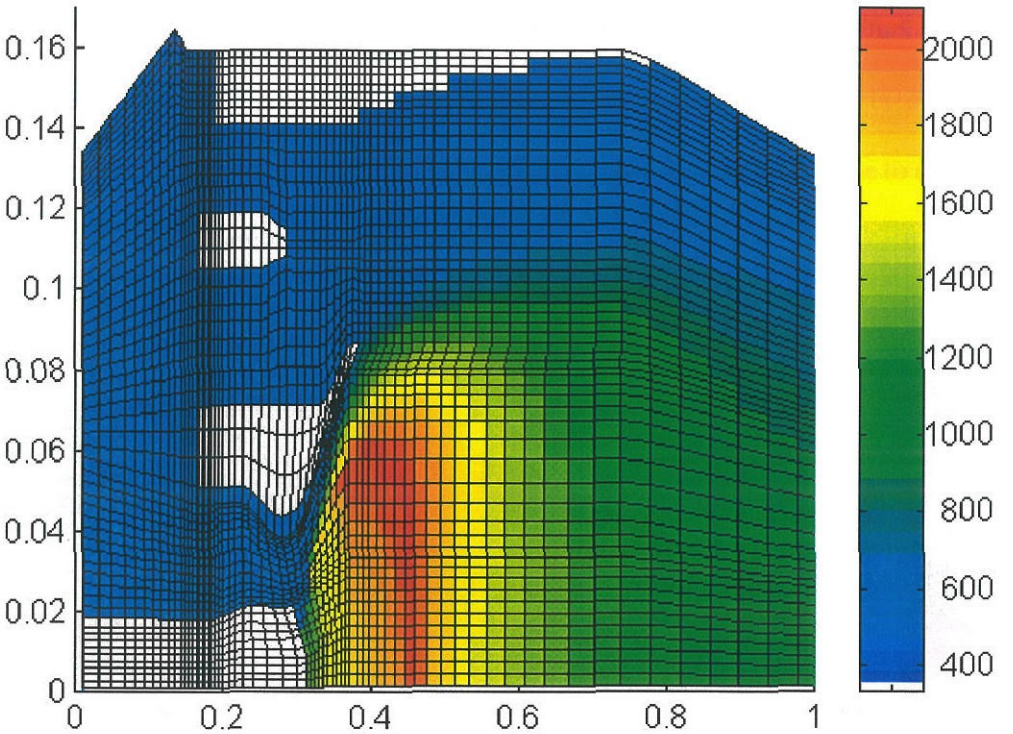

Figure 5-5 Steady State Temperature Field in Gas-Turbine Combustor

In addition to the axisymmetric simulations, a 3-D steady state simulation was performed. The 2-D 57 x 57 cell grid is swept around a 45° slice of the combustor to represent the periodic behavior of one premixer and a single pilot fuel injection hole. The $\pm\theta$-planes were assumed to be periodic. The grid defining the premixer is altered to conform to the proper shape. There are 13 cells in the third dimension. Figure 5-6 shows two slices of the temperature field for this steady state simulation at the K=3 and K=7 planes. Figures 5-5 and 5-6 show many similarities in magnitude of temperature field and basic flame distribution. However, the 3-D simulation displays some interesting differences. The high temperature recirculation zone is broader and shows more extension into the premixed flow. The area downstream of the recirculation zone is not as energetic, which seemingly draws more of the premixed flow into the diffusion flame. This

increased mixing leads to a premixed flame attachment to the outer wall much earlier in the transition region than the 2-D simulation which corresponds to a more complete fuel burn. The exit plane temperature is more uniform and is near the experimentally determined temperature at this point in the flow field. The maximum temperature is also slightly lower, due to a diffusion flame that is more spread out in the 3-D simulation.

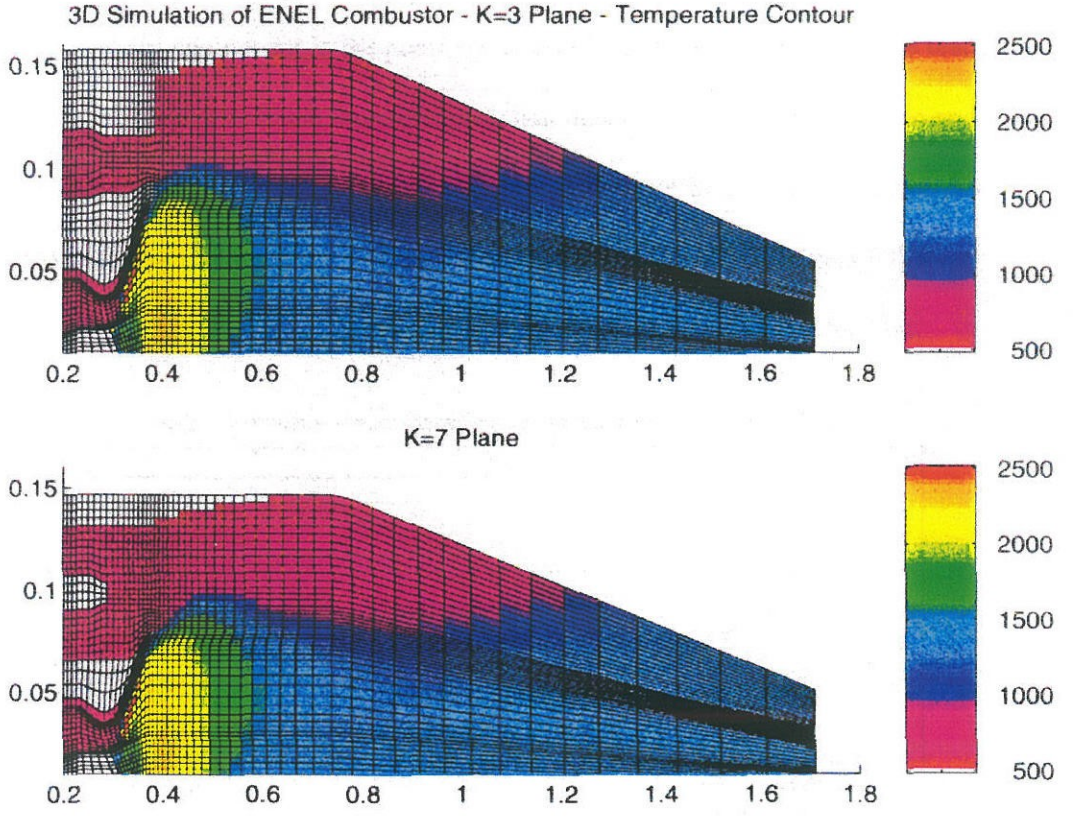

Figure 5-6 3-D Steady State Temperature Contours for Gas-Turbine Combustor

The 2-D temperature field has a large region of cold gas near the top wall in the transition region. Some of this is due to the cold secondary air flow injected tangentially along the wall; however, most of the low temperature region is due to incomplete burning of the premixed flow. Either the ignition set up by the diffusion flame is not strong enough, or the swirling component

of the 2-D simulation does not properly represent the real flow to achieve complete burning. Figure 5-7 shows the fuel mass fraction distribution in the transition region for the 2-D simulation. At x = 0.913 m, there is still a large pocket of fuel near the inlet with a fuel fraction of 0.024. This level is only slightly reduced near the exit plane. This indicates that for the 2-D simulations, the combustion levels are not near completion for the premixed flow. Figure 5-8 shows the fuel mass fraction distribution at various axial locations for the 3-D simulation. The additional 3-D swirl component in the premixed region leads to better stirring of the reactants and the hot products, leading to much more complete combustion in the transition region and at the exit plane. Whereas the maximum fuel mass fraction at the exit in the 2-D simulation is near 0.015, the maximum fuel mass fraction at the exit in the 3-D simulation is near 0.0009, a significant change due mainly to the proper inclusion of swirl in the 3-D simulation.

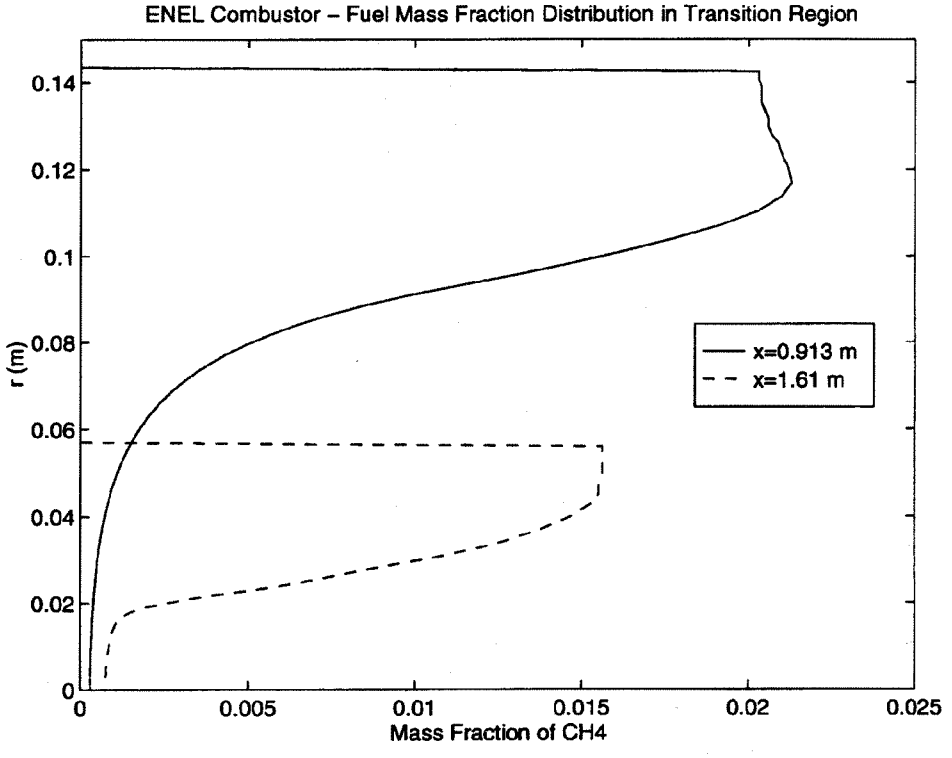

Figure 5-7 Fuel Mass Fraction Distribution in Transition Region

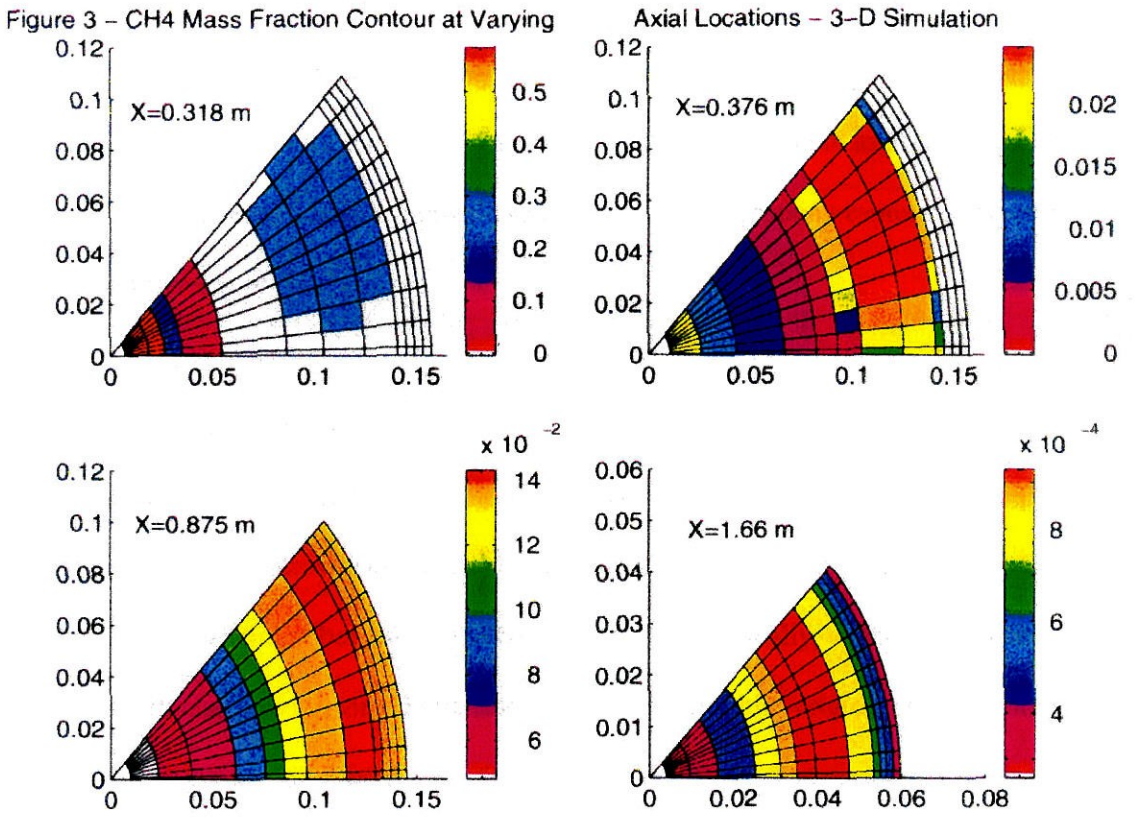

Figure 5-8 Fuel Mass Fraction Contours at Various Axial Locations

As mentioned earlier, knowledge of the system geometry and the steady state temperature field can lead to the determination of the acoustic modes (Benelli et al., 1994). The method is outlined in Appendix A. This analysis technique is applied to the gas-turbine combustor. The results determined that the low frequency modes should be around 160 Hz, 460 Hz, and 700 Hz. These results can provide some guidelines for understanding the transient results.

The steady state results indicate a couple of interesting points that need to be considered when examining the unsteady results in the next section. The results for the mixing in the premixer indicate that the flow field is not completely premixed. This unmixedness could lead to a spatial variation in the temperature field at the flame front, which might be responsible for the

development of oscillations in the gas-turbine combustor. Also, the steady state temperature field indicates that the main flame zone is immediately downstream of the pilot fuel injection and that the premixed flame is delayed into the transition region. The delay is not as pronounced in the 3-D simulations, indicating that axisymmetric simulations are not properly capturing the swirl behavior downstream of the premixer.

5.3 Calculations of Unsteady Flows

The next step in the analysis of this system is numerical simulation of transient flows in the full-scale reacting system. The results should reflect the behavior in the actual experimental combustor. The system has been shown to be unstable experimentally, so these transient simulations will also provide some indication where the instabilities originate in the chamber.

The first simulation is performed for a non-reacting flow. The reaction rates are set to zero in order to examine the basic behavior of the flow field and of pressure waves in the system at a constant temperature with no driving mechanisms. Figure 5-9 shows the results for this cold flow simulation. The initial pressure fluctuations are decaying to zero. A Fourier transform determined that the acoustic modes are 187 Hz, 325 Hz, and 658 Hz. These modes are in reasonable comparison to the modes determined by the finite element method, but it should be noted that this is for a cold flow simulation, not a hot flow as in Section 5.2. These modes can be useful in comparison with the reacting simulation since they can be easily scaled to the proper mean temperature.

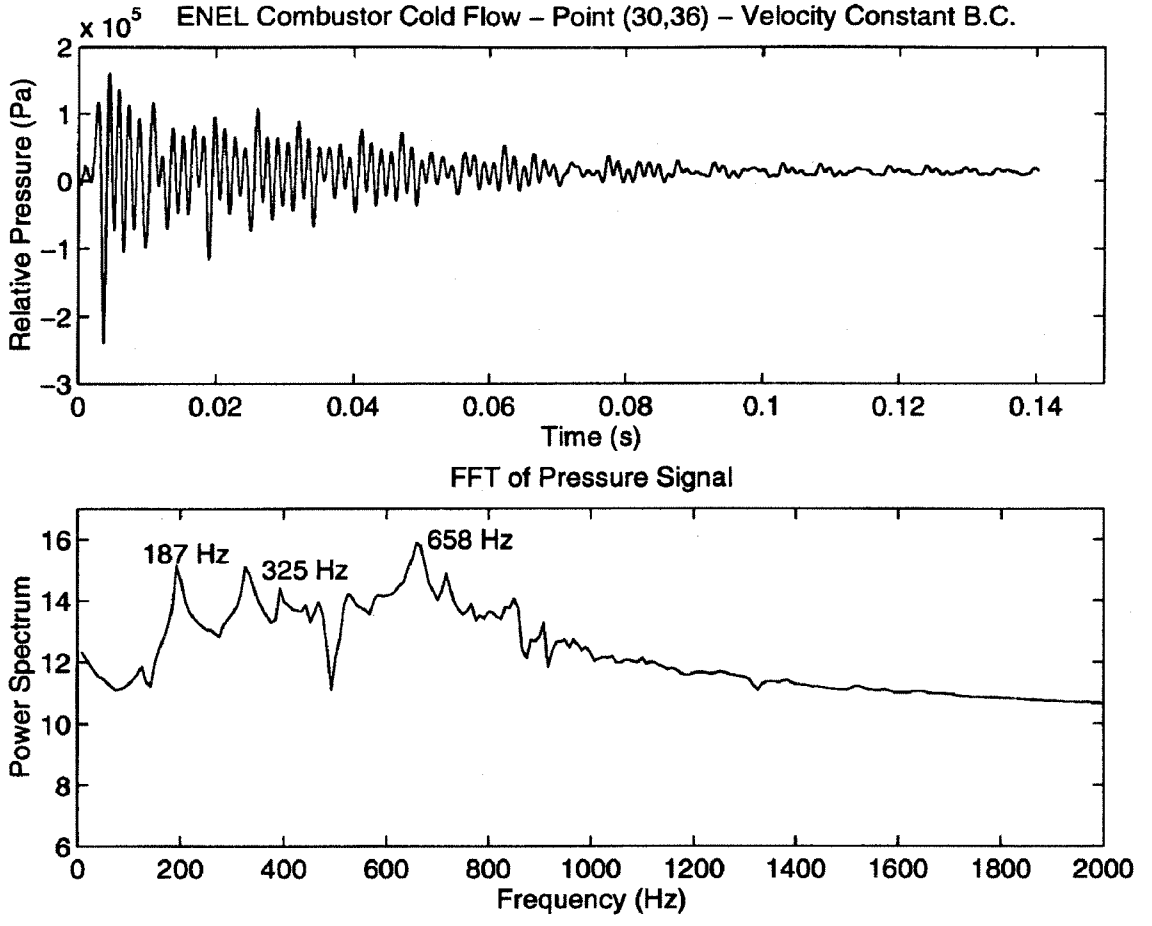

Figure 5-9 Transient Simulation of Non-Reacting Flow in Gas-Turbine Combustor

A transient simulation is then performed for the 2-D axisymmetric flow at maximum load conditions. The time step was taken as 2 μs, which is an order of magnitude below what is required for proper pressure wave calculations between the cells. The default boundary conditions, described in Chapter 2, are used in the case. At the exit plane, the flow increases in speed before entering the turbine blades. The flow should reach Mach 1 at this location which creates an approximately closed boundary for acoustic waves.

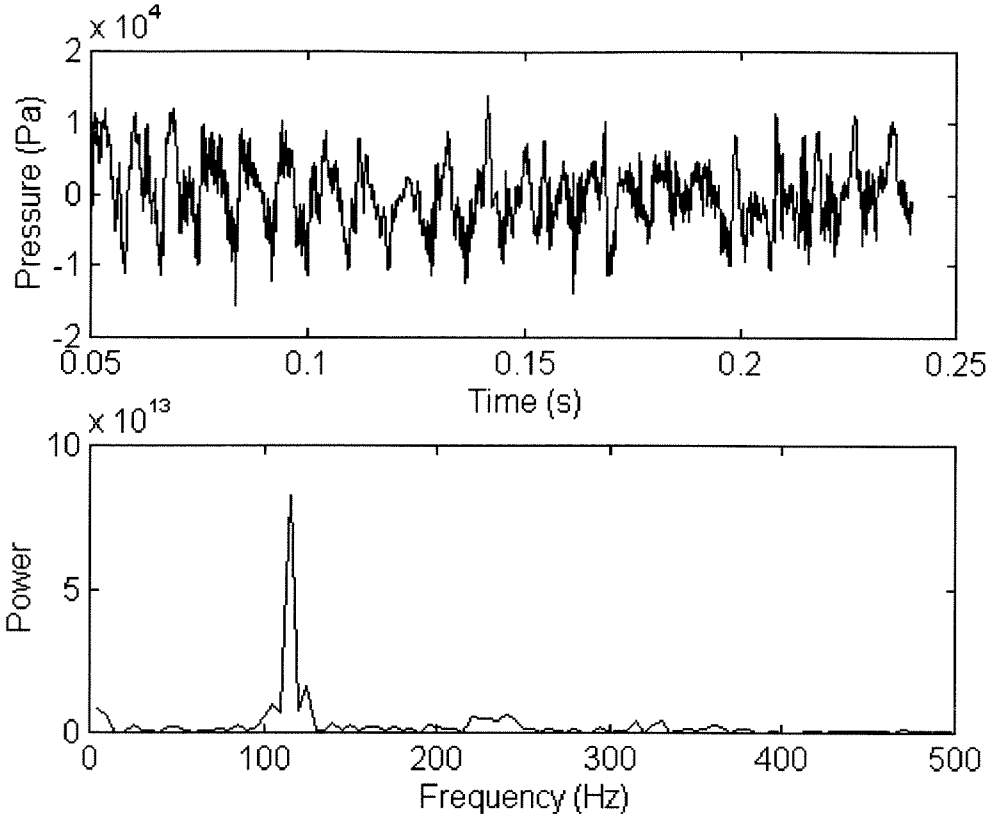

Figure 5-10 Gas-Turbine Combustor at Maximum Load

Figure 5-10 shows the results of the 2-D transient simulation with secondary air flow along the upper boundary as shown in Figure 5-1. The pressure signal is reaching a limit cycle behavior at about 1.5% of the mean pressure in the chamber. The main mode of the oscillation is 115 Hz, which is comparable to the known unstable frequency of 95 Hz experienced during the experimental tests. Figure 5-11 shows the pressure record for a simulation without secondary air flow along the upper boundary. There has been a frequency shift from 115 Hz to 203 Hz for the main unstable mode and the oscillation level seems to be dropping at a later time when compared with the results in Figure 5-10. It is unclear why this change has occurred. The mean acoustic velocity may be higher without the secondary air flow, since the secondary air flow is a cooling mechanism along the upper boundary.

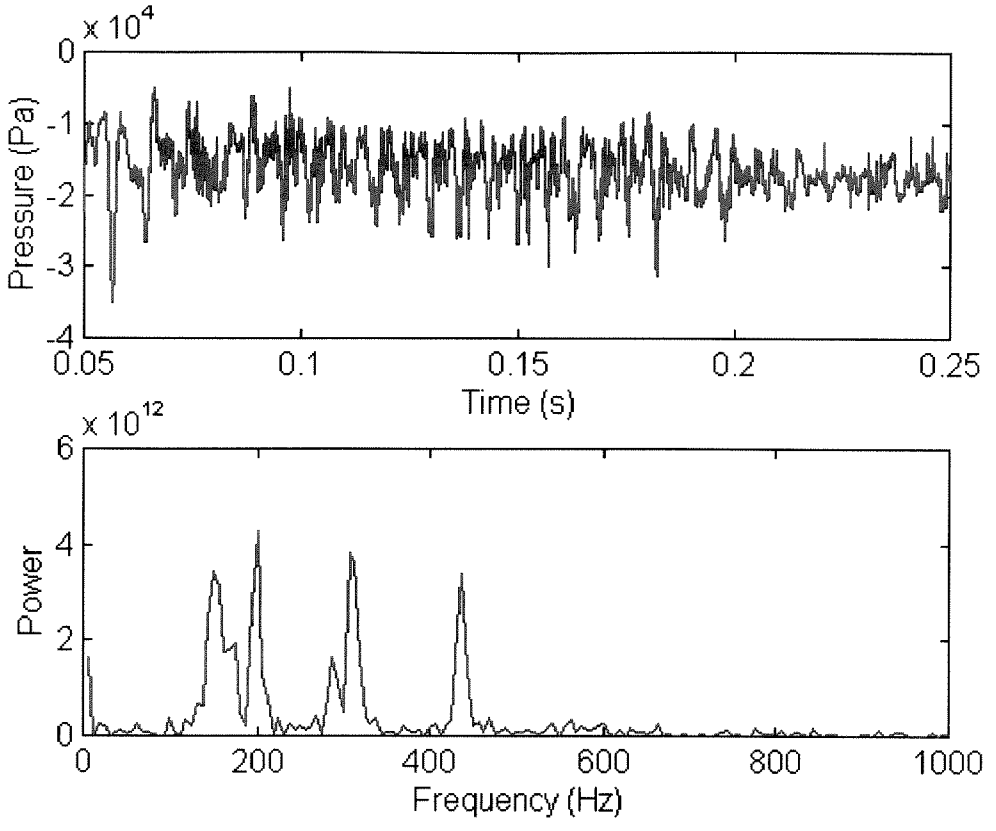

Figure 5-11 Gas-Turbine Combustor without Secondary Air Flow

Figure 5-12 shows the temperature contour and Figure 5-13 shows the axial velocity contour during a cycle of the oscillation for the case with the secondary air flow. There is variation in the properties in the region immediately downstream of the pilot flame and in the premixer. The high temperature in the premixer seems out of place. However, we do not have experimental results detailing the temperature in the premixer for this case (even after repeated requests to ENEL for experimental results to compare with). It may be possible that a high-amplitude pressure oscillation could force the flame back into the premixer, allowing for the type of fluctuations in temperature shown in Figure 5-12. If this were the case, the mixing and subsequent burning at the premixer injectors would be a very important mechanism in the driving of the instability.

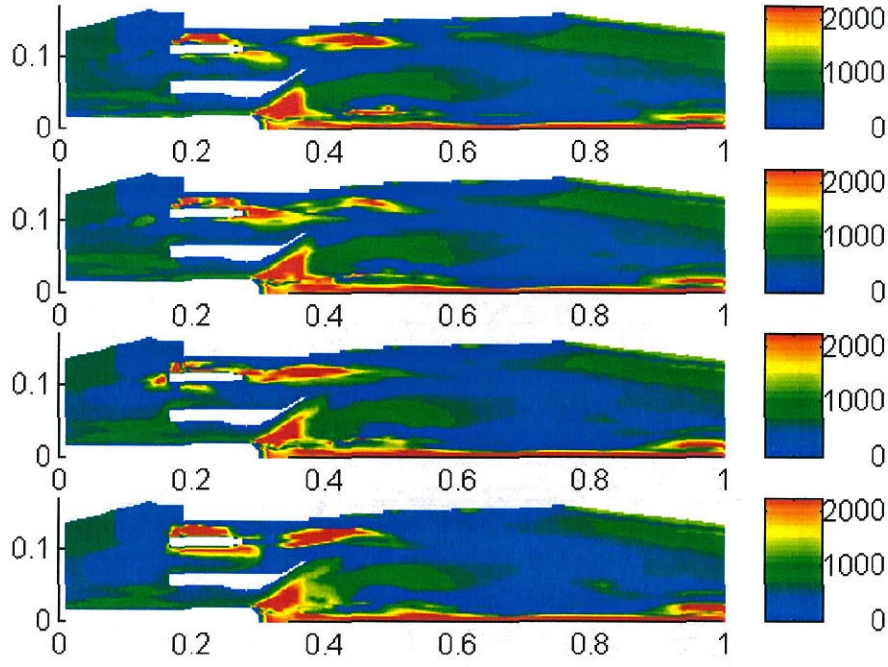

Figure 5-12 Temperature Contours During Cycle of Oscillation (with Secondary Air Flow)

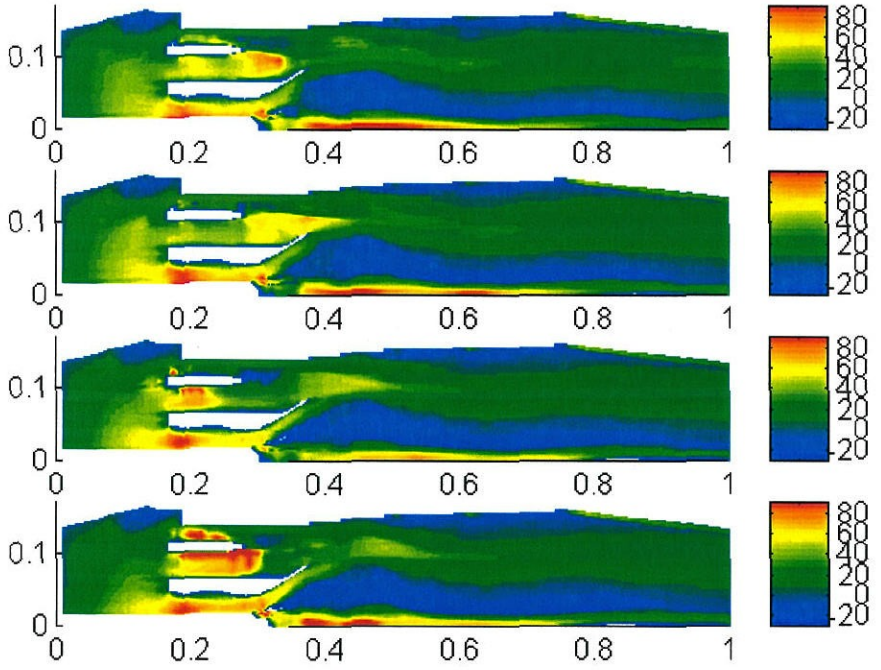

Figure 5-13 Axial Velocity Contours During Cycle of Oscillation (with Secondary Air Flow)

Figure 5-14 shows the temperature contour at a stage of the oscillation without the inclusion of the secondary air flow in the simulation. The high temperature in the premixer is also apparent in this case.

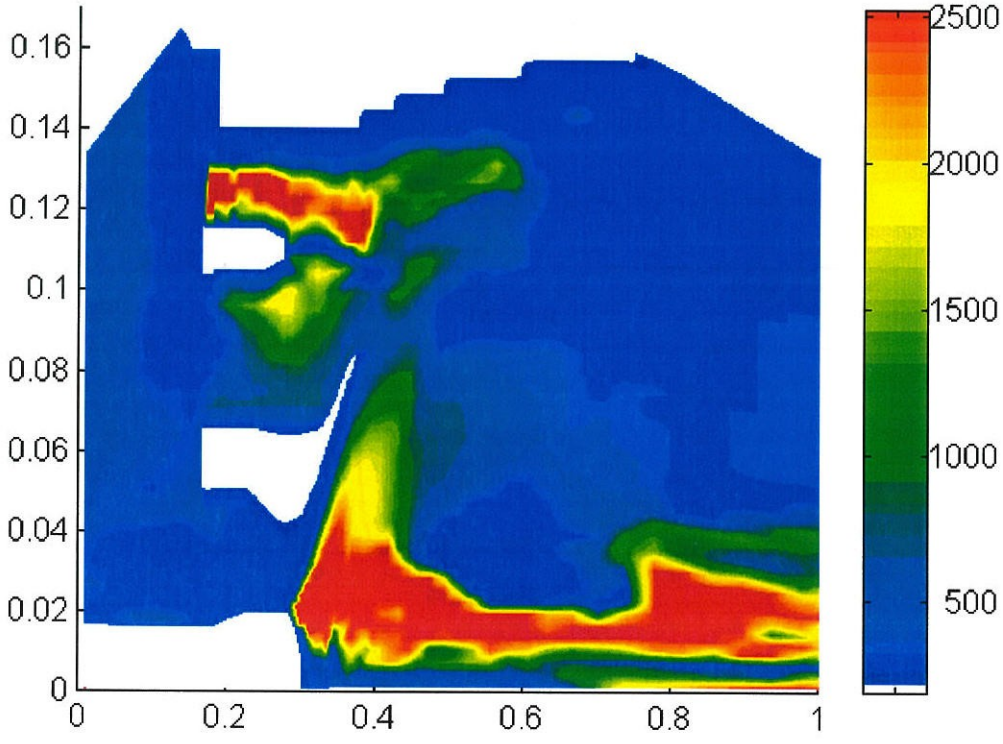

Figure 5-14 Temperature Contours During Oscillation (without Secondary Air Flow)

Figure 5-15 shows the pressure record for a different simulation. For the cases in Figure 5-10 and 5-11, the fuel and air are mixed in the premixer by the inclusion of a fuel source term at the injection locations. For the results shown in Figure 5-15, the fuel and air are premixed at the inlet of the numerical domain, negating any effects the mixing may have on the structure of the instability. The pressure record for this configuration is decaying toward zero, which indicates a stable solution. The temperature contour shown in Figure 5-16 for this case has a maximum in the pilot flame region, but not in the premixer as was the case for the results in Figures 5-12 and 5-14.

This difference in the behavior between a perfectly premixed case and a case in which the mixing is dynamic may give credence to the theory that the unmixedness in the premixer and the interaction with the pressure oscillations leads to the development of an unstable system. However, further cases need to be run to examine this behavior in more detail.

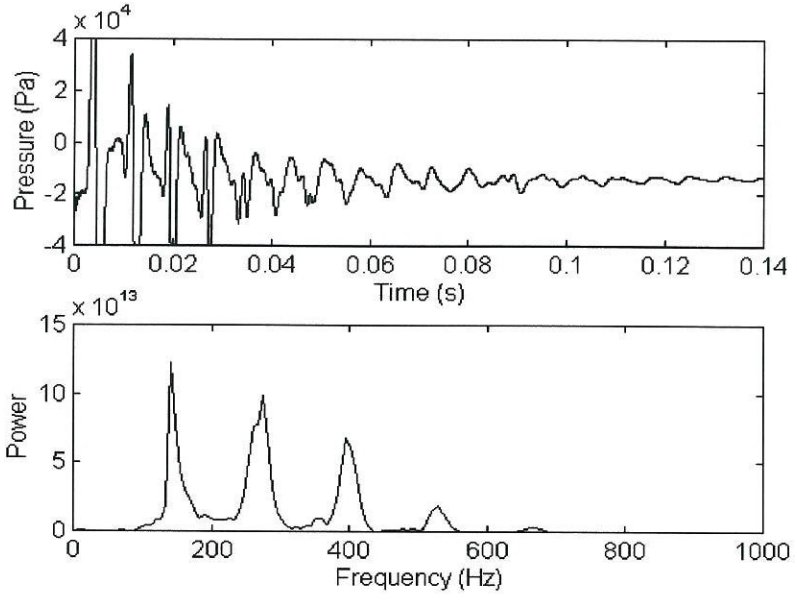

Figure 5-15 Pressure Record with Perfectly Premixed Flow at Inlet

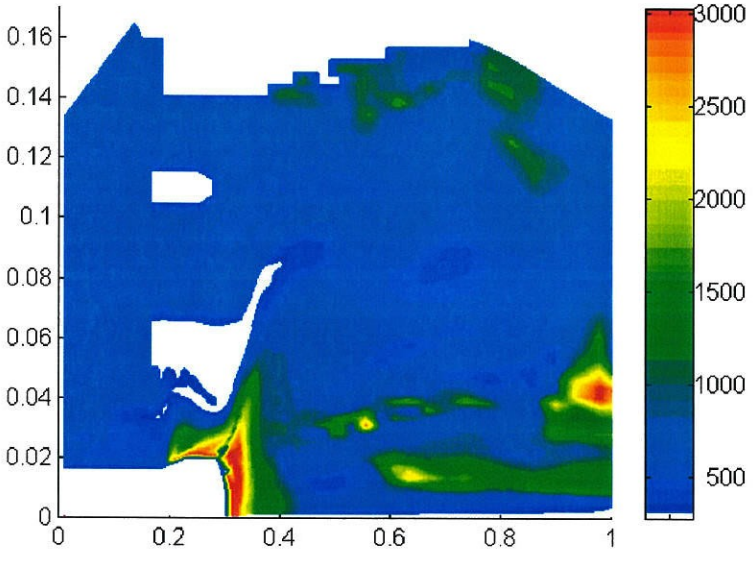

Figure 5-16 Temperature Contour with Perfectly Premixed Flow at Inlet

Overall, the results for the gas-turbine combustor seem to indicate that there could be a possible negative interaction between the mixing in the premixer and the pressure field. This interaction could be what is driving the large-scale instability in the experimental test rig. However, it is imperative that experimental results are obtained for proper comparison with the numerical simulations. Without the comparison, the numerical simulations can only provide a possible theory explaining the cause of the instabilities and cannot make any positive conclusions about the instability or method for correcting the problem.

Chapter Six

Pollutant Production in a Combustion Environment

One of the main concerns of combustion research for the gas turbines is the production of pollutants (NOx, CO, UHC, SOx). Several practical approaches towards reducing NOx production have been based on lowering the overall flame temperature by burning lean. However, as the lean blowout limit is approached, experimental results have shown an increase in the unsteady nature of the flame. This unsteady flame behavior can drive unsteady oscillations within the chamber. These combustion instabilities will impact the level of pollutants produced (e.g., oscillations in the simulation of the dump combustor in Chapter 4 showed an increase in the CO level at the exit plane, but a reduction in the NOx level). It is therefore important to understand how the flow field and the chemical reactions interact not only for their impact on the heat release rate, but also on the species concentrations in the presence of an oscillating flow field.

In this chapter we will first cover the main mechanisms of NOx production along with methods for reducing the production of NOx. We will then describe a framework for incorporating the species conservation equations and results from numerical simulations into the approximate analysis mentioned in Chapter 3. Finally, we will mention how perfectly stirred reactor (PSR) and plugged flow reactor (PFR) models can be used to examine the quasi-steady pollutant levels in the presence of an instability.

6.1 Production Mechanisms for NOx

The pollutant of the greatest concern in the research community at this time is NO and NO_2 which are lumped together under the label NOx. Since the mechanism which produces NO_2 is directly tied to the levels of NO, most works usually focus only on the production of NO. A

review of the mechanisms of pollutant production in combustion environments can be found in an article by Bowman (1975). A more detailed look at NOx formation can be found in an article by Correa (1992c). There are three main mechanisms for NOx formation: the thermal mechanism; the prompt mechanism; and the nitrous oxide mechanism.

The thermal mechanism was first postulated by Zeldovich (1946). The mechanism involves the reaction of atmospheric nitrogen with oxygen atoms. The reaction is given by:

$$O + N_2 \rightarrow NO + N \tag{6-1}$$

with the reaction rate $w = A[N_2][O]\exp(-E_a/RT)$, where A is a constant and E_a is the activation energy for the reaction. $E_a \sim 76$ kcal/mol for this reaction, which means that the production of NO due to this mechanism is only significant for temperatures above 1800 K. The peak production via this mechanism is just on the lean side of stoichiometric and drops off on the lean and rich sides. This is one of the main reasons behind lean premixed combustors to reduce NOx production. Also, due to the exponential dependence on temperature, the reaction rate is very sensitive to temperature perturbations.

Two other fast reactions are combined with (6-1) to form the extended Zeldovich mechanism:

$$N + O_2 \rightarrow NO + O \tag{6-2}$$

$$N + OH \rightarrow NO + H \tag{6-3}$$

Also of importance for this mechanism is that NO formation is linearly dependent on residence time. The longer the reaction is kept at high temperatures, the greater the amount of NO produced. This relates to the results obtained for the pulse combustor results mentioned in the introduction. A higher temperature in the main flame zone led to increased NO, but the residence time at high temperatures was reduced, leading to lower overall NO concentrations at the exit plane when compared with steady state results.

Since thermal NO production is much slower than the main heat release reactions, it was believed that most of the NO production occurred after the flame. However, Fenimore (1970) measured NO levels for a laminar premixed flame. When he extrapolated the curve back to the surface of the burner, the NO levels were not zero. This NO level, noticed in hydrocarbon flames, was labeled the prompt mechanism. The reactions dominating this mechanism are fast and hard to resolve spatially near the burner.

The reaction scheme that describes the prompt mechanism involves hydrocarbon radicals, which are most prevalent in fuel-rich premixed flames. The hydrocarbons react with atmospheric nitrogen via the following reactions (Fenimore, 1970; Iverach et al., 1972):

$$CH + N_2 \rightarrow HCN + N \quad (6\text{-}4)$$

$$CH_2 + N_2 \rightarrow HCN + NH \quad (6\text{-}5)$$

$$C_2 + N_2 \rightarrow 2CN \quad (6\text{-}6)$$

$$HCN + H \leftrightarrow H_2 + CN \quad (6\text{-}7)$$

$$HCN + OH \leftrightarrow CN + H_2O \quad (6\text{-}8)$$

The CN atoms then react with O_2 and OH to form NO by:

$$CN + O_2 \rightarrow OCN + O \quad (6\text{-}9)$$

$$OCN + OH \rightarrow CO + NO \quad (6\text{-}10)$$

Experimental work has shown that the amount of NOx produced via this mechanism is greatest for fuel-rich regions and drops off drastically as the flame goes lean. Since it has been estimated that the prompt mechanism accounts for ~ 30% of NOx formed (Fenimore, 1970), running the system on the lean side of stoichiometric would have a dramatic effect on prompt NO.

The third mechanism developed by Malte and Pratt (1974) is the nitrous oxide mechanism and is important at low temperatures. The mechanism involves the production of N_2O as an intermediate to NO:

$$N_2 + O + M \rightarrow N_2O + M \quad (6\text{-}11)$$

The N_2O is then converted to NO or N_2. N_2O itself does not survive as a significant emission.

Other possibilities for the production of NOx involve any nitrogen contained in the fuel. Many hydrocarbon fuels contain 0.2 - 0.5% nitrogen. The nitrogen compounds will often undergo some transformation before entering the combustor. The nitrogen radicals (NH_i, i=1,2,3,4, HCN, CN, etc.) will then react to form NO.

The other species that makes up NOx is NO_2. The major source of NO_2 is the rapid oxidation of NO:

$$2NO + O_2 \leftrightarrow 2NO_2 \qquad (6\text{-}12)$$

This reaction occurs spontaneously and at ambient conditions. In combustion systems the main NO_2 formation reaction is:

$$NO + HO_2 \rightarrow NO_2 + OH \qquad (6\text{-}13)$$

and the principal removal steps are:

$$NO_2 + H \rightarrow NO + OH \qquad (6\text{-}14)$$

$$NO_2 + O \rightarrow NO + O_2 \qquad (6\text{-}15)$$

There is evidence that the consumption of NO_2 depends on the oxygen content of the flame. Also, at high temperatures, NO_2 removal is increased. NO_2 lifetimes are less than 10 ms for temperatures greater than 1500 K. This indicates that NO_2 emission levels will only be statistically relevant in low temperature combustors or devices that can quench the $NO_2 \rightarrow NO$ mechanism (Miller and Bowman, 1989).

6.2 Methods for Reducing NOx Emission Levels

The methods being developed to reduce the levels of NOx are based on the behavior of the mechanisms involved in NOx production. By running lean, the effects of prompt NO formation can be reduced significantly due to the low concentrations of hydrocarbon radicals.

Other methods make use of the results of the thermal mechanism by trying to reduce the temperature or the time the species spend in a high temperature environment.

Water injection into a gas-turbine combustor has been investigated for NOx reduction (Correa, 1992b). The steam/water injection lowers the temperature in the chamber, which reduces the effects of the thermal mechanism. However, water injection has many side effects including: quenching CO burnout; compromising flame stability; and mechanical corrosion. Also, water injection is not an acceptable method for aircraft gas turbines due to the excess weight. These deficiencies, along with the cost and complexity of adding water injection, make this method impractical for gas-turbine systems.

Another method involves staging the burner. The air inflow is split. Part of it is mixed with the fuel and burned fuel-rich, outside the bounds of significant thermal and prompt NOx production. The mixture is then quenched with the remaining air and then burned fuel-lean. This method can reduce NOx emissions by 50-70% and has been demonstrated experimentally (Sturgess et al., 1993).

One other method currently being pursued for the reduction of NOx emissions is with the processing of the gas downstream of the combustor. This method often involves filtering the output gas through either a catalyst or a system of chemicals that react with the pollutant species to lead to more acceptable products. This work is especially important for modifying older combustors to meet the lower levels of pollutant emissions set by current regulations. Problems with this method are usually the cost of restructuring an existing system with these modifications, and the possibility that the post processing is either not fast enough to lower the pollutants to the desired levels or that the new products formed from the post processing may also not be acceptable emissions.

Due to the complexity of a multi-staged combustor, much of the recent work has been on single stage systems of lean combustion (reviewed by Correa, 1992b). The work is applicable to premixed and diffusion flames; however, due to the non-uniformity of diffusion flames, premixed

flames show the best prospect for reducing NOx emissions. The basic idea of this scheme is to reduce the flame temperature by reducing the equivalence ratio and the corresponding thermal NOx production. The geometry of these systems is usually can-annular in that there are a number of premixer chambers leading into a cylindrical combustion chamber. The premixed flow often flows through an expansion before reaching the flame front to keep the flame out of the premixer to avoid flashback. One of the main difficulties with this approach is obtaining a properly premixed flow. Swirl vanes and fuel injection hole location have been examined as methods for improving the mixing quality of the flow. The swirl vanes are often used as well in an attempt to stabilize the flame. A dump plane with a recirculation region similar to the design tested in Chapter 4 is also a possible choice for maintaining the flame. However, this system is very sensitive to flow conditions and may develop unstable oscillations. Another method of stabilizing the flame, as seen in Chapter 5, involved the use of a diffusion pilot flame. However, the pilot flame burns stoichiometrically and is often the major producer of NOx in a given system.

Recent work with pulse combustors has shown the possibility of reducing the average amount of NOx emissions for a given system as compared with steady state operation. Keller and Hongo (1990) investigated possible reasons for the NOx reduction through lower residence times at high temperatures. During pulsing operation, the temperature dropped off significantly downstream of the main flame zone. This decrease in temperature compared to the non-pulsing case led to a decreased residence time at high temperatures, which led to a lower production of NOx in the pulsing case. Other experimental work by Casentini (1995) examined the flame structure and pollutant levels when the air and fuel injectors were pulsed at a certain frequency. The frequency was varied from 30 Hz to 2400 Hz to examine the impact of certain frequencies. It was found that the NOx levels were reduced by up to 21% and the CO levels by 46% in the presence of pulsing fuel and air flow.

6.3 Coupling of Unsteady Motions with Chemical Kinetics

Pulse combustors contain pressure oscillations that are desired. However, in a gas-turbine combustor, due to the accompanying noise production and structural vibrations, the development of instabilities may be a greater detriment to the system and might not have the same effect on NOx emissions. In order to understand how the reaction rates respond to pressure oscillations and likewise how the reaction rates and subsequent heat release affects the flow field, work needs to be undertaken both experimentally and analytically to look at possible interactions.

The formulation described in Chapter 3 leads to the representation (3-31) of the unsteady pressure field as a collection of nonlinear oscillators driven by energy released by chemical reactions, coupling with the mean flow field, and interactions with the turbulence field. Nearly all published works on combustion instabilities neglect the influences of turbulence and are concerned with stability of small disturbances and some aspects of nonlinear behavior. The details of the chemistry are buried in representations of the unsteady heat release and normally receive little attention.

As described in Appendix C, it is assumed that the unsteady motions can be computed (i.e., by solving the set of equations (C-29)) without specifying details of the chemistry. That assumption implies assigning the fluctuation Q′ of heat release values that depend only on the velocity and thermodynamic variables. Having, in principle, determined the unsteady field, we then turn attention to its influence on the chemical kinetics required to describe the formation of pollutants - here nitrogen oxides. Each of the species, having concentration $Y_i = \rho_i/\rho$, is described by the equation

$$\frac{\partial \rho Y_i}{\partial t} + \nabla \cdot \left(\rho \mathbf{u} Y_i \right) = \nabla \cdot \left(\rho \mathcal{D} \nabla Y_i \right) + w_i \qquad (6\text{-}16)$$

where w_i is the production rate, having dimension s^{-1} (Khalil, 1982).

A perturbation analysis can be performed for (6-16) as was done for the other conservation equations in Appendix C. After using the continuity equation and the assumption that the mean values do not vary with time, the perturbed equation reduces to:

$$\left(\overline{\rho}+\rho'\right)\frac{\partial Y_i'}{\partial t}=\left(-\rho'\overline{\mathbf{u}}-\overline{\rho}\mathbf{u}'-\overline{\rho}\,\overline{\mathbf{u}}-\rho'\mathbf{u}'\right)\cdot\nabla\left(\overline{Y}_i+Y_i'\right)+\nabla\cdot\left(\overline{\rho}\mathcal{D}\nabla\overline{Y}_i\right)+\nabla\cdot\left(\rho'\mathcal{D}\nabla\overline{Y}_i\right)$$
$$+\nabla\cdot\left(\overline{\rho}\mathcal{D}\nabla Y_i'\right)+\nabla\cdot\left(\rho'\mathcal{D}\nabla Y_i'\right)+w_i \qquad (6\text{-}17)$$

The unsteady flow field variables are determined from the approximate analysis given in Appendix C. The reaction rate needs to be expanded in the flow field and species variables. If it is assumed that the production rate is specified by the Arrhenius form, then:

$$w=A\exp\left(-T_a/T\right)\prod_j\left(\rho Y_j/W_j\right)^{C_j} \qquad (6\text{-}18)$$

where A is a pre-exponential constant for the reaction, T_a is the activation temperature, W_j is the molecular weight of species j, and Cj is the exponential factor for the concentration of species j. Expanding (6-18) around the perturbed quantities and letting the sum over j of C_j equal C_T leads to the following:

$$w = A\exp\left(\frac{-T_a}{\overline{T}}\right)\overline{\rho}^{C_T}\left(\prod_j\overline{Y}_j^{C_j}\right)\left[\prod_{k=1,\infty}\exp\left(\frac{-T_a}{\overline{T}}\left(\frac{-T'}{\overline{T}}\right)^k\right)\right]\left(1+\frac{\rho'}{\overline{\rho}}\right)^{C_T}\prod_j\left(1+\frac{Y_j'}{\overline{Y}_j}\right)^{C_j} \qquad (6\text{-}19)$$

The series is only convergent if $T_a/\overline{T}$ is less than one and the perturbations are small. Unfortunately, $T_a/\overline{T}$ is usually much greater than one in practice. Keeping in mind the problem of convergence, if the perturbations are assumed to be small, on the order of 0.1 or lower, then (6-19) can be further expanded to first order:

$$w =A\exp\left(\frac{-T_a}{\overline{T}}\right)\overline{\rho}^{C_T}\left(\prod_j\overline{Y}_j^{C_j}\right)\left[1+\frac{T_aT'}{\overline{T}^2}+C_T\frac{\rho'}{\overline{\rho}}+\sum_j C_j\frac{Y_j'}{\overline{Y}_j}+o(2)\right] \qquad (6\text{-}20)$$

The mean reaction rate is given by:

$$\overline{w} = A exp\left(\frac{-T_a}{\overline{T}}\right)\overline{\rho}^{C_T}\left(\prod_j \overline{Y}_j^{C_j}\right)\left[1 + C_T\frac{\overline{T_a T'\rho'}}{\overline{T}^2\ \overline{\rho}}\right.$$
$$\left. + \sum_j C_j\left(\frac{T_a}{\overline{T}}\frac{\overline{Y_j' T'}}{\overline{Y}_j\ \overline{T}} + C_T\frac{\overline{Y_j'\rho'}}{\overline{Y}_j\ \overline{\rho}} + \frac{C_T T_a}{\overline{T}}\frac{\overline{Y_j' T'\rho'}}{\overline{Y}_j \overline{T}\overline{\rho}}\right) + h.o.t.s\right] \qquad (6\text{-}21)$$

The mean reaction rate has many turbulence correlation terms which need to be obtained by second-order closure of their transport equations. The dominant term in (6-20) is the temperature fluctuation term. The activation temperature is often a large number on the order of 1e4, and consequently, $T_a/\ \overline{T}$ is larger than the values of C_T or C_j. Therefore, the fluctuations in the species levels will be strongly dependent on the oscillating temperature field. Substituting (6-20) back into (6-17), a relation for the fluctuating species mass fraction can be developed as a function of the fluctuating flow field variables. It would be possible to use this relation to examine the local and global behavior of the species levels in the presence of unsteady combustion; however, the higher order terms and possible turbulent correlations would make this a complex method.

The relation (6-20) can also be examined as a possible model source for the combustion response model discussed in Chapter 3. The oscillating heat release is a function of the oscillating production rates for the included species. This relation was given by (3-2) in which the heat release is given by the sum of the reaction rates for the individual species multiplied by the formation enthalpy. By incorporating (6-20) into that heat release relation, the fluctuating heat release is given as a function of the oscillating temperature, density and species mass fraction. The oscillating pressure and density fields are usually substituted for the oscillating temperature field through the ideal gas law, so the heat release is reduced to a function of the density, pressure and species mass fraction. In addition, the relation (6-20) can be substituted into (6-16) in order to solve for the variation of Y_j. It seems possible then to include this relation for the fluctuating mass fraction to provide a complex relation for the heat release given in terms of the mean and fluctuating flow field variables: p, ρ and u.

Another method for the examination of the species mass fractions in the presence of an oscillating flow field is by the use of numerical simulations. The numerical simulations can provide information about the local behavior that can be useful in understanding how the pollutant levels might change in an oscillating environment. However, as has been noted, many of these simulations only make use of a simplified reaction mechanism to reduce the computational expense of a complete numerical simulation. These simplified reaction mechanisms can, nevertheless, provide a reasonable guide as to how the unsteady flow field interacts both locally and on a global scale with the production of various species.

Section 4.4 presented the results for the CO levels within a dump combustor under oscillatory conditions. The steady state CO mass fraction contour shown in Figure 4-20 was computed for an equivalence ratio of 1.3. The contour, when compared with the temperature contour in Figure 4-2, shows that the region of greatest CO level is in the main flame region downstream of the step inlet. This level drops off as the high temperature levels out and the reaction mechanism for the transition from CO to CO_2 dominates. This transition is also the reason why the CO levels within the recirculation zone are lower.

When the time dependent simulation is performed, the location of the main flame region develops an oscillating structure. The vortex dynamics create local pockets of cold reactants that are propagated downstream. The downstream propagation delays the burning and the subsequent location of the flame front. Since the flame front corresponds to the location of the maximum CO levels, the region of maximum CO is forced downstream towards the exit plane. Therefore, on average, the CO levels at the exit plane, as they are defined for this problem, will be higher in the presence of oscillations than in steady flow. For this case, the oscillations have the opposite effect on the NOx levels. Thermal NOx is created when the temperature is high and the levels grow with increasing residence time. The flame oscillations in the dump combustor reduce the mean flame temperature, in turn reducing the reaction rate for the production of NOx. The residence time is also reduced, since the oscillations vary the size of the recirculation zone behind

the step. For both of these reasons, the NOx levels at the exit plane are lower than the steady state values for the case flow configuration.

6.4 PSR and PFR Models for Simulating Combustion System

The numerical results that have been performed up to this point involve a complex geometry representation and the inclusion of a simple chemical mechanism. The main reaction used in the simulations only involved five reaction steps and eight species. However, as has been mentioned, inclusion of all the relevant chemistry within a given simulation could involve as many as 42 species and 300 reaction rates. Therefore, it is not computationally prudent to perform simulations that include a complex geometry and a detailed chemical reaction mechanism. One way around this is to reduce the complexity of the chemical reactions. Another is to reduce the complexity of the geometry while keeping the detailed chemical description. This method is accomplished by the use of perfectly stirred reactor (PSR) and plugged flow reactor (PFR) models. Large sections of the combustor can be grouped together and modeled by average flow properties. In this manner, the entire combustion system could be modeled as connecting PSR and PFR elements.

Most of the research work conducted with the use of PSR and PFR elements involves the calculation of the steady state species levels within a given design. This method of simulating the flow field is very beneficial in pre-design studies in industry where a good estimate of the pollutant levels can be made without too much computational effort (Nicol et al., 1992). Due to the ability to examine the steady state species levels in a given combustor design, work was initiated by Feitelberg (1995) to use PSR and PFR models to examine the influence of oscillations on the species levels within a given combustor design. Feitelberg used a single PSR element for his initial research study. An oscillating pressure term was prescribed at the PSR inlet, which also influenced the incoming equivalence ratio. The oscillating inlet flow was then stepped in

time to determine how the species level within the PSR element behaved under oscillating conditions.

Independently, similar work was performed at Caltech (Swenson and Pun, 1996). The first step in the work ran the PSR simulation for a range of equivalence ratios to determine the steady state influences of temperature and pressure. For a single PSR element, the NOx dependence was determined as:

$$[\text{NOx (15\% Dry)}] = 14.37\ T^{1.905} \exp(-2.622E4/T) \qquad (6\text{-}22)$$

To examine the influences of an oscillating temperature field, a time dependent oscillation was imposed on the steady state relation given by (6-22). At each step in time, it was assumed that the mixture in the PSR was perfectly stirred and had reached quasi-steady levels given by (6-22). This use of the steady state NOx dependence was compared with Feitelberg's results, which ran the simulation with the PSR at distinct time steps throughout the imposed simulation. The main results presented by Feitelberg involved a 2% temperature oscillation. He showed that the average NOx level in the presence of this oscillation amounted to an increase of 2.3% over the mean NOx level at the mean temperature. The results we obtained showed an increase of 2.5% over the mean NOx levels for the same temperature oscillation. Although it is only one matching condition, it seems that these two approximate methods are comparable and may provide quantitative values for pollutant levels within a single PSR or PFR element. However, it should be noted that since the PSR and PFR methods do not accommodate dynamical behavior in a rigorous way (i.e., the results are for a quasi-steady system), research in this area will not provide much insight into the system-wide dynamic response between the chemical species and an unsteady flow field. The PSR and PFR method is better configured to determine the relation of the species levels under a range of conditions to develop relationships like that given by (6-22) that can then be used with a simple oscillating input to determine pollutant level guides in design studies.

Chapter Seven

Conclusions

The initial motivation for this thesis was the desire to obtain detailed information about the dynamics of the flow field in a full-scale gas turbine combustor. The information would be valuable in understanding how the heat release interacts with the flow field in developing unsteady motions. Knowledge of this basic interaction would be beneficial in constructing heat release models and control methodologies for improving the system efficiency and reducing pollutant production. Numerical simulations were chosen as a means of obtaining the flow field information because experimental results are mostly unavailable especially since it is difficult to use experimental diagnostics in a full-scale combustor. Since the desire of the thesis was not the constructing of a numerical method, but the use of such a method in the further exploration of other issues, a commercially available code, ANSWER, was selected. In order to validate ANSWER, additional simple flow configurations were modeled. The three configurations modeled as a part of this thesis were a planar heat source in a tube, a premixed flow in a dump combustor, and a full-scale gas turbine combustor with premixed and diffusion flames.

Modeling the Rijke tube numerically has been accomplished in the past by one-dimensional approximations that only took into account the longitudinal interactions and by approximate analysis techniques like those described in Chapter 3. However, up to this point, there has not been a good simulation using a full Navier-Stokes solver. The results obtained for this thesis were made for two configurations, a constant heat source similar to an electrically heated wire mesh and a premixed flame. The issue of a boundary condition deficiency was exposed during these simulations. A Rijke tube is normally defined as having acoustically open boundaries upstream and downstream of the heat source. We were able to obtain acoustically open boundaries at the upstream and downstream end of the numerical domain but with some

limitations. The frequencies and mode shapes obtained matched theoretical predictions; however, the use of a fixed pressure boundary and the specification of a zero gradient velocity at the inlet in the validation process brought up many issues concerning the stability of the numerical method and the possible over-damping of acoustic motions at the boundary. The ability of the numerical method to calculate a broad range of boundary specifications needs to be explored in more detail in the future to allow the numerical method to be applied to more diverse problems.

The results for this simple configuration did demonstrate that fitting the desired problem to the default boundary conditions could be useful in the examination of the interaction between the heat release and the flow field. The constant heat source in a tube that is acoustically closed at both ends showed unsteady behavior when the heat source was placed at $x = 3L/4$ and steady behavior when the heat source was placed at $x = L/4$. The reason has to do with the phase difference between the oscillating component of the heat release, the velocity and pressure. In both of these positions, the heat release lagged the velocity by about 60°. At $x = 3L/4$, the acoustic pressure also lags the velocity by 90°, allowing positive coupling between the heat release and pressure, which according to Rayleigh's criterion leads to a driven system. Similar results for the premixed flame in an acoustically closed-open tube indicate that a possible heat release model, based on the numerical results, is a time lag model connecting the heat release and the velocity fluctuations. This results could be extended by further studies using the approximate analysis method described in this thesis.

Another result from the Rijke tube simulations was the behavior of the NOx levels. Keller and Hongo (1990) had shown a reduction in the NOx concentration in a pulse combustor when the system was oscillating. The results for the Rijke tube obtained here matched that result, indicating that in the presence of an oscillation, the mean temperature downstream of the heat source is reduced. This, in turn, reduces the NOx production rate and therefore the amount of

NOx at the exit. If the oscillations could be controlled in a real system, it may be possible to apply this result to further reduce NOx concentrations.

The dump combustor results demonstrated a coupling between the vortex shedding and the acoustic frequencies. The unsteady frequencies determined for this flow configuration agreed well with experimental results obtained previously at Caltech and one-dimensional theoretical calculations. The results demonstrated that as long as the boundary conditions are understood, the numerical method could be useful for simulating combustion instabilities. Varying the mass flow rate and the equivalence ratio in the simulations led to a stability map for the system. Both stable and unstable results were obtained depending on the flow configuration. The stability map matched the basic shape of a similar map obtained experimentally at Caltech and could be improved further by a systematic set of numerical simulations.

Determining the coupling between the heat release and the flow field is considerably more complicated for the dump combustor than for the planar heat source in a tube. However, the results are more detailed than those that can be obtained experimentally, allowing for the development of localized heat release models. Knowledge of the heat release models can be useful for the development of active and passive control methodologies. Additional fuel sources and upstream fluctuations of the mixture ratio are being explored experimentally as possible active control mechanisms. These methods can also be explored using the numerical simulations.

Passive control methods can also be examined by the use of numerical simulations. The results with the Helmholtz resonator presented in this thesis demonstrated that the oscillations can be damped. The full-scale numerical simulation of an unstable flow with a Helmholtz resonator as a passive control is original with this thesis. However, the results need to be extended in time to examine the behavior of the oscillations as the hot products in the recirculation zone interact with the cold air in the resonators to change the resonant frequency. A possible de-tuning may occur in this case leading to a resurgence of the oscillation. This de-tuning with a change in temperature has been shown in experimental results.

The results for the dump combustor also showed interesting behavior of the NOx and CO concentrations. The development of the oscillation pushed the main flame zone further downstream, leading to a delay in the production of the pollutants. The delay forced the maximum CO region downstream, leading to an increase in the CO concentration at the exit plane. However, the delayed flame region had the opposite effect on the NOx concentration. By delaying the flame zone, the residence time in the hot flame was reduced, leading to a reduction in the NOx concentration at the exit plane. It is not clear how this information might be applied to real systems, but it does merit further attention.

The full-scale gas turbine combustor is even more complex than the dump combustor. The geometry is more complex and the flow includes a diffusion flame to stabilize the premixed flame and a region at the exit where the flow approaches sonic conditions. Studies of the mixing in the premixer indicate that the flow is not perfectly premixed by the time it reaches the flame front. Variations in the local equivalence ratio lead to unsteady motions that could be amplified. A better designed premixer may be a possible solution to part of the problem of unsteady operation. The numerical simulations could be useful for this design study, but experimental results are needed for validation. The maximum heat release region occurs at the diffusion flame. The interaction of the pressure fluctuations with the fuel and air flow rates may lead to a coupling between the heat release and the pressure field and a driven system. The diffusion pilot flame is also a major source of NOx production due to the stoichiometric burning. If the diffusion flame could be eliminated by better flame holding of the premixed flame, the performance of the system might be improved substantially.

In summary, the numerical code ANSWER worked fairly well in reproducing unsteady acoustic motions in the presence of combustion once the deficiencies of the code were understood and improved. The acoustic frequencies and modes determined for all the simulations matched either experimental results for the same configuration or theoretically determined mode shapes and frequencies. The results indicate that it should be possible to use numerical simulations for

the development of localized heat release models for use in approximate methods. The results showed an ability to study passive control methods numerically, which could also be applied to active control methods in the future. Finally, the numerical results were able to resolve the behavior of NOx and CO production rates in the presence of an oscillation. These results could lead to a further examination of the trade-off between a stable system and the need to reduce the NOx concentrations in gas-turbine systems.

Appendix A

Finite Element Method Applied to Acoustic Wave Equation for the Theoretical Determination of Acoustic Modes

This appendix will outline the method for determining the acoustic mode information for a given geometry and temperature field. This analytical method makes use of a finite element representation of the acoustic equation:

$$\frac{\partial^2 p'}{\partial t^2} - \bar{c}^2 \nabla^2 p' = \bar{\rho}(\gamma - 1) G \frac{\partial p'}{\partial t} \tag{A-1}$$

where G is a complex number representing the spatial element of heat release and local delay of fluctuations of heat in relation to pressure. By separating the spatial and temporal components of pressure, the solution takes on the following form:

$$p' = p'_o(x, y, z) e^{st} \tag{A-2}$$

where $s = \omega_r + i\omega_i$. From this, the propagation equation reduces to:

$$\nabla^2 p'_o + k^2 p'_o + \frac{s\bar{\rho}(\gamma - 1) G(x, y, z, s)}{\bar{c}^2} p'_o = 0 \tag{A-3}$$

where $k^2 = -s^2 / \bar{c}^2$. The domain of integration can be subdivided into a number of subdomains Ω^e to obtain:

$$\sum_{h=1}^{n} \left\{ s^2 M^e_{k,h} + s\left(B^e(s)_{k,h} - C^e(s)_{k,h,} \right) + K^e_{k,h} \right\} u^e_h = Q^{0e}_k + Q^{1e}_k \qquad k = 1, n \tag{A-4}$$

with the following designations:

$$\text{Stiffness Matrix: } K^e_{i,j} = \int_{\Omega^e} \left[\frac{\partial \psi^e_j}{\partial x} \frac{\partial \psi^e_i}{\partial x} + \frac{\partial \psi^e_j}{\partial y} \frac{\partial \psi^e_i}{\partial y} + \frac{\partial \psi^e_j}{\partial z} \frac{\partial \psi^e_i}{\partial z} \right] d\Omega$$

$$\text{Mass Matrix: } M^e_{i,j} = \int_{\Omega^e} \frac{1}{c^2} \psi^e_i \psi^e_j d\Omega$$

Self-Excitement Matrix: $C^e(s)_{i,j} = \int_{\Omega^e} \frac{\rho(\gamma-1)G(x,y,z,s)}{\bar{c}^2} \psi_j^e \psi_i^e d\Omega$

Impedance Matrix: $B^e(s)_{i,j} = \int_{\Gamma_3} \frac{\rho}{Z(x,y,z,s)} \psi_j^e \psi_i^e d\Gamma$

Exchanged Flow: $Q_j^{0e} = \int_{\Gamma_0} \frac{\partial u^e}{\partial n} \psi_j^e d\Gamma$

Outward Flow: $Q_j^{1e} = \int_{\Gamma_1} \frac{\partial u^e}{\partial n} \psi_j^e d\Gamma$

Putting this all together over the entire domain leads to:

$$s^2\left[M^G\right]\{u\} + s\left[B^G(s) - C^G(s)\right]\{u\} + \left[K^G\right]\{u\} = \left\{Q^{1G}\right\} \qquad \text{(A-5)}$$

The eigenvalues for this system can be solved by setting the right-hand side to zero. In order to reduce the complexity of the solution even further, azeroth order approximation can be made by setting the G term to zero, hence no heat input to the system, and by setting the impedance at the boundaries to infinity, which leads to a zero B matrix. This reduction to only the M and K matrices leads to a simple solution method for s and {u}; however, these values are only useful up to the level of the approximations made.

Appendix B

One-Dimensional Theoretical Determination of Acoustic Modes with a Temperature Jump

This appendix will outline the method for determining the acoustic mode information for a one-dimensional tube with a specified temperature jump representative of a planar heat source in a Rijke tube. This method assumes a cosine and sine summation for the fluctuating pressure and velocity:

$$p'=a\cos(kx)+b\sin(kx)$$
$$u'=\frac{1}{\gamma k^2}(-ak\sin(kx)+b\cos(kx)) \tag{B-1}$$

where k is the wave number and is specified as ω/c, where ω is the angular frequency and c is the speed of sound. The domain is broken into two sections at temperature T_1 upstream of the heat source and T_2 downstream of the heat source. The pressure and velocity fluctuations are then given by

$$p'_1=a_1\cos(k_1x)+b_1\sin(k_1x)$$
$$p'_2=a_2\cos(k_2x)+b_2\sin(k_2x)$$
$$u'_1=\frac{1}{\gamma k_1^2}(-a_1k_1\sin(k_1x)+b_1\cos(k_1x)) \tag{B-2}$$
$$u'_2=\frac{1}{\gamma k_2^2}(-a_2k_2\sin(k_2x)+b_2\cos(k_2x))$$

The unknowns are a_1, b_1, a_2, b_2 and ω The first step is to define the boundary condition at the upstream end. For example, if the upstream boundary is acoustically closed, $u'_1 = 0 = b_1$, and if the upstream boundary is acoustically open, $p'_1 = 0 = a_1$. The second step is to define the boundary condition at the downstream end. This will lead to b_2 as a function of a_2 and ω. We can then scale the result by setting one of the remaining terms equal to one. The pressure and velocity matching conditions at the interface provide the final requirements to solve for the

frequency and the mode shapes. The matching conditions are that the pressure and velocity fluctuations are constant at the interface.

As an example of this method, we can solve for a tube of length L = 1.0m, with the temperature jump at $x_f = 0.25$ m. The temperature upstream is $T_1 = 300$ K, and the temperature downstream is $T_2 = 1600$ K. If we assume that the upstream boundary is acoustically closed, $u'_1|_{x=0} = 0$ and therefore $b_1 = 0$. Assuming that the downstream boundary is acoustically open, $p'_2|_{x=L} = 0$ which leads to

$$b_2 = -a_2 (\cos(k_2 L)/(\sin(k_2 L)) \tag{B-3}$$

We now set a1 = 1 and scale the results to this value. The matching condition for the pressure leads to

$$\cos(k_1 x_f) = a_2 \left(\cos(k_2 x_f) - \frac{\cos(k_2 L)}{\sin(k_2 L)} \sin(k_2 x_f) \right) \tag{B-4}$$

The matching condition for the velocity leads to

$$\sin(k_1 x_f) = a_2 \frac{k_1}{k_2} \left(\sin(k_2 x_f) + \frac{\cos(k_2 L)}{\sin(k_2 L)} \cos(k_2 x_f) \right) \tag{B-5}$$

Combining (B-4) and (B-5) results in a function for the angular frequency:

$$\cos(k_1 x_f) = \frac{k_2}{k_1} \sin(k_1 x_f) \frac{\left(\cos(k_2 x_f) - \frac{\cos(k_2 L)}{\sin(k_2 L)} \sin(k_2 x_f) \right)}{\left(\sin(k_2 x_f) + \frac{\cos(k_2 L)}{\sin(k_2 L)} \cos(k_2 x_f) \right)} \tag{B-6}$$

The solutions to this equation are the theoretical acoustic modes. The frequency, $f = \omega/2\pi$, of the first mode is 188.8 Hz, and the frequency of the second mode is 420.9 Hz. Figure B-1 shows the pressure mode shapes for these first two acoustic modes.

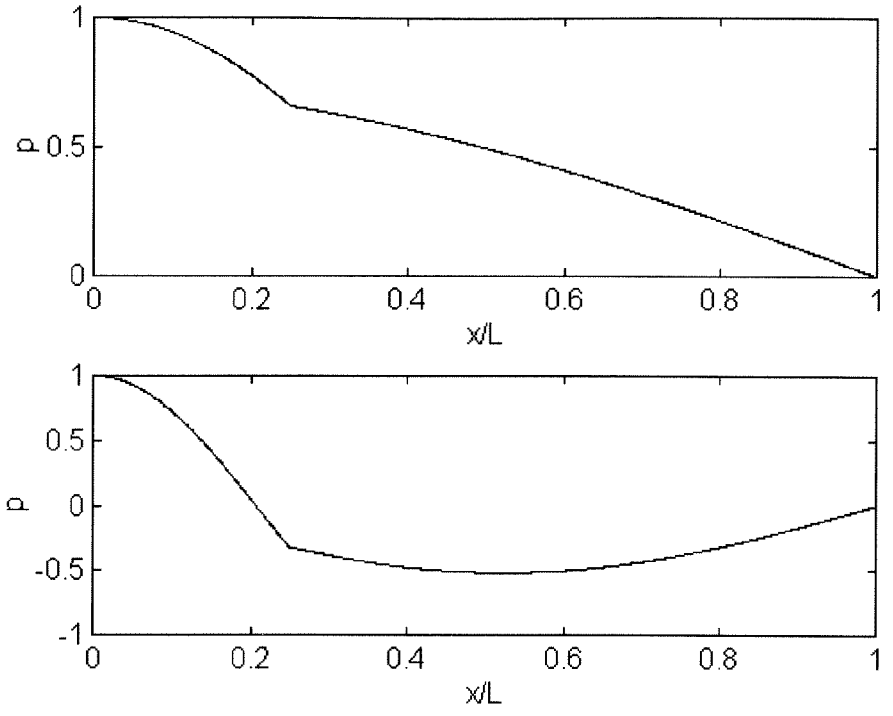

Figure B-1 Theoretical Acoustic Pressure Mode Shapes for First Two Mode Solutions;

$L = 1.0$ m, $x_f = 0.25$ m, $T_1 = 300$ K, $T_2 = 1600$ K

Appendix C

Analysis of Instabilities

This section will present the details behind the development of analytical techniques for the analysis of instabilities within a combustion system. The technique makes use of a method of spatial averaging to simplify the perturbed conservation equations into a series of ordinary differential equations. No new work on the analysis itself will be presented. This section is intended more as background motivation for the numerical work. As has been shown in the previous sections, the numerical simulations can provide key information for the simplified analysis including the acoustic frequencies and mode shapes and the interaction between the heat release and the flow field.

C.1 Formulation of an Approximate Analysis

In order to generalize the results obtained for combustion instabilities and to reduce the complexity of analyzing a real combustion system, approximate methods of analysis have been developed to investigate unsteady motions and coupling between an unsteady flow field and the combustion regime. The analysis provides a means of predicting and interpreting the characteristics of linear and nonlinear oscillations in combustion chambers. Most of the previous work has involved coupling between velocity, pressure and the heat release. Additionally, this analysis should be able to be expanded to incorporate coupling between chemical reaction rates and flow field oscillations. A prerequisite to obtaining quantitative global results with this sort of analysis is careful modeling and explicit calculations of contributing physical processes.

Formulation of the analysis starts with the conservation equations of mass, momentum and energy in the primitive form:

MASS $$\frac{\partial \rho}{\partial t} + \nabla \cdot (\rho \mathbf{u}) = \dot{W} \qquad \text{(C-1)}$$

MOMENTUM $$\frac{\partial}{\partial t}(\rho \mathbf{u}) + \nabla \cdot (\rho \mathbf{u}\mathbf{u}) + \nabla p = \nabla \cdot \tau + \mathbf{F} \tag{C-2}$$

ENERGY $$\frac{\partial}{\partial t}(\rho e_0) + \nabla \cdot (\rho \mathbf{u} e_0) + \nabla \cdot (\rho \mathbf{u}) = \nabla \cdot (\tau \cdot \mathbf{u}) + \nabla \cdot \mathbf{q} + Q + \mathbf{u} \cdot \mathbf{F} \tag{C-3}$$

where ρ, $\mathbf{u}$ and p are the density, velocity and pressure; $e_0 = e + u^2/2$ is the stagnation internal energy ($de = C_v dT$ where T is temperature); τ is the viscous stress tensor; $\mathbf{q}$ is internal heat transfer; and $\mathcal{W}$, $\mathbf{F}$ and Q represent sources of mass, momentum and energy, the last being essentially the heat released in chemical reactions. The equation of state is

$$p = \rho RT \tag{C-4}$$

Standard manipulations of these equations lead to the set

$$\frac{D\rho}{Dt} = -\rho \nabla \cdot \mathbf{u} + \mathcal{W} \tag{C-5}$$

$$\rho \frac{D\mathbf{u}}{Dt} = -\nabla p + \mathcal{J} \tag{C-6}$$

$$\rho C_\upsilon \frac{DT}{Dt} = -p \nabla \cdot \mathbf{u} + \mathcal{Q} \tag{C-7}$$

$$\frac{Dp}{Dt} = -\gamma p \nabla \cdot \mathbf{u} + \mathcal{P} \tag{C-8}$$

$$T \frac{Ds}{Dt} = \mathcal{Q} - RT\mathcal{W} \tag{C-9}$$

where

$$\mathcal{J} = \nabla \cdot \tau + \mathbf{F} - \mathbf{u}\mathcal{W} \tag{C-10}$$

$$\mathcal{Q} = (\tau \cdot \nabla) \cdot \mathbf{u} + \nabla \cdot \mathbf{q} + Q - \left(e - u^2/2\right)\mathcal{W} \tag{C-11}$$

$$\mathcal{P} = \frac{R}{C_\upsilon}\left(\mathcal{Q} + C_\upsilon T \mathcal{W}\right) \tag{C-12}$$

So far as combustion instabilities in a gas turbine are concerned, the contributions from $\mathcal{J}, \mathcal{W}, \tau$ and $\mathbf{q}$ are normally negligible, giving the simple result for $\mathcal{P}$,

$$\mathcal{P} = R\mathcal{Q}/C_v = RQ/C_v \tag{C-13}$$

Nonlinear gas dynamic processes are important in the kinds of problems envisioned here, acting, for example, to produce limit cycles and to couple the turbulent and acoustic fields (Culick, 1995; Burnley, 1996). Experience with analysis of nonlinear combustion instabilities has demonstrated that it is sufficient to carry nonlinear contributions to second order: third order terms seem to generate only quantitative, not qualitative, corrections. The flow field is represented as a sum of a steady mean field and an unsteady fluctuation, $p = \bar{p} + p'$, $\mathbf{u} = \bar{\mathbf{u}} + \mathbf{u}'$, etc. For simplicity here we will assume $\bar{p}$, $\bar{\rho}$and $\bar{T}$ uniform but $\bar{\mathbf{u}}$ must be non-uniform which implies $p(t, \mathbf{r}) = \bar{p} + p'(t, \mathbf{r}), \mathbf{u}(t, \mathbf{r}) = \bar{\mathbf{u}}(\mathbf{r}) + \mathbf{u}'(t, \mathbf{r})$.

Making these substitutions in the conservation equations leads to perturbed equations for momentum and energy:

$$\bar{\rho}\frac{\partial \mathbf{u}'}{\partial t} + \nabla p = -\bar{\rho}\left[\bar{\mathbf{u}}\cdot\nabla\mathbf{u}' + \mathbf{u}'\cdot\nabla(\bar{\mathbf{u}} + \mathbf{u}')\right] - \rho'\frac{\partial \mathbf{u}'}{\partial t} + \mathcal{F}' \tag{C-14}$$

$$\frac{\partial p'}{\partial t} + \gamma\bar{p}\nabla\cdot\mathbf{u}' = -\gamma p'\nabla\cdot(\bar{\mathbf{u}} + \mathbf{u}') - (\bar{\mathbf{u}} + \mathbf{u}')\cdot\nabla p' + \mathcal{P}' \tag{C-15}$$

Taking the time derivative of (C-15) and substituting in the relation for $\partial\mathbf{u}'/\partial t$ from the left-hand side of (C-14) leads to the nonlinear wave equation for p':

$$\nabla^2 p' - \frac{1}{a^2}\frac{\partial^2 p'}{\partial t^2} = h_1 + h_2 + h_3 = h \tag{C-16}$$

where $$h_1 = -\bar{\rho}\nabla\cdot\left[\bar{\mathbf{u}}\cdot\nabla\mathbf{u}' + \mathbf{u}'\cdot\nabla\bar{\mathbf{u}}\right] + \frac{1}{a^2}\left(\gamma\frac{\partial p'}{\partial t}\nabla\cdot\bar{\mathbf{u}} + \bar{\mathbf{u}}\cdot\nabla\frac{\partial p'}{\partial t}\right) \tag{C-17a}$$

$$h_2 = -\bar{\rho}\nabla\cdot(\mathbf{u}'\cdot\nabla\mathbf{u}') - \nabla\cdot\rho'\frac{\partial \mathbf{u}'}{\partial t} + \frac{1}{a^2}\left[\gamma\frac{\partial}{\partial t}(p'\nabla\cdot\mathbf{u}') + \frac{\partial}{\partial t}(\mathbf{u}'\cdot\nabla p')\right] \tag{C-17b}$$

$$h_3 = \nabla\cdot\mathcal{F}' - \frac{1}{a^2}\frac{\partial \mathcal{P}'}{\partial t} \tag{C-17c}$$

and $a^2 = \gamma\ \bar{p}/\ \bar{\rho}$ is the constant speed of sound in the chamber. The pressure boundary condition is determined by the scalar product of the outward normal with (C-14):

$$\nabla p'\cdot\hat{n} = \left(-\mathbf{f}_1 - \mathbf{f}_2 - \mathbf{f}_3\right)\cdot\hat{n} = -\mathbf{f}\cdot\hat{n} \tag{C-18}$$

where, $\mathbf{f}_1 = \overline{\rho}\frac{\partial \mathbf{u}'}{\partial t} + \overline{\rho}[\overline{\mathbf{u}} \cdot \nabla \mathbf{u}' + \mathbf{u}' \cdot \nabla \overline{\mathbf{u}}]$ (C-19a)

$$\mathbf{f}_2 = \rho'\frac{\partial \mathbf{u}'}{\partial t} + \overline{\rho}(\mathbf{u}' \cdot \nabla \mathbf{u}') \quad \text{(C-19b)}$$

$$\mathbf{f}_3 = -\mathcal{F}' \quad \text{(C-19c)}$$

If the right-hand sides of (C-16) and (C-18) are set to zero, then the nonlinear wave equation would allow simple periodic solutions for p′ with a frequency ω_n. The problem would be reduced to solving for the classical acoustic modes of the chamber $\psi_n(\mathbf{r})$. The nonlinear wave equation would simplify to:

$$\begin{aligned} &\nabla^2 \psi_n(\mathbf{r}) + k_n^2 \psi_n(\mathbf{r}) = 0 \\ &\nabla \psi_n(\mathbf{r}) \cdot \hat{n} = 0 \end{aligned} \quad \text{(C-20)}$$

with $k_n = \omega_n / a$.

Since this perturbation analysis assumes the fluctuations to be small, the contributions of h and f are small and the classical acoustic modes can be considered nearly correct. The pressure and velocity fluctuations are assumed to be a product of the acoustic modes $\psi_n(\mathbf{r})$ with a time dependent amplitude $\eta_n(t)$,

$$p' = \overline{p}\sum_{j=1}^{\infty} \eta_j(t)\psi_j(\mathbf{r}) \quad \text{(C-21)}$$

$$u' = \sum_{j=1}^{\infty} \frac{\dot{\eta}_j(t)}{\gamma k_n^2} \nabla \psi_j(\mathbf{r}) \quad \text{(C-22)}$$

Substituting these back into the wave equations for p′, multiplying by ψ_n and averaging over the chamber volume leads to the set of time dependent equations for the amplitude of the fluctuations:

$$\ddot{\eta}_n + \omega_n^2 \eta_n = \mathbf{F}_n \quad \text{(C-23)}$$

where

$$\mathbf{F}_n = -\frac{a^2}{\bar{p}E_n^2}\left\{\int h\psi_n dV + \oiint f\psi_n dS\right\}$$
$$E_n^2 = \int \psi_n^2 dV \qquad \text{(C-24)}$$

In this manner, the set of partial differential equations has been simplified to a set of ordinary differential equations.

With the approximation to second order noted above, the forcing function F_n, defined by (C-24), can eventually be written

$$-\frac{\bar{p}E_n^2}{a^2}F_n = \bar{\rho}I_1 + \frac{1}{a^2}I_2 + \bar{\rho}I_3 + \frac{1}{a^2}I_4 + \oiint \bar{\rho}\frac{\partial \mathbf{u}'}{\partial t}\cdot \hat{n}dS - \int \frac{1}{a^2}\frac{\partial \mathcal{P}'}{\partial t}\psi_n dV \qquad \text{(C-25)}$$

where

$$I_1 = \int (\bar{\mathbf{u}}\cdot\nabla\mathbf{u}' + \mathbf{u}'\cdot\nabla\bar{\mathbf{u}})\cdot\nabla\psi_n dV$$
$$I_2 = \frac{\partial}{\partial t}\int (\gamma p'\nabla\cdot\bar{\mathbf{u}} + \bar{\mathbf{u}}\nabla\cdot p')\psi_n dV$$
$$I_3 = \int \left(\mathbf{u}'\cdot\nabla\mathbf{u}' + \frac{\rho'}{\bar{\rho}}\frac{\partial \mathbf{u}'}{\partial t}\right)\cdot\nabla\psi_n dV \qquad \text{(C-26)a,b,c,d}$$
$$I_4 = \frac{\partial}{\partial t}\int (\gamma p'\nabla\cdot\mathbf{u}' + \mathbf{u}'\nabla\cdot p')\psi_n dV$$

In deriving these formulas for the integrals I_1-I_4, some use has been made of the classical acoustics relations, $\bar{\rho}\mathbf{u}_t' = -\nabla p'$ and $p_t' = -\gamma\bar{p}\nabla\cdot\mathbf{u}'$, a step consistent with the order to which the equations have been written. The approximation can be justified by carrying out a two-parameter expansion of the original conservation equations, the two small parameters being Mach numbers characterizing the steady and unsteady fields.

Further reduction in the complexity of the problem can be achieved by time averaging the wave equation (C-23) after first breaking each $\eta_n(t)$ term into:

$$\eta_n(t) \approx r_n(t)\cos(\omega_n t - \phi_n(t)) = A_n(t)\sin(\omega_n t) + B_n(t)\cos(\omega_n t) \qquad \text{(C-27)}$$

A set of differential equations can be developed from this for the progression of $A_n(t)$ and $B_n(t)$:

$$\frac{dA_n}{dt} = \frac{1}{2\pi}\int_{t}^{t+\tau} F_n \cos(\omega_n t')dt'$$
$$\frac{dB_n}{dt} = -\frac{1}{2\pi}\int_{t}^{t+\tau} F_n \sin(\omega_n t')dt' \qquad \text{(C-28)}$$

where $\tau = 2\pi/\omega_n$. Similar relations may be derived for $r_n(t)$ and $\phi_n(t)$.

C.2 Acoustic Parameters and Combustion Response Models

The approximate analysis requires information about the flow field that is commonly not easily determined from experiments. Numerical simulations provide an opportunity to understand the behavior of the mean flow field in various geometrical configurations which could be valuable for calculating various terms of the approximate analysis. The numerical simulations also provide a means for analyzing the acoustic frequencies and mode shapes and the interaction of the heat release with the flow field.

There are two main numerical methods for the determination of the acoustic frequencies and mode shapes. The first uses the temperature field and the geometry of the chamber to calculate the theoretical frequencies and mode shapes. For 2-D and 3-D flows, this calculation can be performed with the use of a finite element method described in Appendix A. For 1-D flows, the method described in Appendix B can be used to determine the theoretical frequencies and mode shapes. Another method uses the results of the transient numerical simulations to determine the frequencies and mode shapes. Since it was determined in Section 2.5 that the numerical simulations calculate the proper acoustic behavior, taking into account the boundary conditions, a fast Fourier transform of the output signal provides the power levels of the frequency components. By stepping through a cycle of the oscillation, the structure of the acoustic modes can be determined. This method was shown earlier to work for the simple case of the Rijke tube.

In addition to the gas dynamic terms, combustion response models are important for the approximate analysis. The form of the response model is highly dependent on the combustion chamber environment. An example of the response in a solid propellant rocket is related through the mass burning rate at the surface, given by:

$$\dot{m}_b' = (\bar{\mathbf{u}}\rho' + \mathbf{u}'\bar{\rho} + \mathbf{u}'\rho')\cdot(-\hat{n}) = [\text{ad hoc formula}] \qquad \text{(C-29)}$$

Various models for this mass burning rate can be included in the perturbation analysis to produce systems of equations which contain both the nonlinear gas dynamics and other nonlinear response terms.

As the results for the Rijke tube have demonstrated, the combustion response can be analyzed in more detail with the numerical simulations. These detailed results can be used to develop models of the combustion response in both reacting and non-reacting flows. The electrically heated mesh is a very simple case in which the numerical results can be compared with a simple analysis to determine a basic form of the combustion response. Figure C-6 showed that the acoustic modes for the numerical Rijke tube are basically cosines, with a slight deviation at the heat source location. Because of this we can assume the following forms for the pressure and velocity fluctuations:

$$\begin{aligned} p' &= \bar{p}\cos(kx)\cos(\omega t) \\ u' &= \bar{u}\sin(kx)\sin(\omega t) \end{aligned} \qquad \text{(C-30)}$$

where $k = \pi/L$ for our test case. By setting q' equal to various functions of p' and u' and integrating over a period of the oscillation, we can calculate the spatial value of Rayleigh's parameter, $R(x)$. The regions where $R(x) > 0$ should correspond to a driven situation and $R(x)$ to a damped situation.

A first assumption that $q' = p'$ leads to a situation where the system is driven at all points in the chamber, except at L/2 where there is a pressure node. However, the numerical results in Section 3.1.2 showed that the first mode was only unstable when the heat release was placed in the later half of the chamber, so this assumption for a model is not accurate. A second

assumption of $q' = u'$ seems reasonable; however, R(x) in this case is basically zero at all values of x, indicating that the system will never be driven with this basic model. Other researchers (Raun et al., 1993) have guessed that q' is a product of u' and p', either as $q' = u'p'$ or $q' = |u'p'|$. The calculation of the Rayleigh's parameter in both of these cases yields a zero value for all x locations, indicating that both of these models do not conform with the numerical and experimental results. Examining the behavior in Figure 3-6, we see that the heat release oscillation lags the velocity fluctuation and leads the pressure fluctuation by T/8, where T is the period and is equal to 1/f. This implies two possible models. The first is $q'(t) = p'(t + T/8)$ which leads to the same R(x) behavior as $q' = p'$, which does not match the behavior of the oscillation in the numerical case when the heat release was placed at L/4 instead of 3L/4. The other model is $q'(t) = u'(t - T/8)$, which leads to a driven case when $x > L/2$ and a damped case when $x < L/2$. This simple model, which is a basic n-τ model, captures the behavior of the heat release for the numerical simulation of the electrically heated wire mesh. The physical basis for a velocity lag model for the electrically heat wire mesh is that when the velocity is increased, the temperature of the air at the wire mesh is decreased and the heat convection is increased after a given lag time. For the premixed flame, the velocity increase at the flame front will increase the mass of reactants and therefore will increase the amount of energy added to the system after a certain lag time. The lag times for these different systems may not necessarily be the same as is seen in the lag difference between Figures 3-9 and 3-15.

References

Abdel-Gayed R.G., Bradley D., and Lung F.K.-K. (1989) "Combustion Regimes and the straining of Turbulent Premixed Flames," Combustion and Flame, Vol. 76, pp. 213-218.

Annaswamy A.M., El Rifai O.M.,Fleifil M. et al. (1998) "A Model-Based Self-Tuning Controller for Thermoacoustic Instabilitiy," Combustion Science and Technology, Vol. 135, pp. 213-240.

Bayless, C. (1994) "Less is More: Why Gas Turbines Will Transform Electric Utilities," Public Utilities Fortnightly.

Bayliss A., Leaf G. K. and Matkowsky B. J. (1992) "Pulsating and Chaotic Dynamics Near the Extinction Limit," Combustion Science and Technology 84:253-278.

Benelli G. (1995) Personal Communication.

Benelli G., Cossalter V., and DeMichele G. (1994) "Combustion Driven Oscillation in Large Combustion Systems for Power Generation."

Benelli, G., Cossalter, V., and Da Lio, M. (1993) "Advances in Numerical Simulation of Pulsating Combustion at ENEL," Combustion Science and Technology 94:317-335.

Borghi R. (1985) in *Recent Advances in the Aerospace Sciences*, (C. Bruno and C. Casci, eds.), Plenum, New York.

Boussinesq V. J. (1877) "Theorie de l'Ecoulement Tourbillant," Mem. Pres. Acad. Sci., Vol. 23, p 46.

Bowman C. T. (1975) "Kinetics of Pollutant Formation and Destruction in Combustion.".

Bradshaw P., Ferriss D. H., and Atwell N. P. (1967) "Calculation of Boundary Layer Development using Turbulent Energy Equation," J. Fluid Mechanics, Vol. 28, p. 593.

Bray, K.N.C. and Moss J.B. (1977) "A Unified Statistical Model of the Premixed Turbulent Flame," *Acta Astronautica*, Vol. 4, pp. 291-319.

Brederoe, V. De and Bradshaw, P. (1972) "Three-Dimensional Flow in nominally Two-Dimensional Separation Bubbles. Flow Behind a Rearward-Facing Step," I.C. Aero Report 72-19.

Brouwer J., Ault B. A., Bobrow J. E., and Samuelsen G. S. (1990) "Active Control for Gas Turbine Combustors" 23rd Symposium (International) on Combustion, The Combustion Institute pp. 1087-1092.

Buchlin J.-M. and Planquart P. (1995) *Industrial Computational Fluid Dynamics*, Lecture Series 1995-03, Von Karman Insitute.

Burnley V. (1996) "Nonlinear Combustion Instabilities and Stochastic Sources," Ph.D. Dissertation, Department of Aeronautics, California Institute of Technology.

Caentini F., Hermann J., Vortmeyer D. and Gleis S. (1997) "NO and CO Reduction by Pulsating the Air Flow on a Swirl Spray Burner," Fourth International Conference on Technologies and Combustion for a Clean Environment," Lisbon.

Candel S., Veynante D., et al. (1990) 'Flamelet Descriptions of Turbulent Combustion," 9th International Heat Transfer Conference, Jerusalem, Israel.

Carrier G. F. (1955) "The Mechanics of Rijke Tube," Q. Appl. Math, Vol. 12, p. 383.

Casentini F. (1995) "Pulsated Combustion on a Swirl Spray Burner: Influence on NOx Emissions and Flame Structure," Ph.D. Thesis, Department of Energy, Politecnico Di Milano, Milan, Italy.

Catlin C.A. and Lindstedt R.P. (1991) "Premixed Turbulent Burning Velocities Derived from Controlled Reaction Models with Cold Front Quenching," Combustion and Flame, Vol. 85, pp. 427-439.

Choi Y.-H. and Merkle C.L. (1993) "The Application of Preconditioning in Viscous Flows," Journal of Computational Physics," Vol. 105, pp. 207-223.

Chorin A.J. (1967) "A Numerical Method for Solving Incompressible Viscous Flow Problems," Journal of Computational Physics, Vol. 2, pp. 12-26.

Chu B.-T. and Kovasznay S.G. (1958) "Non-Linear Interactions in a Viscous Heat-Conducting Compressible Gas," Journal of Fluid Mechanics 3:494-514.

Chu Y., Dowling A.P., and Glover K. (1998) "Robust Control of Combustion Oscillations." In *Proc. 1998 IEEE Conference on Control Applications*, pp. 1165-1169, Trieste, Italy.

Collyer A. A. and Ayres D. J. (1972) "The Generation of Sound in a Rijke Tube Using Two Heating Coils," J. Phys. Appl. Phys, Vol. 5.

Correa S. M. (1992a) "Carbon Monoxide Emissions in Lean Premixed Combustion," Journal of Propulsion and Power, Vol. 8, No. 6, pp. 1144-1151.

Correa S.M. (1992b) "A Review of NOx Formation Under Gas-Turbine Combustion Conditions," Combustion Science and Technology 87:329-362.

Correa S.M. and Shvy W. (1987) "Computational Models and Methods for Continuous Gaseous Turbulent Combustion," Progress in Energy and Combustion Science 13:249-292.

Culick F.E.C. (1963) "High Frequency Oscillations in Liquid Rockets," AIAA Journal, Vol. 1, No. 5, pp. 1097-1104.

Culick F.E.C. (1966) "Acoustic Oscillations in Solid Propellant Rockets," Astronautica Acta, Vol. 12, No. 2, pp. 113-126.

Culick F. E. C. (1971) "Nonlinear Growth and Limiting Amplitude of Acoustic Oscillations in Combustion Chambers," Combustion Science and Technology, Vol. 3, No. 1, pp. 1-16.

Culick F. E. C. (1976) "Nonlinear Behavior of Acoustic Waves in Combustion Chambers, Parts I and II," Acta Astronautica, Vol. 3, pp. 714-757.

Culick, F.E.C. (1988) "Combustion Instabilities in Propulsion Systems," AGARD Conference Proceedings, Paper 1, 450.

Culick F.E.C., Paparizos L., Sterling J. and Burnley V. (1991) "Combustion Noise and Combustion Instabilities in Propulsion Systems," AGARD Conference on Combat Aircraft Noise, AGARD CP 512.

Culick F.E.C. and Yang V. (1992) "Prediction of the Stability of Unsteady Motions in Solid Propellant Rocket Motors," AIAA Progress in Aeronautics and Astronautics Series 143:719-779.

Culick F.E.C. (1994) "Some Recent Results for Nonlinear Acoustics in Combustion Chambers," AIAA Journal 32:146-169.

Culick F.E.C. (1995) "Nonlinear Acoustics in Combustion Chambers with Stochastic Sources," Jet Propulsion Center Document CI95-6, California Institute of Technology.

Culick F.E.C. (1996) "A Note on Ordering Perturbations and the Insignificance of Linear Coupling in Combustion Instabilities," To be published in Combustion Science and Technology.

Di Martino, P., Cinque, G.,Paduano, C., and Cirillo, L. (1994) "Numerical Study of Swirling Reacting Flow in a Can-Type Combustor," AIAA Paper No. AIAA-94-3044.

Duclos J. M., Veynante D., andPoinsot T. (1993) "A Comparison of Flamelet Models for Premixed Turbulent Combustion," Combustion and Flame, 95:101-117.

Dupoirieux, F. and Desaulty M. (1995) "A Coherent Research Effort on Combustion: The A3C Operation.".

Durbin M. D., Vangsness M. D. and Ballal D. R. (1994) "Characteristics of Swirl Flames in a Step Combustor," AIAA Paper No. 94-3272.

Entezam B., VanMorrhen W. K., and Majdalani J. (1997) "Modeling of a Rijke Tube Pulse Combustor using Computational Fluid Dynamics," Published by AIAA, with permission.

Feikema D., Chen R., Driscoll J. F. (1990) "Enhancement of Flame Blowout Limits by the Use of Swirl," Combustion and Flame, Vol. 80, pp. 183-190.

Feitelberg, A. S. (1995) "The Perfectly Stirred Pulsed Reactor," Eastern States section meeting of the Combustion Institute, Wercester Polytechnic Institute 217-220.

Fenimore C. P. (1970) "Formation of Nitric Oxide in Premixed Hydrocarbon Flames," Thirteenth Symposium (International) on Combustion, The Combustion Institute, Pittsburgh, PA pp. 373-380.

Flandro G. (1967) "Rotating Flows in Acoustically Unstable Rocket Motos," Ph.D. Dissertation, California Institute of Technology, Department of Aeronautics.

Flandro G. (1974) "Solid Propellant Acoustic Admittance Corrections," Journal of Sound and Vibration, Vol. 36, No. 3, pp. 297-312.

Flandro G. (1995) "Effects of Vorticity on Rocket Combustion Stability," Journal of Propulsion and Power, Vol. 22, No. 4.

Flugge S., Editor (1961) *Hanbuch der Physik*, Vol. XI, Acoustics 1, Springer-Verlag, Berlin, pp. 1-128.

Fric T. F. (1993) "Effects of Fuel-Air Unmixedness on NOx Emissions," Journal of Propulsion and Power, Vol. 9, No. 5, pp. 708-713.

Givi P., Madnia C. K. et al. (1990) "DNS, LES and Stochastic Modeling of Turbulent Reacting Flows."

Glarborg P., Miller J. A. and Kee R. J. (1986) "Kinetic Modeling and Sensitivity Analysis of Nitrogen Oxide Formation in Well-Stirred Reactors," Combustion and Flame, 65:177-202.

Goldin G.M. and Menon S. (1998) "A Linear Eddy Model for Steady-State Turbulent Combustion," AIAA Paper No. 96-0519.

Greene W. D. (1990) "Triggering of Longitudinal Combustion Instabilities in Rocket Motors," Masters Thesis, The Pennsylvania State University, Department of Aerospace Engineering.

Gutmark E., Parr T. P., Hanson-Parr D. M.,Schadow K. C. (1991) "Closed-Loop Amplitude Modulation Control of Reacting Premixed Turbulent Jet," AIAA Journal, Vol. 29, N. 12, pp. 2155-2162.

Hadjinieolaou M. and Goussis D.A. (1999) "Asymptotic Solution of Stiff PDEs with the CSP Method: The Reaction Diffusion Equation," SIAM J.Sci. Comput., Vol. 20, pp. 781-810.

Harlow, F. H. and Nakayama P. I. (1967) "Turbulent Transport Equations," Physics of Fluids, Vol. 10, p. 323.

Harrje D.T. (ed.) (1972) *Liquid Propellant Rocket Combustion Instability*, NASA SP-194.

Hautman D. J., Dryer F. L., Schug K. P. and Glassman I. (1981) "A Multiple-Step Overall Kinetic Mechanism for the Oxidation of Hydrocarbons," Combustion Science and Technology, 25:219-235.

Hayder M.E. and Turkel E. (1995) "Nonreflecting Boundary Conditions for Jet Flow Computations," AIAA Journal, Vol. 33, pp. 2264-2270.

Hewson J. C. (1995) "Reduced Mechanisms for Hydrocarbon and Nitrogen Chemistry in Diffusion Flames," CECR Report 95-01, Center for Energy and Combustion Research, University of California, San Diego.

Hirsch C. (1988) *Numerical Computation of Internal and External Flows, Vol. 1 and 2*, John-Wiley and Sons, New York.

Houpt P. K. and Goodman G. C. (1990) "Active Feedback Stabilization of Combustion for Gas Turbine Engines."

Iverach D., Basden K.S. and Kirov N.Y. (1972) "Formation of Nitric-Oxide in Fuel-Lean and Fuel-Rich Flames," Fourteenth Symposium (International) on Combustion, The Combustion Institute, Pittsburgh, PA, pp. 767-775.

Jones W. P. and Launder B. E. (1973) "Predictions of Low Reynolds Number Phenomena with a two Equation Model of Turbulence," Int. J. Heat and Mass Transfer, Vol. 16, p. 1119.

Jones W.P. and Kakhi M. (1998) "PDF Modeling of Finite-Rate Chemistry Effects in Turbulent Non-Premixed Jet Flames," Combustion and Flame, Vol. 115, pp. 210-229.

Jonsson V. K. and Sparrow E. M. (1966) "Turbulent Diffusivity for Momentum in Concentric Annuli," J. Basic Eng., V. 88, p. 550.

Joshi N.D., Epstein M.J., Durlak S., Marakovits S., and Sabla P.E. (1994) "Development of a Fuel Air Premixer for Aero Derivative Dry Low Emissions Combustors," ASME Paper No. 94-GT-253.

Kailasanath, K., Gardner, J. H., Oran, E. S., and Boris, J. P. (1991) "Numerical Simulations of Unsteady Reactive Flows in a Combustion Chamber," Combustion and Flame 86:115-134.

Keller J.O. and Hongo I. (1990) "Pulse Combustion: The Mechanisms of NOx Production," Combustion and Flame 80:219-237.

Khalil, E. E. (1982) *Modelling of Furnaces and Combustors*, Abacus Press.

Kuo K. K. (1986) *Principles of Combustion* John Wiley and Sons, New York.

Lam S. H. and Goussis D. A. (1994) "The CSP Method for Simplifying Kinetics," International Journal of Chemical Kinetics 26:461-486.

Launder, B. E. and Spalding, D. B. (1972) *Lectures in Mathematical Models of Turbulence*, Academic Press.

Ledder G. and Kapila A. K. (1991) "The Response of Premixed Flames to Pressure Perturbations," Combustion Science and Technology, 76:21-44.

Lee D., Yeh C.L., Tsuei Y.M., and Chou J. (1993) "Numerical Simulations of Gas Turbine Combustor Flows," Journal of Propulsion and Power, Vol. 9, pp. 322-328.

Leonard G. and Correa S. (1990) "NOx Formation in Premixed High-Pressure Lean Methane Flames," Fossil Fuels Combustion Symposium.

Lepelletier T.G. and Raichlen F. (1987) "Harbor Oscillations Induced by Nonlinear Transient Long Waves," Journal of Waterway Port Coastal and Ocean Engineering, ASCE, Vol. 113, pp. 381-400.

Levine J.N. and Baum J.D. (1981) "A Numerical Study of Nonlinear Instability Phenomena in Solid Rocket Motors," AIAA Paper No. 81-1524.

Libby P.A. and Williams F.A. (editors) (1994)*Turbulent Reacting Flows*, Academic Press, London.

Lieuwen T., Neumeier Y., and Zinn B.T. (1998) "The Role of Unmixedness and Chemical Kinetics in Driving Combustion Instabilities in Lean Premixed Combustors," Combustion Science and Technology, 135:193-211.

Liu, R. and McGuirk, J. J. (1995) "Prediction of Combustion Induced Oscillations using a Pressure-Correction Method," ASME paper no. 95-GT-336.

Lores E. M. and Zinn B. T. (1973) "Nonlinear Longitudinal Instability in Rocket Motors," Combustion Science and Technology, Vol. 7, No. 6, pp. 245-256.

Madnia C. K., Frankel S.H., and Givi P. (1991) "Direct Numerical Simulations of the Unmixedness in a Homogeneous Reacting Turbulent Flow," Chemical Engineering Communications, Vol. 109, pp. 19-29.

Malte P. C. and Pratt D. T. (1974) "Measurement of Atomic Oxygen and Nitrogen Oxides in Jet-Stirred Combustion," Fifteenth Symposium (International) on Combustion, The Combustion Institute, Pittsburgh, PA pp. 1061-1070.

Malte P. (1996), University of Washington, Private Communication.

Manna M. and Vandromme D., Lecture Series Directors (1996) *Combustion and Turbulence in Two-Phase Flows*, Lecture Series 1996-02, VonKarman Institute.

McDonald J. P. and Mellor A. M. (1995) "Design of Inlet Conditions for High Pressure NOx Measurements in Lean Premixed Combustors," ASME Paper No. 95-GT-136.

McVey J.B., Padget F. Cc, et al. (1993) "Evaluation of Low NOx Combustor Concepts for Aeroderivative Gas Turbine Engines," Journal of Engineering for Gas Turbines and Power, Vol. 115, pp. 581-587.

Mellor A. M., Editor (1996) "NOx and CO Emissions Models for Gas-Fired, Lean-Premixed Combustion Turbines," Final Report, December 1996, Vanderbilt University.

Meneveau C. and Poinsot T. (1991) "Stretching and Quenching of Flamelets in Premixed Turbulent Combustion," Combustion and Flame, 86:311-332.

Menon, S. and Jou W.-H. (1991) "Large-Eddy Simulations of Combustion Instability in an Axisymmetric Ramjet Combustor," Combustion Science and Technology, Vol. 75, pp. 53-72.

Merk H. J. (1957) "Analysis of Heat-Driven Oscillations of Gas Flows: II. On the Mechanism of the Rijke Tube Phenomenon," Applied Scientific Results, A6:402-420.

Merkle C.L. and Choi Y.-H. (1988) "Computation of Low-Speed Compressible Flows with Time-Marching Procedures," International Journal for Numerical Methods in Engineering, Vol. 25, pp. 293-311.

Miller J.A. and Bowman C.T. (1989) "Mechanism and Modeling of Nitrogen Chemistry in Combustion," Progress in Energy Combustion Science 15:287-338.

Miller R. S., Frankel S. H., Madnia C. K. and Givi P. (1993) "Johnson-Edgeworth Translation for Probability Modeling of Binary Scalar Mixing in Turbulent Flows," Combustion Science and Technology, 91:21-52.

Moss W.D., Baker S. and Bradbury L.S.J. (1979) "Measurements of Mean Velocity and Reynolds Stresses in Some Regions of Recirculating Flows," in *Turbulent Shear Flows 1* (ed. F. Durst, B.C. Launder, F.W. Schmidt and J.H. Whitelaw). Springer.New York.

Nandula S. P., Pitz R. W., Barlow R.S. and Fiechtner G. J. (1996) "Rayleigh/Raman/LIF Measurements in a Turbulent Prmixed Combustor," AIAA Paper No. 96-0937.

Nee V. W. and Kovasznay L. S. G. (1969) "The Calculation of the Incompressible Turbulent Boundary Layer by a Simple Theory," Physics of Fluids, V. 12, p. 473.

Newburry D.M. and Mellor A.M. (1995a) "Characteristic Time Model Correlation of NOx Emissions from Lean Premixed Combustors," ASME Paper No. 95-GT-135.

Newburry D. M. and Mellor A. M. (1995b) "Semi-Empirical Predictions and Correlations of NOx Emissions from Utility Combustion Turbines," ASME Paper No. 95-GT-70.

Nicol D., Malte P.C., Lai J., Marinov N.N., and Pratt D.T. (1992) "Nox Sensitivities for Gas Turbine Engines Operated on Lean-Premixed Combustion and Conventional Diffusion Flames," ASME Paper No. 92-GT-115.

Oran E. S. and Gardner J. H. (1985) "Chemical-Acoustic Interactions in Combustion Systems," Progress in Energy and Combustion Science, 11:253-276.

Oran E.S., and Boris J.P. (1987) *Numerical Simulation of Reactive Flow*, Elsevier, New York.

Peters N. and Ludford G. S. S. (1983) "The Effect of Pressure Variations on Premixed Flames," Combustion Science and Technology, 34:331-344.

Peters N. (1986) "Laminar Flamelet Concepts in Turbulent Combustion," Twenty-First Symposium (International) on Combustion, The Combustion Institute, Pittsburgh, PA.

Poinsot and Lele (1992) "Boundary Condition for Direct Simulations of Compressible Viscous Flows," Journal of Computational Physics, Vol. 101, pp. 104-129.

Prandtl L. (1925) "Bericht uber Untersuchung zur Ausgebildeten," ZAMM, Vol. 5, p. 136.

Prasad K. (1994) "Interaction of Pressure Perturbations with Premixed Flames," Combustion and Flame 97:173-200.

Pun W., and Hixson D. (1999) Personal Communication.

Raun R.L., Beckstead M.W., Finlinson J.C., and Brooks K.P. (1993) "A Review of Rijke Tubes, Rijke Burners and Related Devices," Prog. Energy Combust. Sci., Vol. 19, pp. 313-364.

Rayleigh J.W.S. (1878) Nature, Vol. 18, p. 319.

Richards G. A., Yip M. J., Robey E., Cowell L., Rawlins D. (1995) "Combustion Oscillation Control by Cyclic Fuel Injection," 1995 ASME Turbo Expo, Houston, TX.

Rizk N.K. and Mongia H.C. (1993a) "Semi-analytical Correlations for NOx, CO and UHC Emissions," Journal of Engineering Gas Turbine and Power, Transactions of the ASME 115:612-619.

Rizk N.K. and Mongia H.C. (1993b) "Three-Dimensional Gas Turbine Combustor Emissions Modeling," Journal of Engineering Gas Turbine and Power, Transactions of the ASME 115:603-611.

Roquemore W.M., Reddy V.K., et al. (1991) "Experimental and Theoretical Studies in a Gas-Fueled Research Combustor," AIAA Paper No. 91-0639.

Rowley C.W. and Colonius T. (1998) "Discretely Nonreflecting Boundary Conditions for Linear Hyperbolic Systems," Submitted to J. Computational Physics October 1, 1998.

Runchal A.K. (1977) "Comparative Criteria for Finite-Difference Formulations for Problems of Fluid Flow," Inter. Journal for Numerical Methods in Engineering, Vol. 11, pp. 1667-1679.

Saxena V. and Pope S.B. (1999) "PDF Simulations of Turbulent Combustion Incorporating Detailed Chemistry," Combustion and Flame, Vol. 117, pp. 340-350.

Schadow K. C. and Gutmark E. (1992) "Combustion Instability Related to Vortex Shedding in Dump Combustors and Their Passive Control," Progress in Energy and Combustion Science, 18:177-232.

Schadow K.C., Gutmark E., Parr T.P., Parr D.M., Wilson K.J., and Crump J.H. (1987) "Large Scale Coherent Structures as Drivers of Combustion Instability," AIAA Paper No. 87-1326.

Seywert C. and Isella G. (1999) Personal Communication.

Sirignano W. A. (1964) "Theoretical Study of Nonlinear Combustion Instability: Longitudinal Mode," Ph.D. Thesis, Princeton University, Princeton, New Jersey.

Sirignano W. A. and Crocco L. (1964) "A Shock Wave Model of Unstable Rocket Combustors," AIAA Journal, Vol. 2, No. 7, pp. 1285-1296.

Smith D.A. and Zukoski E.E. (1985) "Combustion Instability Sustained by Unsteady Vortex Combustion," AIAA Paper No. 85-1248.

Smith T.M. and Menon S. (1998) 'Subgrid Combustion Modeling for Premixed Turbulent Reacting Flows," AIAA Paper No. 98-0242.

Spalding D. B. (1971) "Mixing and Chemical Reaction in Steady Confined Turbulent Flames," Thirteenth Symposium (International) on Combustion, The Combustion Institute, Pittsburgh, PA.

Steele R. C., Tonouchi J. H., Nicol D. G., Horning D. C., Malte P. C., and Pratt D. T. (1996) "Characterization of NOx, N_2O and CO for Lean-Premixed Combustion in a High Pressure Jet-Stirred Reactor," ASME Paper No. 96-GT-128.

Steele R.C., Jarrett A.C., Malte P.C., Tonouchi J.H., and Nicol D.G. (1997) "Variables Affecting NOx Formation in Lean-Premixed Combustion," Journal of Engineering for Gas Turbines and Power: Transactions of the ASME, Vol. 119, pp. 102-107.

Sterling, J.D. (1987) Longitudinal Mode Combustion Instabilities in Air Breathing Engines, Ph.D. Thesis, Daniel and Florence Guggenheim Jet Propulsion Center, California Institute of Technology, Pasadena, CA.

Sterling J.D. and Zukoski E.E. (1987) "Longitudinal Mode Combustion Instabilities in a Dump Combustor," AIAA Paper No. 87-0220.

Sturgess G. J., Sloan D. G., et al. (1991) "Flame Stability and Lean Blowout," ISABE Paper No. 91-7037.

Sturgess G. J., Sloan D. G., et al. (1992) "Design and Development of a Research Combustor for Lean Blowout Studies," Journal of Engineering for Gas Turbines and Power, Vol. 114, pp. 13-19.

Sturgess G.J., McKinney R.G., and Morford S.A. (1993) "Modification of Combustor Stoichiometry Distribution for Reduced NOx Emission from Aircraft Engines," Journal of Engineering for Gas Turbines and Power, Vol. 115, pp. 570-580.

Subramaniam S. and Pope S.B. (1999) "Comparison of Mixing Model Performance for Non-Premixed Turbulent Reactive Flow," Combustion and Flame, Vol. 117, pp. 732-754.

Swenson G., Pun W. and Culick F.E.C. (1996) "Nonlinear Unsteady Motions and NOx Production in Gas Turbine Combustors."

Toh H. and Hosoi J. (1994) "Development of a Low-NOx Combustor," AIAA Paper No. 94-2900.

Tonouchi J.H., Held T.J. and Mongia H.C. (1998) "A Semi-Analytical Finite Rate Two-Reactor Model for Gas-Turbine Combustors," Journal of Engineering for Gas Turbines and Power: Transactions of the ASME, Vol. 120, pp. 495-501.

Torres H, Lieuwen T., Johnson C., Daniel B.R., and Zinn B.T. (1999) "Experimental Investigation of Combustion Instabilities in a Gas Turbine Combustor Simulator," AIAA Paper No. 99-0712.

Veynante D., Lacas F., and Candel S. (1989) "A NewFlamelet Combustion Model Combining Premixed and Non-Premixed Turbulent Flames," AIAA Paper No. 89-0487.

Von Karman T. H. (1930) "Mechanische Ahnlichkeit und Turbulenz," Proc. 3rd Int. Congress Appl. Mech., Stockholm, pt. 1, p. 85.

Watson W.R. and Myers M.K. (1991) "Inflow-Outflow Boundary Conditions for Two-Dimensional Acoustic Waves in Channels with Flow," AIAA Journal, Vol. 29, pp. 1383-1389.

Weiss J. M. and Smith W. A. (1995) "Preconditioning Applied to Variable and Constant Density Flows," AIAA Journal Vol. 33, No. 11, pp. 2050-2057.

Yu K, Lee S., Trouve A., Stewart H., and Daily J.W. (1987) "Vortex-Nozzle Interactions in Ramjet Combustors," AIAA Paper No. 87-1871.

Zinn B. T. and Powell E. A. (1970) "Application of the Galerkin Method in the Solution of Combustion Instability Problems," Proceedings of the 19th International Astronautical Congress, 3:59-73.

Zinn B. T. and Lores E. M. (1972) "Application of the Galerkin Method in the Solution of Nonlinear Axial Combustion Instability Problems in Liquid Rockets," Combustion Science and Technology, Vol. 4, No. 6, pp. 269-278.

Zsak, T. W. (1993) An Investigation of the Reacting Vortex Structures Associated with Pulse Combustion, Ph.D. Thesis, Daniel and Florence Guggenheim Jet Propulsion Center, California Institute of Technology, Pasadena, CA.